Vibro-Acoustic Health Monitoring of Bearings using Signal Processing Techniques

THESIS

Submitted in partial fulfillment
of the requirements for the degree of

DOCTOR OF PHILOSOPHY

by

Satish Mohanty
ID No. 2011PHXF418P

Under the Supervision of

Dr. Karunesh Kumar Gupta
&
Dr. Kota Solomon Raju

BITS Pilani
Pilani | Dubai | Goa | Hyderabad

BIRLA INSTITUTE OF TECHNOLOGY & SCIENCE, PILANI

2016

Dedication

"To my Ma, Bapa and

my Brother, Sisters & my nephews

and

Best ever friends

and the unseen vibrations guiding me

to visualize the eclectic side of me and the nature  *"*

BIRLA INSTITUTE OF TECHNOLOGY & SCIENCE

PILANI-333031 (RAJASTHAN) INDIA

CERTIFICATE

This is to certify that the thesis entitled **"Vibro-Acoustic Health Monitoring of Bearings using Signal Processing Techniques"** submitted by **Satish Mohanty,** ID No. **2011PHXF418P** for award of Ph.D. of the Institute embodies original work done by him under my supervision.

Signature of the Supervisor	Signature of the Co-Supervisor
Name: Dr. K. K. Gupta	Name: Dr. Kota Solomon Raju
Designation: Assistant Professor	Designation: Principal Scientist
Date: 31 /12/ 2016	Date: 31 / 12/ 2016

Vibro-Acoustic Health Monitoring of Bearings using Signal Processing Techniques

THESIS

Submitted in partial fulfillment
of the requirements for the degree of

DOCTOR OF PHILOSOPHY

by

Satish Mohanty
ID No. 2011PHXF418P

Under the Supervision of

Dr. Karunesh Kumar Gupta
&
Dr. Kota Solomon Raju

BITS Pilani
Pilani | Dubai | Goa | Hyderabad

BIRLA INSTITUTE OF TECHNOLOGY & SCIENCE, PILANI

2016

Dedication

"To my Ma, Bapa and

my Brother, Sisters & my nephews

and

Best ever friends

and the unseen vibrations guiding me

to visualize the eclectic side of me and the nature  *"*

BIRLA INSTITUTE OF TECHNOLOGY & SCIENCE

PILANI-333031 (RAJASTHAN) INDIA

CERTIFICATE

This is to certify that the thesis entitled **"Vibro-Acoustic Health Monitoring of Bearings using Signal Processing Techniques"** submitted by **Satish Mohanty,** ID No. **2011PHXF418P** for award of Ph.D. of the Institute embodies original work done by him under my supervision.

Signature of the Supervisor	Signature of the Co-Supervisor
Name: Dr. K. K. Gupta	Name: Dr. Kota Solomon Raju
Designation: Assistant Professor	Designation: Principal Scientist
Date: / / 2017	Date: / / 2017

Acknowledgements

I would like to take this opportunity to convey my heartfelt gratitude and indebtedness to my supervisor, Dr. Karunesh Kumar Gupta and Co-supervisor Dr. Kota Solomon Raju for all their support, guidance and supervision during my research tenure.

I owe a debt of gratitude to my Doctoral Advisory Committee members Prof. Surekha Bhanot and Prof. Navneet Gupta, for their valuable support and comments that have shed a new light on several aspects of the research work. I owe my sincere gratitude to Prof. Anu Gupta and Prof. V. K. Chaubey for providing me the requisite facility to carry out my doctoral research. I would like to show my gratitude to Dr. Abhijit Asati, convener, Doctoral Research Committee for all his support and useful suggestions.

I wish to express my humble gratitude to Vice Chancellor, Director, and Deans, BITS-Pilani, Pilani Campus for providing me the opportunity to pursue my doctoral studies. I express my gratitude to Prof. S. K. Verma, Dean-ARD, Prof. H. R. Jadhav, Associate Dean-ARD & SRCD, for their official support and encouragement. I extend my thanks to SRCD and ARD staff for their valuable support.

I owe my appreciation to Prof. B. K. Rout for his valuable suggestion during the research objective. I acknowledge each and every individual to dispense their time and support. The time spent at BITS-Pilani was inspiring and commendable. I am thankful to Mahesh Saini, Tulsiram Sharma, Bahadur Singh, Ravindra Kumar, Manoj Jangir, Ashok Saini, and Amitabh Jangir, Bridi Chand, Sanjay Bhargava and the people of BITS-workshop for their affluent and unflinching support. I would like to express my appreciation to Dr. P. Bhanu Prasad, Vikrant Mishra, Pramod Tanwar, Vipin Sharma of CEERI-Pilani for their kind support.

I would like to thank my entire Ph.D. cohort for their inspiration during my tenure at the wonderful campus. I would cherish happy moments spent with my friends at BITS-Pilani, Pilani campus for my whole life. Finally, I would also like to thank my Maa and Bapa in inspiring and imparting the faith that created the craving for knowledge, whether in humanity or science. Finally, I would like to thank my family for their commendable support to carry out my research.

Satish Mohanty

Abstract

Rolling element bearings have diverse applications in various industrial sectors and fields that need motion. The rapid demands of bearings have put the question on their reliability to avoid malfunction and failure. The assessment of their reliability has given a new dimension to the condition monitoring (CM) equipments & tools. The current survey shows that the overall demand of the CM market is expected to reach 2.45 billion USD by 2020. The demand and supply have made the field of CM lucrative as well as sensitive. In general, CM relies on the advanced sensor technologies and signal processing methods to diagnose machinery and their related faults. Especially, to anticipate bearings CM (BCM), various sensors like accelerometer, acoustic emission (AE), ultrasonic, thermal imaging, microphone and motor current signature analysis (MCSA) etc. are used prevalently. Out of these sensing methods, vibration based sensing finds usages of around 87% for reliable fault diagnosis and detection. Recently, microphone sensors have given a new dimension to the CM due to their significant improvement in the sensitivity and bandwidth, as well as their coherence with vibration.

The goal of the thesis is to analyze vibration and acoustic signals from the bearings using statistical and signal processing techniques like; kurtosis, crest factor, energy, probability density function (pdf), empirical mode decomposition (EMD) and variational mode decomposition (VMD). In this thesis, three signal processing methods are proposed to identify faults related to bearings.

Initially, adaptive empirical mode decomposition and principal component analysis (EMD-PCA) based average kurtosis technique followed by Fourier, envelope, cepstrum and cepstral envelope (FECCV) techniques are proposed to detect bearing defects from the vibration signature. In this method, the initial verification is conducted to address the effect of sample length and standardization on the spectral characteristic of FECCV techniques. It is observed, the standardization along with large sample length can be used to detect inner race defect (IRD) and outer race defect (ORD) effectively without the use of complex algorithms, however, it cannot detect ball defect (BD). Similarly, the effects of EMD and envelope detection on the spectral characteristics of decomposed modes are tested for various faulty signals. The EMD-PCA based average kurtosis technique is used to generate a

modified signal to enhance the fault frequencies. These methods are validated on experimental data sets of Case Western Reserve University (CWRU).

The second approach proposes a unitary sample shifted probability density function based on Kolmogorov and Smirnov test (KS-test) performed on Case Western Reserve University data sets. In this approach, two probability density functions namely, Laplacian and rectangular functions with variable window sizes are generated using sampling rate, sample length and number of impulses generated during the experimentation. These distribution functions are further used as a unitary sample shifted window over the faulty signals to generate frame based crest factor (FCF), frame based kurtosis (FKS) and frame based energy (FE) time series signals. It is observed that the sensitivity of these time series signals increases with the change in the shape parameter and boundary value of the probability density function. The fault detection sensitivity of Laplacian distribution function is better than rectangular distribution function.

Apart from vibration, the acoustic signals are gaining prominence as either one can be the cause, and the other, its effect. Therefore, the third method is proposed to analyze coherence characteristics of acoustic and vibration signals in detecting bearing defects at variable rotating speeds. In this method, these two signals are decomposed concurrently using EMD and VMD. The actual mode representing the fault frequency and the shaft speed are identified using correlation coefficient (CC) and log-variance based selection approach. It is observed that the performance of acoustic signal is better than vibration using VMD at higher speed, whereas, EMD performs better at lower speed.

Moreover, the present results show that the sensing and signal processing techniques play a vital role in extracting fault features of the system under test.

Table of Contents

List of Figures

List of Tables

List of Abbreviations & Symbols

Symbols	Notations
ADC	Analog to digital converter
AE	Acoustic emission
AM	Amplitude modulation
BCM	Bearing condition monitoring
BD	Ball defect
CEEMD	Complete ensemble EMD
CF	Crest factor
CF	Correlation functions
CLF	Clearances factor
CWRU	Case Western Reserve University
DAQ	Data acquisition
DGBB	Deep groove ball bearing
EDM	Electrical discharge machining
EEMD	Ensemble empirical mode decomposition
EMD	Empirical mode decomposition
FCF	Frame based crest factor
FE	Frame based energy
FECCV	FFT, envelope, cepstrum and cepstral envelope
FFT	Fast Fourier Transform
FKS	Frame based kurtosis
FM	Frequency modulation
HHT	Hilbert-Huang Transform
ICA	Independent component analysis
ICP	Integrated circuit piezoelectric
IF	Impulse factor
IMF	Intrinsic mode function

IRD	Inner race defect
KS-Test	Kolmogorov and Smirnov test
KS	Kurtosis
LOS	Line of sight
MCSA	Motor current signature analysis
ORD	Outer race defect
PCA	Principal component analysis
PDF	Probability density function
RMS	Root mean square
RPM	Revolution per minute
RPS	Revolution per second
RTD	Resistance temperature detector
SD	Standard deviation
SK	Spectral kurtosis
SK	Skewness
SNR	Signal to noise ratio
SUT	System under test
SVM	Support vector machine
Var	Variance
VMD	Variational mode decomposition
WVD	Wigner Ville distribution
ZCR	Zero crossing
B_d	Ball diameter
C_i	Decomposed mode
N_b	Number of ball
N_δ	Number of impulses
P_d	Pitch diameter
$\frac{df}{f_{FM}}$	Modulation index
f_{Gn}	Fractional Gaussian noise
f_{bd}	Ball defect frequency
f_{ir}	Inner race frequency
f_{or}	Outer race frequency
f_s	Spin frequency of shaft

r_n	Residual mode
w_k	Center of gravity
$\bar{x}$	Mean
x_{AM}	Amplitude modulated
x_{FM}	Frequency modulated
x_{PH}	Periodic harmonic
x_{PS}	Periodic signal
x_{QP}	Quasi-periodic
x_{TS}	Transient signal
$\emptyset$	Contact angle
B	Diversity
CC	Correlation coefficient
H	Hurst
K	Mode index
N	Sample length
Λ	Lagrangian multiplier
C	Covariance

CHAPTER 1
Introduction

The industrial revolution has increased the dependency on bearings and their demand is expected to increase by $104.5 billion USD by 2018, globally. Primarily, the state of the machine or the system under test (SUT) needs a complete understanding of various bearing condition monitoring techniques (BCM). These techniques solely depend on the types of the sensor and the signal processing methods adapted to anticipate the incipient faults. The selection of sensors plays a vital role and it depends on the condition of the system to be tested. Nowadays, the researchers are focusing on BCM using vibration and acoustic/microphone sensors due to their close dependency and characteristics. Apart from these sensing methods, various statistical and non-linear signal-processing methods have paved their way to intercept the information required for condition monitoring (CM). In general, signal processing and analysis are the mathematical envelopes that help to decode and understand the existence of different patterns in nature. The true form of the signals depends on various parameters i.e. the property of the source from where it evolved, the propagating channels, interaction with other signals, and finally, the realizing system and the mathematical operators involved in the realizations/extraction of these signals. Therefore, the perfect analogy related to fault can be realized only if the variation in the patterns at different stages during propagation can be assimilated using the inverse mathematical model in its true form. This analogy is too complex and indeed need an affluent understanding of each mathematical operator acting on the signals and their influence that change the actual characteristics.

As every divided kingdom falls, so every mind divided between many studies confounds and saps itself.

— Leonardo da Vinci

1.1 Background

Condition monitoring or health monitoring has gained its prime importance in recent days, whether it is for humans or machines. Condition monitoring of rolling element bearings has leveraged its importance in providing smooth dynamics to devices/systems that need motions. These rolling elements have found their applications since the Stone Age and long been used by human civilizations to drive towards development. In the early days, as the demands were less, perception based analysis was the main tool to diagnose the state of the machines. With the change in demand and to mitigate risk, sensors and signal processing methods are used to shape the field of condition monitoring. The broad spectrum of the bearing condition monitoring market and the demands to anticipate their condition has given a new dimension to the researchers to understand their characteristics as the bearings roll towards the future.

1.2 Motivation

The rapid growth in the industrial sectors has given new dimensions to the bearing condition monitoring (BCM) market to avoid catastrophic failure during operation. It has wide applications in various sectors and fields, wherever there is need for motion, i.e. automobile, railways, electric motor, steel plants, power generation units and cement plants etc. The condition monitoring of the of the bearings is important to avoid unexpected failure, increase mean time between failure, decrease in repair and overhaul timing and decrease downtime so as to minimize cost and maximize production efficiency. These are affected by the coupling, misalignment, and surrounding environment etc., and can be monitored using various sensors like vibration, temperature, pressure, Acoustic emission, Ultrasonic, oil quality, Eddy current, thermal imaging, and perception based analysis etc. However, BCM monitoring using vibrations is widely used to detect fault, and contributes approximately 87% relative to other sensors. Recently, microphone sensors have marked their interest among the researchers, even though their applications are limited to noise-free environments. Therefore, the selection of sensors plays a major role to anticipate the real world physical data. As the sensitivity, bandwidth of operation and operating environmental conditions affect the performance of sensors, therefore, the system needs to be examined carefully before subjecting these sensors to the field. However, the question arises about the selection

of sensors and their usability that can suit to a particular experimental setup. Apart from sensors, the communication protocols, and the type of the analog to digital converter (ADC) used to communicate with the computer play a vital role. The property of the ADC i.e. the quantization bit level, noise floor and the sampling rate of the devices must be known for faithful acquisition of desired noise and vibration signals. During data acquisitions, if the sampling rate and data acquisition time are not chosen properly the signal may misrepresent the actual information. Similarly, during the data acquisitions using sensors and data acquisition (DAQ) devices, the signals may be corrupted by the propagating channels and create a deviation in the amplitude and frequencies. Therefore, the effect of modulations and the noise induced by the surroundings make the signal analysis complicated. Recently, the rapid developments of nonlinear and non-stationary signal processing algorithms have made the signal analysis better in the presence of noise. Nevertheless, the selection of a signal processing algorithm needs an understanding about the system to be observed, and the alterations done during propagations. Generally, signal processing methods use different mathematical operators to extract information hidden in the signals by inverse mathematical model i.e. if the sequences of the mathematical operators are not set properly then it may dilute the information content. Therefore, care should be taken during extraction and analysis process of the signals as it is not only biased by its design, but also by the surrounding artefacts.

1.3 Research Objectives

The field of BCM is complex and rich with sensors and signal analysis techniques. Therefore, to intercept faults, the practicality of the mathematical functions governing the system must be known clearly and the nature of the signal must be decided prior to the projection of signal processing algorithms. The objectives of the thesis are to diagnose and extract the signals emanating from the bearing using various signal processing methods. The flow of the investigation and analyses are as follows:

1. Preliminary investigation of technological know-how related to BCM.
2. Selection of sensors and DAQ card based on the past and the current trend to acquire signals (accelerometer and microphone).
3. Implementation of various signal processing and statistical methods like kurtosis, crest factor, energy, probability density functions, EMD, VMD etc.

4. Proposed algorithms by fusion of different statistical and signal processing techniques and validation on bearing data sets provided by Case Western Reserve University (CWRU) [1].
5. Proposed fusion of advanced non-linear signal processing techniques and correlation analysis methods to anticipate the characteristics of vibroacoustic signals at variable speeds.

1.4 Thesis Outline

The research work carried out in this thesis is organized as follows:

CHAPTER 1 elaborates different aspects of bearing conditions monitoring, challenges, and objectives, defining the sensing and signal processing methods to analyze the health of the bearings. It also outlines the methods and analyses adopted in the subsequent chapters to diagnose fault related to bearings.

CHAPTER 2 outlines the various aspects of BCM and the types of faults related to bearings. It covers the need analysis of the current research based on the global market survey conducted on CM. Apart from the market survey, the various aspects of different sensors like vibration, temperature, pressure, Acoustic emission, Ultrasonic sensors, oil quality, Eddy current, thermal imaging, and MCSA etc. are discussed with their advantages and limitations. Similarly, different aspects of signal processing methods, particularly time domains, frequency domain; time-frequency domains are reviewed with their advantages and disadvantages. Along with the signal processing methods, specifically, the different forms of kurtosis are reviewed in fault detection. Similarly, various non-linear and non-stationary signal-processing techniques like wavelet, local mean decomposition, Wigner-Ville distribution, empirical mode decomposition and variational mode decompositions are investigated with their contributions in the field of fault diagnosis.

CHAPTER 3 proposes an adaptive EMD-PCA based average kurtosis technique to detect lower dimension defects in the bearings. Initially, the Hilbert transform is applied to periodic (PS), quasi-periodic (QP), transient (TS), frequency modulated (FM), amplitude modulated (AM), amplitude-frequency (AM-FM) modulated signals to observe the change in their spectrums. The proposed analysis is divided into two parts (a) effect of standardization and sample length on fault identification, (b) signal decomposition, mode de-correlation and

modified signal generation. The proposed algorithm is validated on Case Western Reserve University (CWRU) data sets.

CHAPTER 4 proposes unitary sample shifted rectangular and Laplacian distribution functions to detect faults. This chapter is divided into two sections; in the first section, Kolmogorov and Smirnov test is used to identify the associated probability density function (pdf) of CWRU data sets. In the second section, the proposed algorithm is used to generate frame based crest factor (FCF), frame based kurtosis (FKS) and frame based energy (FE) time series signals. These time series signals for different distribution functions are analyzed to identify incipient faults in the bearings.

CHAPTER 5 addresses the effectiveness of vibration and acoustic sensors in identifying faults related to bearings. In this chapter, accelerometer and microphone sensors are used simultaneously to acquire signals from the experimental setup. In the proposed technique, the effect of variable speeds on the vibration and acoustic signals of IRD are studied concurrently using EMD and VMD. The fault frequencies are identified from the correlation coefficient (CC) and log-variance trend of decomposed modes.

CHAPTER 6 concludes the results obtained from the three different proposed algorithms. This chapter also gives an insight into the future scope and direction for further studies related to BCM.

CHAPTER 2
Literature Survey

Bearing condition monitoring (BCM) plays a vital role in various industries like aerospace, pharmaceutics, automobile, marine, power plants, petrochemicals etc. The applications are unlimited in the incipient fault diagnosis of bearings to avoid malfunction and hazards. The objectives of BCM are to optimize various parameters i.e. fast and accurate measurement with minimization in the cost of sensing; reliable monitoring of the system with minimal maintenance cost, increasing the life of the equipment, and avoiding breakdown in the long run etc. The optimization can be addressed using the advanced sensors and signal processing techniques. However, the selection of sensor for a system under test (SUT) is the real challenge for the condition monitoring engineer, as a broad range in sensing technologies like vibration sensors, temperature sensors, pressure sensors, AE sensor, Ultrasonic sensors, oil quality sensors, Eddy current sensing, thermal imaging etc are available to diagnose health. Similarly, the field of signal processing techniques is rich with algorithms; however, the implementation and implication of algorithms truly depend on the system to be monitored. Signal processing is the mathematical tool that performs addition, multiplication, shifting, scaling convolution, integration, and differentiation etc. to extract buried information content from the signal. Thereby, actual information content of the initially evolved signal in its true form can be realized affluently. Since, the law of nature is not always reversible; however, it can be, if the statistical properties acting on the system are made symmetrical. The influence of nature on the signals and the clarity in the de-segmentation can put the real facet in front of the analyst.

If you want to find the secrets of the universe, think in terms of energy, frequency, and vibration.

– ***Nikola Tesla.***

2.1 Introduction

All matter in the universe transfers information in the form of waves, either using light or sound waves. This act is possible due to the vibration or oscillations of particles. Generally, light and sound are the soul of all the living and assumed non-living matters, and transfer

information in the form of vibrations. Nature, the master of the universe controls its plays through vibration [2]. Bringing the non-living equipments closer to the human society adds up living values. These values call for a regular observation and can be addressed as condition monitoring (CM). The CM is very complex and needs expert knowledge to intercept the language the machinery conveys. Therefore, it needs researchers from diversified fields to profoundly understand the problems and provide the best solution accordingly. It is the process to anticipate the state of the machinery through their languages expressed in form of vibration, acoustic, and temperature etc. Nowadays, the field of CM has tremendous impact on modern society as machines are required to operate 24×7 without breakdown or failure. It has stretched its boundaries to various industries such as petrochemical, pharmaceutics, mining industries, marine, power plant industries etc. Due to rapid growth in the world economy and the increased dependency on machinery, the market share for CM is expected to rise in future. Based on surveys, the CM market can be divided into monitoring by types, applications, geographical region and the process as shown in Fig. 2.1. The projected market share for CM is expected to reach 2.45 Billion USD by 2020 [3]. CM is divided into three stages, firstly, the identification of the system under test (SUT) and its surrounding; secondly, the selection of sensors and their feasibility to adapt and acquire the signals; finally, the signal processing techniques to extract the information [4,5]. The factors like SUT, sensors and signal processing that are associated with CM are shown in Fig. 2.2.

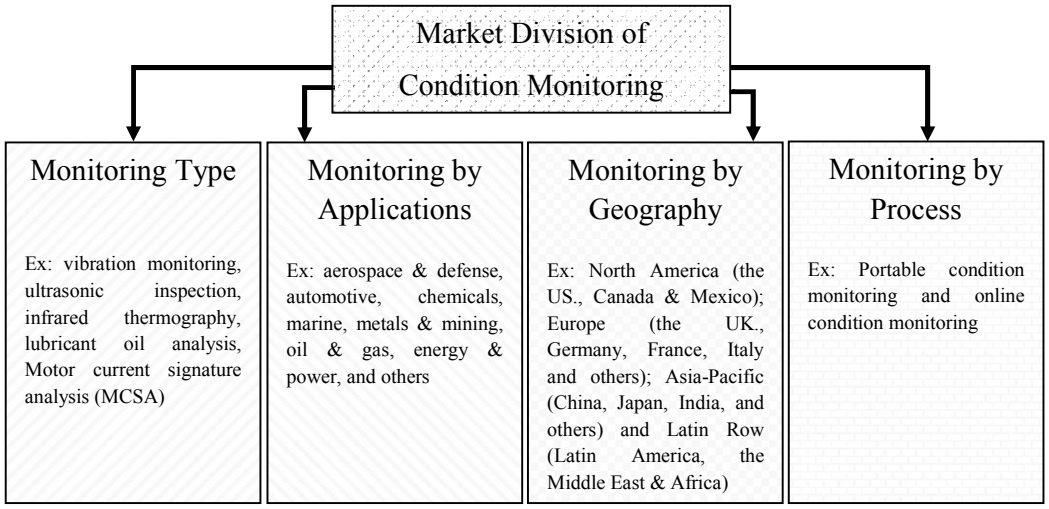

Figure 2.1 Market survey on machine condition monitoring

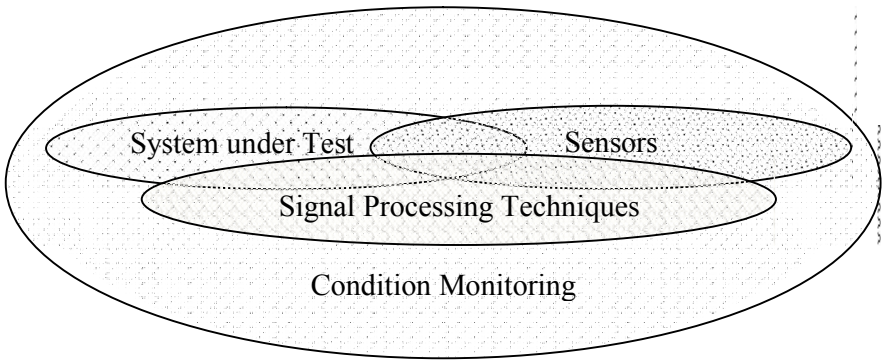

Figure 2.2 Factors associated with condition monitoring

2.2 System under Test

The initial task of CM is to understand about the system under test (SUT). Various SUT are bearings, machine tool, compressor, engine, turbine, gearbox, centrifugal fans, planetary gears etc. [6]. However, the thesis concentrates more on defect frequency analysis of deep groove ball bearings (DGBB) of induction motor and independent bearings. It was observed in the past that most of the failures in the induction motors are due to broken rotor bar, rotor mass imbalances, the stator winding fault, crawling, overload, over or under voltage and bearing faults etc. [7]. However, 51% of failures in the machinery are due to bearings [8], and is shown in Fig. 2.3. Based on the applications, the bearings can be classified into journal bearing (axial load), guide bearings (back and forth motions) and thrust bearings (axial loads) [9]. Basically, the bearings are manufactured using ceramic, chrome steel, stainless steel, and plastics etc. The requirements are subjected to the applications and field of studies; the areas of studies are shown in Fig. 2.4.

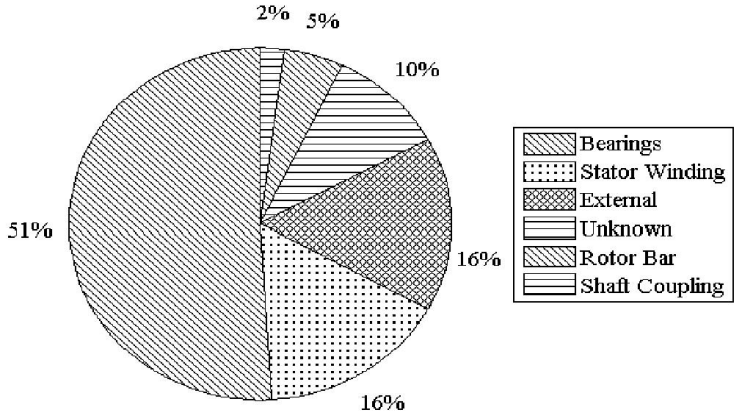

Figure 2.3 Causes of motor failure

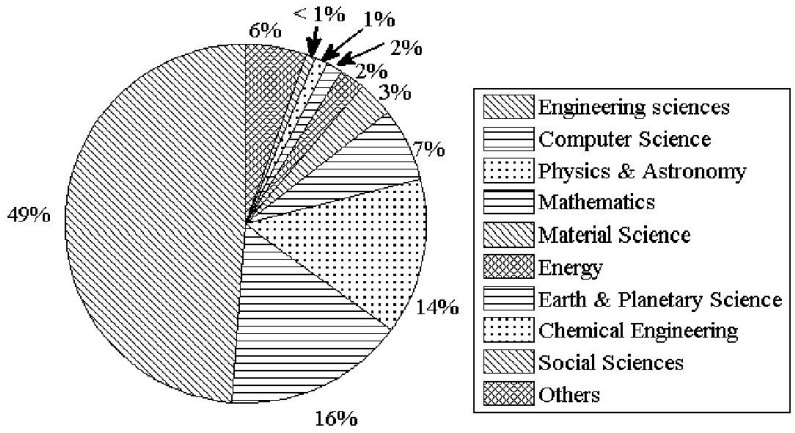

Figure 2.4 Application of condition monitoring in different disciplines (Scopus index database)

Based on the level of interception of faults, CM of bearings can be segregated mainly into detection, diagnosis, and prognosis [10]. The method of detection deals with identifying the fault, whereas the diagnosis goes deeper in analyzing the cause, as well as, the nature of the fault. The prognosis is based on the method of calculating the remaining life before failure or remaining useful life. However, the research work is projected more on diagnosis rather than prognosis, even though both are closely related. Similarly, based on severity of the failure the bearing failure can be divided into four stages i.e. stage-1, stage-2, stage-3 and stage-4 [11]. Generally, the stage-1 indicates an initial failure symptom and generates shock pulses in the ultrasonic frequency bands. The signals generated by this stage can be detected using AE and ultrasonic sensors. The prime reason for the generation of fault at this level is caused by the lack of lubrication. The stage-2 fault occurs due to minor defects of bearing that leads to excitation of mounted resonance, and found to be in the frequency band between 2000-8000 Hz. However, the actual bearing defect frequencies along with the sidebands appear at the end of second stage. In the third stage, the bearing defect frequencies like inner race, outer race and ball defects are more prominent and can easily be traced using vibration sensors. At this stage defects can be visualized clearly or partially using naked eye. Generally, the bearings are subjected to replacement at this stage in order to avoid malfunction in the machineries or in equipments. Finally, the stage four is considered as the last stage of bearing life and produces more noisy signals rather than resonance in the spectrum. The observed frequency spectrum is dominant in the lower frequency band and

the operator should avoid running the equipment at this stage [12]. Some of the recent failures occurred due to malfunctions in bearings are shown in the Fig 2.5.

(a) (b)

Figure 2.5 (a) Turbines on fire, Palladam, Tamil Nadu, India (2016) (b) Freight train collapse in Taiwan (2013) (Courtesy: Google)

It is observed from the literature that bearings are the most vital part that may need continuous monitoring to avoid fatalities. Therefore, the details about the physical specification and its operating condition need to be analyzed prior to intercepting the faults. The basic physical specification of the bearing consists of inner race, outer race, ball, and cage as shown in Fig. 2.6 [13]. From the physical dimensions and the operating speed, the different fault frequencies of the bearing for the fixed outer race can be calculated using the following equations [14].

$$f_{or} = f_s \frac{N_b}{2}\left(1 - \frac{B_d}{P_d} cos\phi\right) \tag{2.1}$$

$$f_{ir} = f_s \frac{N_b}{2}\left(1 + \frac{B_d}{P_d} cos\phi\right) \tag{2.2}$$

$$f_{bs} = f_s \frac{P_d}{2B_d}\left(1 - \frac{B_d^2}{P_d^2} cos^2\phi\right) \tag{2.3}$$

$$f_{ftf} = \frac{f_s}{2}\left(1 - \frac{B_d}{P_d} cos\phi\right) \tag{2.4}$$

Where, f_s is the spin frequency of shaft, N_b is the number of balls in the bearing, B_d is the ball diameter, P_d is the pitch diameter and ϕ is the contact angle, and f_{or}, f_{ir}, f_{bs}, f_{ftf} are the outer, inner, ball spin and train frequencies of the bearing respectively.

Generally, for proper condition monitoring of the bearings, the shaft speed, inner race, outer race and ball defect frequencies are commonly used. However, the frequencies calculated using these equations at various shaft speeds may alter in the practical case due to skidding in the bearings [15]. In practical applications, inner or outer race can be stationary; however, for most of the applications, outer race is fixed when the inner is rotating. As the inner race is directly coupled to the transmission shaft, the effect of bubbling on the shaft may directly affect its actual characteristics. The signals from the inner race have to pass through the balls, outer race and the housing before they are acquired by the sensors. Therefore, the complexities in the transmission medium generate non-linear and non-stationary signals [16]. The most predominant and stationary signals are produced by the outer race faults, and it is easy to detect these compared to inner and ball defects. The most perplexed signal is produced by the ball defect and observed to be buried inside the noise. Many times during manufacturing and testing process of the bearings, the ball defects are unnoticed by the sensors due to its random rotating dynamics [17,18].

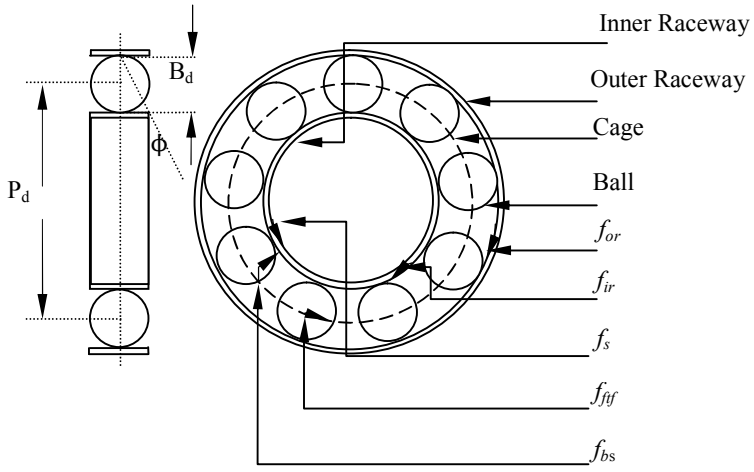

Figure 2.6 Bearing physical specification

After successful evaluation of the defects, the cause of defect needs to be addressed properly i.e. whether it is due to manufacturing or mishandling during operation. The most common defects are caused due to improper handling, contamination of foreign materials,

insufficient lubrication, misalignment, false Brinel and high temperature etc. [19]. As the controllability on working condition is too difficult to achieve, therefore, to prevent damage and malfunction, the SUT needs to be diagnosed continuously.

2.3 Selections of Sensors

Selection of sensor/sensors for a particular system is the real challenge faced by the engineers. Some of these systems operate under high temperature and pressure. The specific sensors need to be identified based on the system to be monitored and the feasibility of mounting. If the system to be monitored is located at a remote location, then non-contact sensors can be used to monitor the system. Further, the selection of sensors also depends on the frequency and intensity characteristic to be observed and the working environment. Once the system under test is identified, the desired sensor for the particular type of the applications can be segregated. The selection of sensors plays a vital role in anticipating the actual information transferred by the physical condition monitoring system under test. The CM systems can be categorized based on their maximum likely hood for a particular data type i.e. temperature, sound, vibration etc. The data will decide the selection of a particular sensor or a combination of sensors. The data is nothing but the parameter most influenced by the SUT i.e. the form of energy indicating the fault characteristics. These energies can exist in any one of the forms such as acoustic, vibrations and temperature. The different sensors used for CM are vibration sensors, temperature sensors, pressure sensors, AE sensor, Ultrasonic sensors, oil quality sensors, Eddy current sensing, thermal imaging, and perception based analysis etc. [20]. In general, thermal imaging is preferred when the SUT operates at high temperature, whereas acoustic sensors are mostly preferred in oil and gas industries to detect leakages. For early and observable frequency detection beyond 20 kHz, Acoustic Emission (AE) sensors are preferred. Similarly, the fault can be diagnosed using other sensors like Eddy current sensors, radiographic inspection systems, and microwave inspection systems etc. [21,22]. The realization of the true anatomy of any system is possible due to the rapid development of the sensor technology and the data acquisition (DAQ) cards. The CM of the bearings can be accessed using these types of sensors and the usability depends on the sensitivity of the sensors as well as the faults stages as shown in Fig. 2.7 [23].

The signal acquisition from the SUT can be broadly classified based on the parameters to be monitored i.e. electrical or mechanical. The observed mechanical parameters are sound, temperature and vibration; whereas the direct electrical fluctuations are considered as a part of electrical parameter analysis technique. The classification of different sensing methods based on their physical significance is shown in the Fig. 2.8 and discussed in the following sections [20,24].

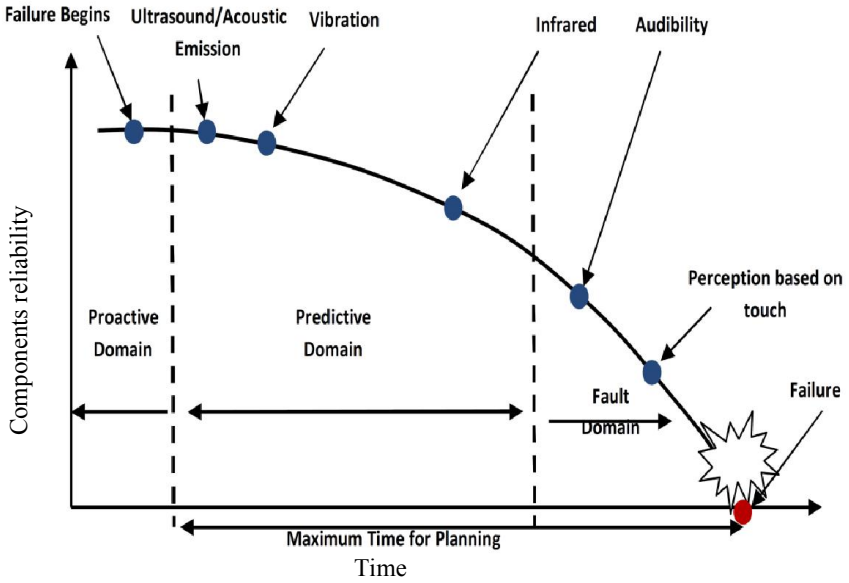

Figure 2.7 Components reliability graph over time

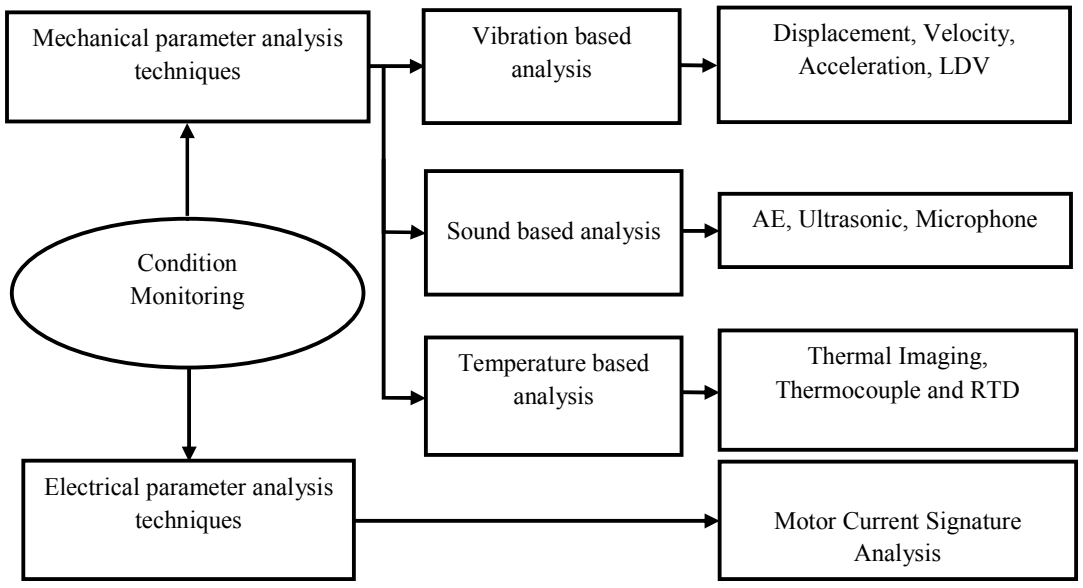

Figure 2.8 Condition monitoring and respective sensors

2.4 CM using Mechanical Parameter Analysis Techniques

The mechanical parameter analysis techniques can be divided based on the signals and their form and are discussed as follows;

2.4.1 Vibration Based Analysis

The vibration signals can be measured from acceleration, velocity and displacement depending on the conversion carried out by the sensors [25]. Various sensors related to vibration are discussed in detailed and as follows;

a) Measurement using Displacement Sensor

Motion sensing using vibration can be divided into three types' acceleration, velocity, and displacement. The selection of vibration sensors depends on detailed knowledge about the system to be monitored [26]. Generally, the motion sensing using displacement sensors are used only when the frequency to be monitored is of lower value. Displacement sensors are used to measure the shaft vibration, speed and rotor positions. These types of sensors can be placed in orthogonal positions to measure the degree of imbalance in the shaft and can be observed using the polar plots. The displacement measurements using Eddy current probes are used to check the shaft vibration from its relative motion w.r.t. sensor probe, and are used to measure low-frequency vibrations (0-10 Hz). In this paper [27], Peton *et al*. have used ADRE 408 DSPi (Dynamic Signal Processing Instrument) along with the Bently Nevada's 3500 Series vibration monitor system to control shaft vibration of air cooled generator.

b) Measurement using Velocity Sensor

The velocity sensor was the first to be used in condition monitoring as it remains constant regardless of frequency and also it is easier to install as compared to displacement sensor. However, at low frequency below 10 Hz and high frequency above 1 kHz the effective sensitivity of the sensor decreases as shown in Fig. 2.9 [28]. However, it can be used in the mid frequency range of the vibration (10-1000 Hz) for effective signal acquisition. Therefore, the analyst must prepare a list of questionnaires on what exactly is to be monitored and their frequency band of operations before subjecting these sensors in the

actual field [29]. Generally, piezoelectric (PE) or integrated circuit piezoelectric (ICP) sensors are mostly used in vibration measurements to avoid unwanted external current excitation circuit [30]. Even the velocity can be measured using the accelerometer sensor, however the effect of boundary condition due to integration [31,32,33] change the actual frequency characteristics. Therefore, the irregularities occurring in phase and amplitude due to transformations have significant impact on signal recovery related to vibration and are detailed in [34].

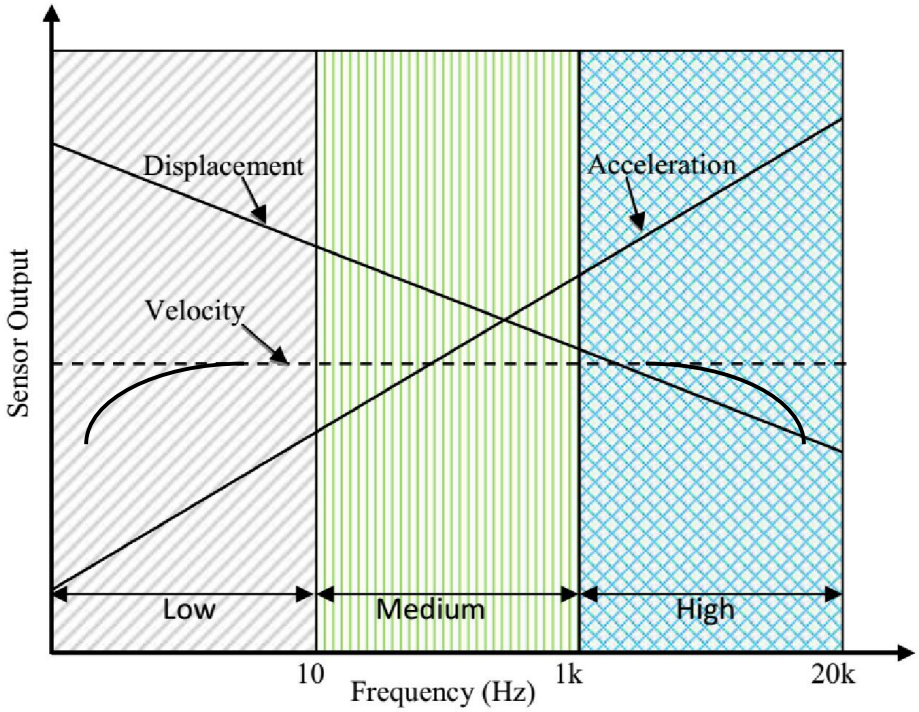

Figure 2.9 Frequency response of accelerometer, velocity and displacement sensors

c) Measurement using Accelerometer Sensor

The advancement and the complexities associated with the CM have created tremendous dependency on sensing methods as well as on the advanced signal processing and analysis techniques. Based on the demand and applications of CM systems, two different types of accelerometer sensors can be used i.e. static and dynamic. Piezoelectric based accelerometers are suitable to measure dynamic acceleration rather than static acceleration (MEMS capacitive accelerometer can measure both static and dynamic accelerations), but these are rugged in nature and the frequency can range between DC to approximately 20 kHz

[35,36]. Generally, the vibration measurement using accelerometer has better sensitivity & signal to noise ratio (SNR) as compared to vibration measurement using velocity sensor. But, as far as the optimization of sensitivity and the 'g' are concerned, it fails to satisfy both due to its design as well as technical issues [37,38]. However, the vibration of SUT must be known before the selection of these sensors based on the ‘g’ and sensitivity. Similarly, prior precaution must be taken before mounting the accelerometer, as the frequency responses may change with the change in the mounting techniques [39,40].

d) Measurement using Laser Vibrometer

Vibration due to fault can be measured using single and multi-point vibrometer [41,42]. Generally, laser vibrometer operates at a modulating frequency of 40 MHz and can be used to detect faults in the bearings. In [43], Polytec laser vibrometer PSV-400 is used to detect faults and the presence of significant harmonics, however, the performance degrades in detecting the low-intensity amplitudes present in the inner race. In [44], the authors have compared the effectiveness of laser vibrometer (displacement and velocity) and accelerometer sensor for detecting bearing faults. It is observed that the laser vibrometer response in terms of velocity is better than that of accelerometer sensor. The main advantages of laser vibrometer are non-contact, wide frequency band of operations, measurable distance up to several meters and good mobility etc. Similarly, the disadvantages of laser vibrometer are due to the interaction of speckle noise in vibration due to unsmooth housing surface, vibration measurement of only stationary objects; issue of line of sight (LOS) [45]; and it only detects the low amplitude and high-frequency vibration [46].

2.4.2 Sound-Based Analysis

Sound is the most powerful phenomena that can be used to detect irregularities in wave patterns generated due to anomalies in the bearings. It can be measured using AE, Ultrasonic sensors, and microphone etc., and each of these sensors has certain advantages and disadvantages in BCM.

a) Measurement using Change in Audible Sound

Change in audible sound pattern recognition is an age old classical method used in machinery to detect faults. In this approach perception based acoustic analysis is used to

infer the sound coming from the screwdriver placed on the housing. Whittaker *et al.* [47] have discussed different classical methods as well as the modern acoustic sensing in detail that can be used to detect faults in the mechanical systems. The main advantage of this method is that it need not require sophisticated technology rather an expert who can segregate the fault based on perceived sound. But, the perception based analysis fails to detect the early fault and lack in discriminating the fault types.

b) Measurement using AE Sensor

Research in the field of AE has been the topic of study for the past four decades. Generally, the AE sensors are used to detect the stress wave radiated by the materials due to crack or plastic deformations. These sensors are responsive in the frequency band between 1 kHz to 10 MHz and are available in many variants (1045S-200 kHz-1300 kHz, 2045S- 300 kHz-2200 kHz, 5045S-500 kHz-4000 kHz) [48]. Many researchers have compared AE with vibration sensors and observed its performance to be better than vibration in early fault detection [49,50,51]. In spite of its certain advantages, it fails to analyze the fault quantitatively rather than qualitatively, and is prone to surrounding noises due to their low SNR (difficult to discriminate between actual signal and noisy signal). In [52], the authors have compared four different AE sensors from Physical Acoustics (PAC) i.e. PAC R15, PAC NANO30, Digital Wave B1025, and the Glaser-type conical sensor to analyze their effectiveness in signal acquisition based on their aperture. Similar study was also carried out by Yongzhi Qu *et al.* [53] to differentiate between AE and vibration sensors. It is observed that even though the AE sensors need higher sampling rate as compared to vibration sensors; they are free from mechanical resonance.

c) Measurement using Ultrasonic Emission

Ultrasonic sensors generate self-excited high-frequency acoustic signals between 20 kHz to 100 kHz to detect faults in mechanical systems. They differ from AE in terms of the detection techniques i.e. AE detects stress wave generated by the system to be monitored and ultrasonic generates self-excited signals to detect faults. The AE and ultrasonic also differ by their frequency band of operation. The ultrasonic sensors have certain advantages like good SNR, analyze the fault quantitatively and need a minimum target surface area to detect fault [54,55]. However, the ultrasonic sensors are limited by the sensing distance and are prone to

the change in the environmental conditions. In [56], the authors have compared the ultrasonic sensor with the vibration sensor for bearing fault diagnosis for low speed bearings and observed that ultrasonic sensors are better than vibration sensors at low speed. Similarly, in [57], Sawalhi *et al.* have tested various types of ultrasonic sensors and their significance in fault diagnosis. In this paper, the authors have used the Ultra Track 750 sensor to detect the fault in the bearing for different fault dimensions and at various speeds. It is observed that even though the AE and vibration sensors can be used to detect faults, however, the ultrasonic sensor takes the advantage in terms of its non-invasive mounting technique [58].

d) Measurement using Microphone

The microphone can be used to diagnose the fault in the bearing and closely resembles the classical hearing based analysis, but it is more precise in detecting faults. In [59], the authors have used the accelerometer, AE and microphone (BAST YG 20107067) to identify the fault in the journal bearings. It is observed that the performance of acoustic sensor is found to be better between 1.5 kHz to 10 kHz. Similarly, the authors in [60] have investigated the bearing vibrations of the rail using multiple microphones. It is observed that the particular microphones are sensitive above 2 kHz. In recent years, researchers are focusing more on acoustics to detect fault in the bearing along with the vibration sensors, even though there is a lot more to be done to it [61].

2.4.3 Temperature Based Analysis

Due to the change in operating conditions, lubrication, intrusion of foreign materials and faults etc., the temperature of the bearing increases. Therefore, the increase in the temperature can be used as an asset to sense the defects and can be detected using thermal imaging and infrared sensors etc.

a) *Measurement using Thermal Imaging*

Thermal imaging uses thermal cameras to sense the change in temperature at various operating states of the machinery and can be used in different fields of CM [62]. The study shows that the infrared radiation exists in the body operating above 0^0 Kelvin. In [63], the authors have used thermal imaging (Gobi- 640-GigE3, an uncooled long-wave infrared (LWIR)) and vibration sensors to detect bearing faults. It is observed that these sensors are independent of the wave propagations, unlike AE and vibration signals which are affected by

the propagating medium. Thermal images have the advantage of detecting the fault even in the absence of light [64]. However, the thermal camera gives erroneous result when the medium is obstructed by glossy or shiny surfaces.

2.5 CM using Electrical Parameter Analysis Techniques

The behavior of the system can be analyzed directly at the motor end, as the driving end characteristics change with change in operating conditions of the coupled devices. The behavior of this type of system can be monitored using current sensor connected to the power supply of the motor and is briefed in the following sub-sections.

a) *Motor Current Signature Analysis*

The faults can be monitored from the change in the current or the voltage characteristics of the driving device. The fluctuations in the motor current can be monitored using a current sensor and the analysis is called as motor current signature analysis (MCSA) [65,66]. The MCSA (A622-Tektronix Hall-effect current probe) experiences the change in the harmonic content of the signal with change in the condition of the system under observation [67].

MCSA is the direct way to measure the change in the current either due to fault in stator, rotor, or in the bearings. The change in the loading or abnormality in the machine may drift the current level. The authors, in [68,69,70], have discussed different aspects of measuring faults using MCSA and its contributions in identifying faults along with other sensing techniques. The main advantage of this method is that it can monitor the system effectively without direct involvement of mounting on to the platform. But, it cannot be used for early fault detection as the change in current is difficult to observe in the spectrum, due to low signal to noise ratio (SNR) [71]. The current sensing and vibration sensing methods are compared by Bellini *et al.* to evaluate the effectiveness of each of these in identifying faults [72].

Finally, it is observed that the fault can be identified by different sensors, but, the traditional vibration based sensing contributes to approximately 87% of the fault detection, due to its reliability and is shown in Fig. 2.10. However, to locate the exact position of the fault and early fault detection, AE sensors are used prevalently. The selections of sensors are now broadening with the development of technologies and the future of BCM is expected to incline towards multiple sensors fusion and processing techniques. To understand different

sensors and their real-time applications, Hodge *et al.* in [73] have corroborated their usability in detail.

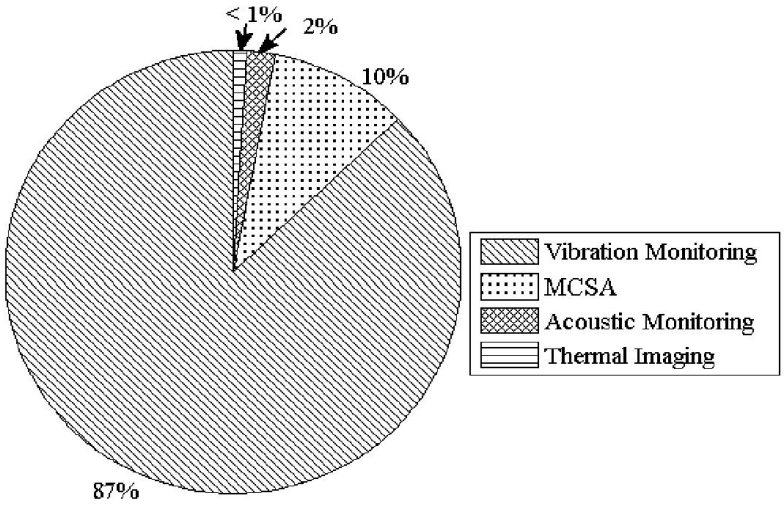

Figure 2.10 Sensing methods in fault detection (Scopus index database)

2.6 Mounting of Sensors

Apart from the selection of sensors, mounting plays a vital role in useful signal acquisitions. Generally, the characteristic of vibration signals changes with the change in the mounting techniques followed during data acquisitions. In general, vibration is caused due to the back and forth moment of the shaft or the structure, and produces signals in the axial and radial (vertical and horizontal) directions. Depending on the type of the bearings and structure, the sensors are mounted accordingly. For example, if misalignment is caused by the axial moment of the structure or the bearings (thrust bearing), then two different displacement sensors can be mounted in orthogonal positions to detect the misalignment from the Lissajous patterns [74]. Similarly, the velocity sensors are used to monitor low to mid band frequency of vibrations and preferably mounted on to the mounting base of the system.

However, the mounting techniques followed for the accelerometer sensors have significant contribution in proper signal acquisitions as compared to the velocity and displacement sensors. It is observed that the frequency and amplitude response of the accelerometer sensor changes with the change in the mounting techniques adopted and is shown in the Fig. 2.11 [75]. It can be mounted in all the three directions (axial, horizontal and vertical) of the measuring system using different mounting techniques as shown in the

Figs. 2.12 & 2.13 [76, 77]. When it comes to analyzing the effects of mounting on faults, the ball and inner race bearing faults are least affected by the vertical or the horizontal mounting, when the outer race is fixed. The effect of various positions of the sensors on the signal characteristics are analyzed by Smith *et al*. in [78]. It is observed that for the same setup, by changing the position of the sensors the signal characteristic changes, therefore, some of the results may be favorable whereas some may not be.

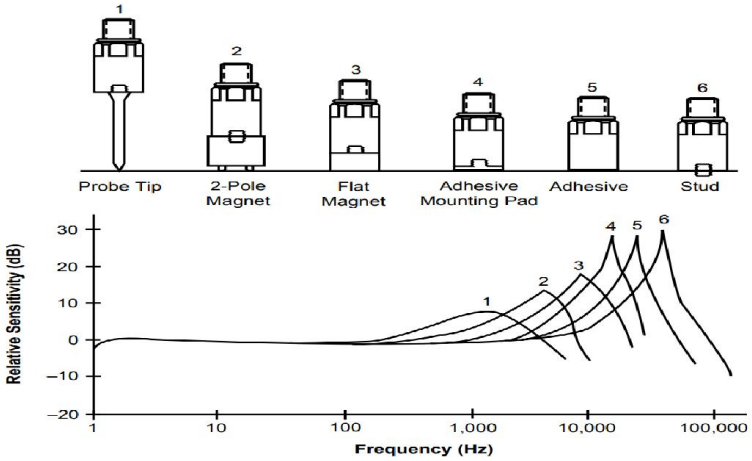

Figure 2.11 Frequency response of accelerometer sensors for various mounting techniques

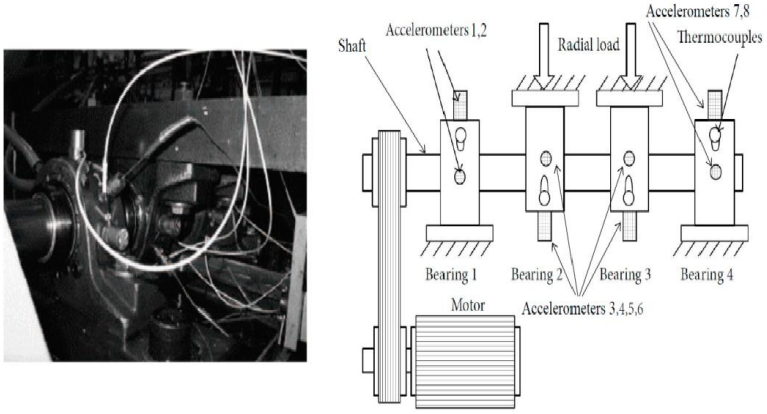

(a) (b)

Figure 2.12 Bearing test rig and sensors placement illustration (a) actual (b) schematic

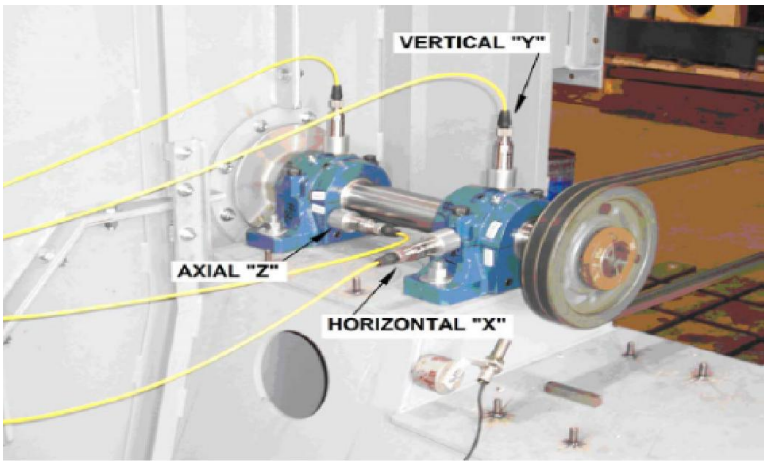

Figure 2.13 Bearing vibration measurement using vertical, horizontal and axially mounted sensors

Generally, AE sensor follows the same mounting techniques as that of the accelerometer sensors, and is free from background noise generated due to variable transmission paths [79]. In [80], Yongyong *et al.* have mounted the sensor in the radial direction of the bearing to analyze the rubbing effect of the shaft with the stationary housing. It is observed that the mounting should be carried out in such a way that low attenuation is achieved at the sensor position, irrespective of the optimal propagation path [81]. Similarly, the precautions related to the mounting techniques are defined by the American Society for Testing and Materials (ASTM) sub-committee E07.04 [82]. However, as compared to AE sensors, microphones and ultrasonic sensors do not make use of the surface mounting techniques, but the proximity of the measuring system and the direction matters a lot. In case of ultrasonic sensors, the proximity and the surroundings affect its performance as it uses the air as the transmission medium; therefore, the mounting position needs to be closer as per technical specification of the sensor. However, it has the advantage of detecting short wave airborne sound signals that are directional and localized [83]. In the case of a microphone, it can be mounted from an external stable holder or platform and can be placed anywhere along the periphery of the housing. But, precautions need to be taken such that direct air pressure from the bearings or shaft should not interact with the microphone [84].

Thermal imaging is not that widely used in BCM due to high cost, but as far as mounting is concerned, it needs to be placed at any suitable position to get a clear picture of thermal effect. However, during mounting, it should be placed in such a way that the reflections from glossy surface do not fall directly on the camera. Apart from these sensing

techniques, current based sensing has an advantage over all other techniques as it is independent of the structural design/position of the SUT. Nowadays, researchers are focusing more on the advanced acoustic and vibration sensors to figure out the correlation between these two phenomena and their usability in anticipating bearings and gear box faults as shown in the Fig. 2.14 [85, 86].

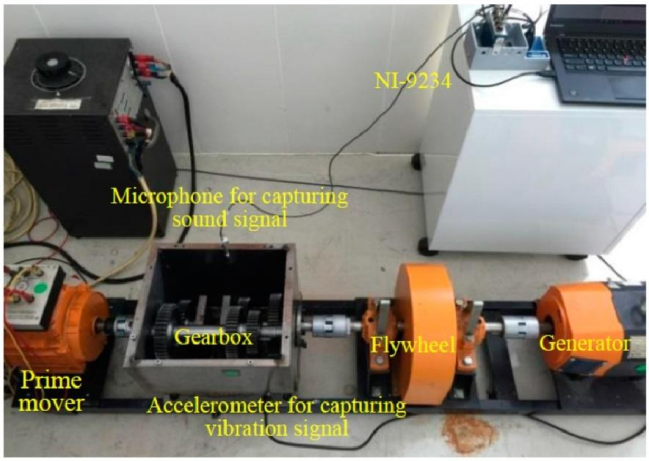

Figure 2.14 Gearbox diagnosis using accelerometer and microphone

The advantages and disadvantages of the different sensors that can be used for BCM are summarized in Table 2.1 [87,88,89,90]. Even though these sensors have certain advantages and disadvantages but, the fusion of different sensors can increase the reliability of the CM systems.

Table 2.1 Advantages and disadvantages of various sensors used in BCM

	Advantages	Disadvantages
Displacement	✓ Simple to install ✓ Good response in middle range of frequencies ✓ Withstand high temperature ✓ Do not require external power ✓ Lowest cost	o Low resonant frequency & phase shift o Cross noise o Big and heavy o Require electronic integration for displacement
Velocity	✓ Measure static and dynamic displacements ✓ Exact response at low frequencies ✓ No wear ✓ Small and low cost	o Electrical and mechanical noise o Bounded by high frequencies o Not calibrated for unknown metal materials o Require external power o Difficult to install

Accelerometer	✓ Good response at high frequencies ✓ Can withstand high Temperature ✓ Small size ✓ Required low sampling rate	o Sensitive to mounting o Require electronic integration for velocity and displacement translation
Laser vibrometer	✓ Non-contact ✓ Wide frequency band of operations ✓ Measurable distance up to several meters and good mobility	o Affected by speckle noise due to unsmooth housing surface o Vibration measurement of only stationary objects o Line of sight (LOS) o Only detects the low amplitude and high-frequency vibration
Audible sound (Perception based analysis)	✓ Does not need sophisticated technology rather an expert ✓ Can be analyzed using simple screwdriver	o It fails to detect early fault o Lack in discriminating different fault types
AE	✓ It is better compared to vibration in early fault identifications ✓ It is free from transmission path noise of the measuring device	o These sensors analyze the fault qualitatively rather than quantitatively o Prone to surrounding noises due low SNR o High cost o High sampling rate required
Ultrasonic	✓ Non invasive (airborne ultra-sound) ✓ Analyze the fault quantitatively	o Affected by medium of propagation of sound o Expert is required to decide whether to go for contact or non-contact depending on the condition of the SUT
Microphones	✓ Non-invasive ✓ Wider spectral measurement band (small diaphragm) ✓ Sensitivity low	o Affected by surrounding noise o Directional to high frequency sound o Costly
Themal Imaging	✓ Instantaneous results ✓ Larger area can be diagnosed	o Inaccurate for close range in the temperature o High cost
MCSA	✓ Need not require direct mounting	o Cannot be used for early fault

	or closest possible positions from the platform ✓ Direct current or voltage fluctuation can intercept the fault	detection o Limited by low signal to noise ratio (SNR) o With accuracy sensor cost increases

2.7 Nature of Signals

Nature is quite perplexing and always ready to reveal its secrets in due course of time. The thirst to understand nature can be achieved by decoding its phenomena. Signals in nature exist in many forms and can be gravitational waves, sound wave, vibrations, rotation of the planetary systems and much more or the whole Universe itself. The contours of information in the signals are true for all the living or non-living bodies in a certain form. The history of signal and its processing dates back to the days when the existing started searching for its existence. Different existing bodies anticipate information in one form or other. Human civilizations have crossed their boundaries to decode the content in signals to leverage their importance. The extraction of signals and their analysis is a typical issue in signal processing. The signal processing techniques purely depend on the natural operations the signal incurred during propagation, and in interactions with other independent components. The intermixing of signals depends on the arrival and directional pattern followed at the sensor position and the alteration carried out by the acquisition devices. The acquisition and processing devices like sensors and analog to digital (ADC) converter alter the nature of the signal. Therefore, to properly realize the signals, higher bit and proper sampling rate of ADCs are required to reconstruct the real world signals in its true form. The prime factors that influence the ADCs are the sampling and the least significant bit (LSB) value [91]. This paper suggests that for proper reconstruction of signal the practical sampling rate should be at least ten times the maximum required frequency. But, as far as the LSB is concerned it should be as low as possible so that the minute fluctuation in the signal intensities can be captured and consequently the round off error due to quantization can be avoided.

Similarly, as far as extractions of signals are concerned, the signal processing methods are rich with algorithms, but implementation and implication of algorithms truly depend on the system to be monitored. Signal processing is a mathematical tool or the combination of different mathematical operators i.e. addition, multiplication, shifting, scaling, convolution,

integration, and differentiation etc. Depending on the signal's interaction with other relative signals and the interacting mediums, it can be classified as; periodic, non-periodic, stationary, non-stationary, linear, non-linear, chaotic and pseudo-random or truly random. These changes in the properties are due to the interacting channels, their behavior and the influence of one signal on another. Based on the mathematical interactions, or more technically the modulations, the signals can be classified as amplitude modulated (AM), frequency modulated (FM) and phase modulated (PM). Generally, non-stationarity is a property associated with FM, whereas, nonlinearity is due to AM. The combined effect of both produces non-linear and non-stationary signals or else, otherwise called as AM-FM. In case of bearing fault analysis the generation of AM, FM or both depend on whether the outer or inner race is stationary, and the type of the faults associated with it. If the inner race has a small defect, then the defect frequency may shift up and down by the shaft rotational frequency at the bearing load zone. The frequency shifting mechanism can produce sidebands in the frequency spectra or the amplitude modulated signals in the time domain. Whereas, there will be no effect of modulation for the outer race as the signal persists at the load zone of the bearing. The deviation in the frequency from the actual fault frequency occurs for non-stationary elements. For ball defects, the defect frequency will be modulated by the fundamental train frequency (FTF) rather than the shaft rotational frequency [92,93,94,95]. Sometimes, the deviation in the frequencies and amplitude may occur due to the problem inside the induction motor bearings [96]. Therefore, the time series modulating signals generated due to different effects can be analyzed in the time domain, frequency domain, and time-frequency domain to infer the condition of SUT. The segmentation of different analysis methods that can be adapted for fault identification of bearings are shown in Fig. 2.15.

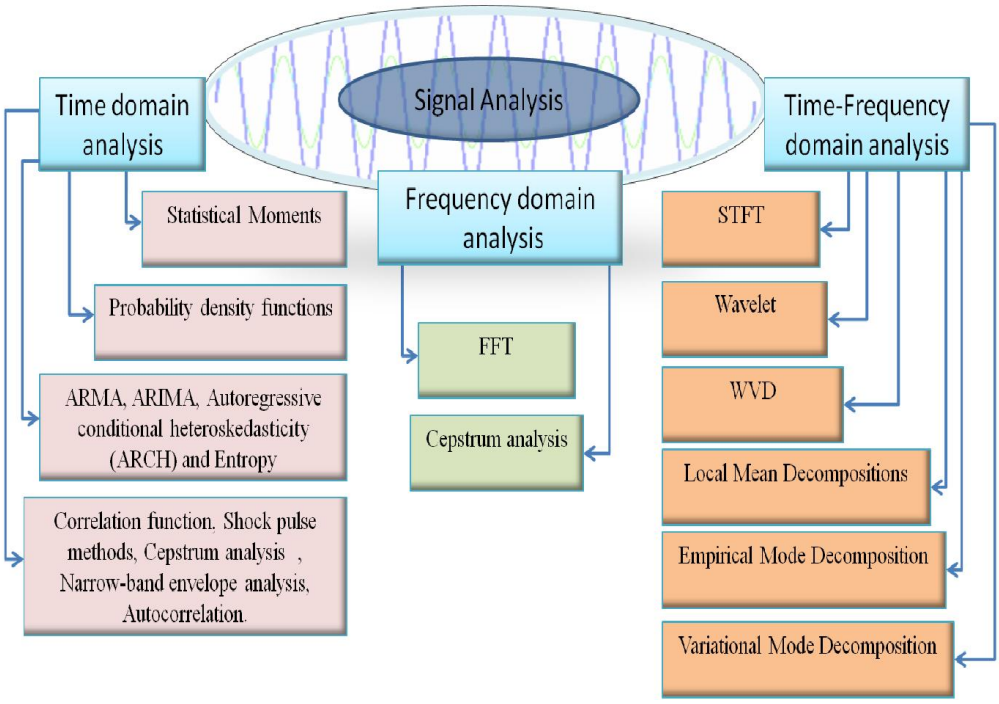

Figure 2.15 Signal analysis methods used for fault detection of bearings

2.8 Time Domain Analysis

The process of analyzing the signal in time has simple as well as complex aspects and it holds all the information related to the SUT. The time series are influenced by outliers and discontinuity due to the intermediate acquisition devices [97,98]. An outlier can be divided into additive outliers (AO), innovative outliers (I0), level shift (LS) outliers or transitory change (TC) outliers [99]. These outliers can change the depth and types of modulation in the time series signals. Time domain analysis is divided into many parts i.e. waveform feature analysis, statistical feature extraction, orbit analysis, and time series modeling [100]. Similarly, different functions that can be used to quantify the information in the signals are mean, median, mode, RMS, variance, standard deviation (SD), peak, crest factor (CF), kurtosis (KS), number of zero crossing (ZCR), skewness, clearance factor and impulse factors, probability density functions, correlation function, shock pulse methods, band pass filtering prior to analysis, power and cross-power spectral density functions, transfer and coherent functions, cepstrum analysis, narrow-band envelope analysis, factor of crest , k factor and defect factor, autocorrelation, ARMA model, ARIMA model (Box-Jenkin), autoregressive conditional heteroskedasticity (ARCH) and entropy etc. [101,102,103,104].

Out of these time domain analysis techniques, mean is the simpler and commonly used method that indicates faults with an increase in its value. Generally, the first order moment, the mean, is affected by shifting, but not the variance. However, with change in distribution functions the skewness changes, thereby, mean gives inaccurate information related to the fault. Similarly, the analysis can be performed using mean, median and mode simultaneously, however, this is true only when the signals are either normal or uniformly distributed. Similarly, RMS and peak value can be used as a fault indicator as reported by Joel *et al.* [105], but these cannot be used to anticipate weak and early faults as reported in [106]. Similarly, variance and standard deviation can be used to indicate the stability and dispersion of the group of data about the mean. Crest factor, one of the fault indicators, can be used to extract information by using the ratio between peak and RMS value. But all these methods do not look into the actual distribution of the signal. As compared to the above discussed methods, kurtosis i.e. the fourth order moment can be used to anticipate an early fault, but it is sensitive to the change in the distributions and the defect dimensions [107, 108]. Similarly, the number of zero crossings can be used as an asset to evaluate the nature of the signal as reported by Osuagwu *et al.* [109]. In this paper, the authors have discussed the underlying concept between resonance and zero crossing rates, and they observed that high-energy resonance generated due to fault can differentiate between healthy and faulty bearings. However, if the defects do not generate resonance, then this method is impractical in real time applications. The impulse factor and clearance factor are similar to the crest factor and kurtosis respectively, and are robust to the change in the operating conditions. Similarly, Shanon entropy used in communications can be applied as a tool to estimate the bearing fault, and is generally used to depict the amount of randomness in the signals [110,111]. However, the entropy fails to solve uncertainty problems associated with the selection of parameters in the bearings. It is observed from the above discussions that the prime factor affecting the signal analysis is the probability density function (pdf). In case of bearings, the pdf changes with the change in the operating conditions and state of the SUT. Even though it can give correct approximation about the nature of the signal, however, it is affected by the sampling rate, sampling length and operating condition of the systems [112]. It is observed that the statistical techniques as well as pdf can be applied suitably to analyze the time domain signals, but the selection of any particular technique may not justify the accuracy of the results. However, many researchers have used the kurtosis as an estimator in

time and frequency domain to evaluate the state of the bearings [113,114]. Based on the survey, the workflow of the thesis is concentrated more towards kurtosis and its impact on fault detection related to bearings.

2.8.1 Kurtosis

Out of all these analysis methods, statistical moments are the classical method to analyze the health of the bearings as in Table 2.2 [115]. In this table x_n is defined as the time domain sampled signal, $\bar{x}$ is the mean and N is the number of discrete samples. To apprehend the characteristic of the signals, higher order moments like kurtosis are used predominantly as fault predictor without training. Analysis using kurtosis can directly indicate the fault in the bearing with least computational complexity and can be used as an indicator in visualizing the spectrum. But, as the signal complexity and distribution changes, only the basic moments may not provide the correct answer to the many problems. Therefore, the capabilities of the moments along with other non-linear and non-stationary synthesis techniques, either in time or frequency domain, can be used for fault diagnosis. For the past three decades, researchers have used kurtosis extensively in the field of condition monitoring to detect faults, in spite of its sensitivity to the sampling rate and sample size. Thereby the thesis focuses more on kurtosis as a fault estimator.

In general, evaluation of kurtosis on the global time scale does not consider the effect of intrinsic modulation and the distribution functions associated with the signals. In [116], the faults in the bearings are analyzed using SK (spectral kurtosis) and maximum correlated kurtosis deconvolution method. In [117], the faults in the bearings are identified using SK and K-nearest neighboring distance method. The precision in the signal analysis is achieved by exploiting the signal in the frequency domain and thereby calculating the kurtosis and other statistical parameters to evaluate the fault [118,119]. The kurtosis in the frequency domain using short-time Fourier transform (STFT) has been used by many researchers in the past to identify faults in the bearings [120,121]. However, the spectrum separation using STFT technique fails to analyze multi-resolution signals, therefore for better segregation of the signals wavelet transforms are used extensively [122, 123]. In [124], extended Shannon function is used to determine the wavelet coefficient and autocorrelation power spectrum, to identify the bearing characteristic fault. Similarly, wavelet energy spectrum along with

envelope detection method is used to identify faults in the bearings [125,126]. Also the non-parametric adaptive analysis method like empirical mode decomposition (EMD) is used prevalently along with kurtosis to detect the faults in the bearings [127]. In [128], the authors have used the spectral kurtosis and the support vector machine (SVM) to detect wheel bearing fault in railways. In [129], the authors have used SVM, along with Hilbert-Huang Transform (HHT) to identify faults in bearings. Even though, these methods classify the faults for diagnosis and prognosis processes, they need prior knowledge of the degrading rate of signals. The spectral kurtosis (SK) needs demodulation using envelope to separate out the harmonics from the actual fault frequencies even after the use of wavelet, HHT, and EMD [130,131,132]. For practicality of the bearing fault analysis, in [133], the authors have investigated various methods to diagnose fault using Case Western Reserve University bearing data sets. Similarly, the faults in the bearings are also identified using adaptive variational mode decomposition (VMD) method to avoid mode mixing problem in EMD [134,135].

Table 2.2 Statistical parameter estimations

Parameters	Equations	Parameters	Equations
Mean	$\frac{1}{N}\sum_{n=1}^{N} x_n$	Shape factor	$\frac{\text{RMS}}{\frac{1}{N}\sum_{n=1}^{N}\lvert x_n\rvert}$
Root Mean Square (RMS)	$\sqrt{\frac{1}{N}\sum_{n=1}^{N} x_n^2}$	Entropy	$\sum_{n=1}^{N} p_n . log_2 p_n$
Peak Value (P_v)	$\frac{1}{2}[x_{max} - x_{min}]$	Skewness	$\frac{\frac{1}{N}\sum_{n=1}^{N}(x_n - \bar{x})^3}{\sigma^3}$
Variance (σ^2)	$\frac{\sum_{n=1}^{N}(x_n - \bar{x})^2}{N}$	Impulse factor (IF)	$\frac{P_v}{\frac{1}{N}\sum_{n=1}^{N}\lvert x_n\rvert}$
Standard deviation (σ)	$\sqrt{\frac{\sum_{n=1}^{N}(x_n - \bar{x})^2}{N}}$	5th normalized moment	$\frac{\frac{1}{N}\sum_{n=1}^{N}(x_n - \bar{x})^5}{\sigma^5}$
Crest factor (CF)	P_v/RMS	6th normalized moments	$\frac{\frac{1}{N}\sum_{n=1}^{N}(x_n - \bar{x})^6}{\sigma^6}$
Kurtosis (KS)	$\frac{\frac{1}{N}\sum_{n=1}^{N}(x_n - \bar{x})^4}{\sigma^4}$	Clearance factor (CF)	$\frac{P_v}{\left(\frac{1}{N}\sum_{n=1}^{N}\lvert x_n\rvert\right)^2}$

Recently, some of the algorithms like symbolic dynamic filtering (SDF) and intrinsic characteristic-scale decomposition (ICD) have been compared along with the traditional signal processing techniques like Fourier transform, Hilbert envelope spectrum, original local mean decomposition and spectral kurtosis techniques in the real time bearings fault diagnosis [136].

2.9 Frequency Domain Analysis

The most efficient and powerful frequency synthesis and analysis technique, to date, is FFT [137]. The complexity in the determination of the wavelength or the maxima-minima perplexes the signal analysis in the time domain. To extensively understand the different frequency components in the signals without focusing much on the time of arrival, Fast Fourier transform (FFT) can be used. FFT distinctively represents a signal along the frequency band and is still the most powerful technique used prevalently in bearing fault diagnosis [138]. However, factors like degradation, misalignment and unbalancing etc. decreases the SNR, thereby sidebands are generated around a significant peak. Therefore, non-coherent envelope detection method is used to separate out the sidebands generated due to modulations. As the carrier or modulated frequency is unknown to the analyst in the time domain, therefore, for more complex signals, the non-coherent demodulation techniques are used to demodulate the signals [139]. Various non-coherent amplitude demodulation schemes are AM demodulation using low pass filter, Hilbert Transform and square law demodulation etc.

All these demodulation techniques can anticipate the actual information only when the resonating frequencies or the modulating carriers are significant. These methods may not work for the suppressed carrier signals, as demodulation may shift the signal to lower frequency band. Therefore, these demodulation algorithms are effective only when the modulated signal and its side bands are significant. However, if the side bands are corrupted by noise, then these methods may produce erroneous results. For such conditions, cepstrum analysis followed by FFT can be used to decode the signal from the carriers.

2.10 Time-Frequency Domain Analysis

Ideally, the signals are independent vector components at appropriately chosen tapping point of the sensors. The cumulative effect of vector multiplications or additions, or the

mathematical operations the signals incur during transmission may modify the actual signal characteristics. The physical condition of transmission media at a particular time instant creates phase, frequency, and amplitude alteration to the basic generated signals. The alteration in the signal characteristics can be predicted using various signal processing approaches that use inverse mathematical operators to anticipate the actual information contents in the signals. The different time-frequency analysis techniques used to extrapolate the information are Short-Time Fourier Transform (STFT), Wavelet Transform [140,141,142], Wigner-Ville distribution (WVD) [143], local mean decomposition (LMD) [144] and Hilbert-Huang Transform (HHT) [145,146,147] etc. respectively. These analysis techniques work by mathematical manipulation carried out on the sample length and the distribution functions, and indirectly use FFT to reconstruct the signal in the local scale rather than in the global scale. As the signal at different tapping points suffers from time delay, it creates frequency modulation, and it can be segregated using STFT. However, it depends on the selection of window based signal energy level and cannot be used for multi-resolution analysis. For multiresolution analysis, wavelet transforms are used predominantly. However, the determination of wavelet coefficients needs prior information related to the signal before extracting the energy efficiently. Similarly, WVD has better time-frequency resolution as compared to wavelet, however, it is affected by cross term due to bilinear characteristic for multi-component signals. To better analyze frequency and amplitude modulated signals simultaneously, EMD can be used over wavelet and WVD [148]. In the literature, EMD has been used by various researchers in spite of its issues related to noise and sampling rate [149]. Similarly, LMD, the alternate of EMD, has been used intrinsically to decompose a signal into modes, and it is reported to perform better in some of the cases [150]. This algorithm uses moving average instead of using cubic spline interpolation to decompose signals into series of AM-FM signals. However, EMD has gained its popularities among researchers working on condition monitoring and many modifications have been reported since its development [151]. Recently, Dragomiretskiy *et al.* have proposed variational mode decomposition (VMD) to analyze amplitude and frequency modulated signals (AM-FM) and further, they have compared their algorithm with EMD for different synthetic as well as practical signals [152]. However, it is not fully adaptive, as the decomposition mode and constrains bandwidth must be decided by the user to check the actual energy of the signal for different center frequencies. For our study, we have used basic

EMD as it is fully adaptive compared to VMD, and the contribution of each of these algorithms in CM of bearings are shown in Fig. 2.16 (studies are based on Scopus list searched on 21-08-2016). Further, to enhance the signal extraction process, fusion of different signal processing methods can be used to classify the signals [153]. Therefore, statistical optimization techniques like principal component analysis (PCA), support vector machine (SVM), independent component analysis (ICA) need to be followed by non-linear and non-stationary signal processing methods [154,155,156]. There are many such techniques that can be used to anticipate fault in the bearings and these processing techniques are unlimited. However, before signal analysis, a very broad understanding is required about the algorithms and their significance in the analysis of time varying faults.

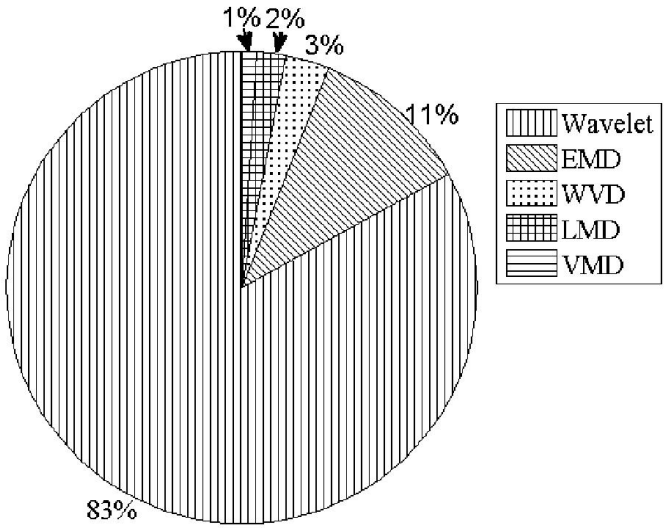

Figure 2.16 Contribution of signal processing algorithms in fault detection

2.11 Conclusion

The literature survey shows that the uses of different sensors in the field of condition monitoring have significant contributions and their application depends on the field of study. From the survey, it is observed that the vibration sensing is the most reliable and age old method and contributes around 87% towards the bearing fault analysis. However, the comparison of one sensing method with another is too difficult, and it can only be applied to certain sensor families with similar bandwidth and sensitivity. Generally, these types of comparison are done based on familiar sensors and their usability in sensing the faults without much focus on their sensitivity and the frequency response. As vibration sensors have a wide variety with different sensitivity, bandwidth of operation and the *g* value,

therefore, comparing even one sensor family with another can change the perception of signal detection and analysis. Eventually, the sensor which performs better for one experimental test bench may not perform in the same fashion in another scenario due to radical behavior of the SUT. Similarly, as far signal processing is concerned various time, frequency and time-frequency analysis techniques can be used to diagnose the fault related to bearings. Moreover, there is no unique solution to many problems. However, the simple analysis tool like kurtosis has gained popularity both in time as well as in the spectral domain to evaluate fault related to bearings, in spite of its sensitivity to the data sample length. Apart from time domain, kurtosis has gained popularity in the frequency domain using SK to detect faults, but the demodulation steps remain unaltered and are carried out using non-coherent Hilbert transform techniques. For better segmentation of multi to mono-components, wavelet transform techniques were the favorites among the researchers. More recently, EMD and VMD have gained their popularity over wavelet due to the adaptive property and the mathematical capabilities in analyzing nonlinear and non-stationary signals.

CHAPTER 3
Fault Detection and Analysis-An Experimental Approach

The fault detections related to bearings have gained significant importance in industries with increase in their applications. The detection of their states needs a clear picture of the evolving signals and their associated modulations. In general, the signals emanating from the bearings are amplitude and frequency (AM-FM) modulated and can be separated out into monotonic modes using empirical mode decomposition (EMD) and the non-linearity can be removed using envelope detection method. In this chapter, a divide-combine and conquer rule is adapted based on EMD-PCA based average kurtosis technique to diagnose bearings. Prior to the selection of the intrinsic mode function (IMFs) based on average kurtosis, principal component analysis (PCA) is applied to de-correlate the correlated modes. These de-correlated modes that are above the average kurtosis are assimilated together to form a new signal. This method is applied to different faulty signals i.e. IRD, ORD and BD of the bearings. These selected signals are finally analyzed using spectrum, envelope, cepstral and cepstral envelope analysis techniques (FECCV). It is observed that the proposed method effectively diagnoses bearing defects by the combinational approach and increases the sensitivity of the signal analysis.

Real knowledge is to know the extent of one's ignorance. Life is really simple, but we insist on making it complicated

- Confucius

3.1 Introduction

Rolling element bearings provide smooth dynamics to systems by reducing friction and have marked their stand in every field. The increase in demand for bearings has given a wide window of opportunities and challenges to the researchers. Therefore, the developments in sensing and data acquisition systems have added a sustainable value to the field of condition monitoring to avoid fatalities. In spite of the real world data acquisition system and sensors, the complexities of the signals make their analysis complicated. Generally, the signals

generated by the bearings are considered to be AM-FM [157]. The non-stationarity and the nonlinearity associated with these signals calls for a multi-lingual mathematical function to decode the information from the noise. The separation and segmentation of these signals can be done adaptively using EMD. This method has been used by many researchers in the field of condition monitoring to infer the actual signal buried in the noise. EMD has proven to be the most efficient and adaptive method in translating the multi-tone signal into a series of multilevel variable frequency components called modes [158]. Similarly, the fault can be identified using the morphological operators (dilation, erosion, opening and closing) and their usability is tested on the Case Western Reserve University (CWRU) bearing data set as reported in [159]. In this paper the inner race, outer race and ball defects for higher dimension defect size are identified using Beucher gradient and top hat based morphological filter, however, it fails to predict the lower dimension defects. To detect signal in presence of noise, in [160], fusion of various classifiers are proposed to detect bearing defects. It also discusses about other classifier methods and their usability in detecting faults. However, the time series analysis using kurtosis has significant importance as its value increases with the increase in fault, and can be used as an indicator to decode state of the bearings effectively [161 162]. Many researchers have even calculated the time and spectral kurtosis from the wavelet decomposed signals [163,164], however, it is constrained by the selection of mother wavelet.

Even though the signals are decomposed to their mono-components using various transformation techniques, still they retain some non-linearity. When the signals are modulated by a single carrier, the age old envelope detection (used in communication) technique can be applied to separate out signal from the carrier. However, if there are multiple sidebands around one or many carriers, then the sensitivity of envelope detection diminishes. Generally, the non-coherent Hilbert transform based technique is preferred over square law demodulation technique to avoid aliasing [165]. These analyses are carried out to identify the effect of amplitude modulation in the bearing diagnosis and demonstrated for the synthetic data as discussed in [166]. Along with envelope analysis, cepstral analysis can be used to analyze signals from the gear, bearing and propeller shaft and it is found to be efficient in detecting faults even in the presence of multiple sidebands [167].

It is observed that there are numerous signal processing methods that can be used to anticipate information from the bearings. The proper selection of signal processing method is tough to identify and every technique has certain advantages and disadvantages. Therefore, to better analyze the signal, this chapter concentrates on EMD-PCA based method as compared to other classifier fusion techniques, to address the fault in the bearings [168, 169]. Here, a standardized adaptive non-parametric EMD-PCA based average kurtosis technique followed by analysis using FECCV is proposed. Generally, the signals need to be filtered before being processed, but the filtration can alter the information content, so adaptive filtration using EMD is achieved through kurtosis based intrinsic mode function (IMF) approach. Before processing using the aforementioned algorithm, the signal can be rescaled using normalization or standardization methods (preprocessing), but it is suggested to go for standardization rather than normalization when the data has lots of variations [170]. The standardization brings down the extracted signals to a zero mean and unit variance signal irrespective of the nature of the input [171]. The EMD-PCA technique eliminates the noise and increases orthogonality between the decomposed modes; as a result decreases the usage of number of IMFs. Finally, FECCV spectrum analysis methods are employed to detect and demodulate the non-linearity in the signals.

3.1.1 Standardization

The signal from the bearings can be random, chaotic, stationary or non-stationary etc., and these properties limit the direct use of any signal processing algorithms in their crude form. Generally, the researchers assume the signal from the bearings as Gaussian [172], however, it is affected by sampling rate, and sample length assumed for the analysis [173]. Generally, the healthy bearing follows Gaussian distribution, and it changes to other distributions with the degradation in the bearings [171]. To properly analyze the signal, it needs to be characterized or transferred to the standardized Gaussian distribution prior to any processing (mean=0, standard deviation =1 and kurtosis=3). Therefore, by standardization (control the variation in the signals), firstly, the erratic behavior of the carrier is reduced in the presence of additive Gaussian noise by the proper selection of larger sample length [174]. As padding cannot differentiate closely spaced peaks and also induces more noise in the signal [175], the analysis is carried out for higher sample length, relative to the sampling rate of the signal. Finally, the signals are z-score normalized to bring down the signal to a

normalized floor irrespective of the nature of the input and are listed in (3.1) and (3.2) respectively.

$$\bar{x} = \frac{1}{N}\sum_{n=1}^{N} x[n] \tag{3.1}$$

$$z = \frac{x[n] - \bar{x}}{\sigma} \tag{3.2}$$

where, $x, \overline{x}, z, \sigma$ and N are the actual vibration signal, mean, normalized and standard deviation and sample length of the signal respectively.

3.1.2 Normalization

Similarly, apart from standardization, the signal can be normalized, even though they are used interchangeably. The preprocessing done using normalization can affect signals having outliers, and thereby, the distribution function may get skewed for larger outliers. Normalization of vibration signals is usually performed by taking the deviation of the actual data from the minimum (range between 0 and 1) and dividing by the difference of its extrema. The normalization is carried out using the equation as in (3.3) [176].

$$z(i) = \frac{x(i) - x_{\min}}{[x_{\max} - x_{\min}]} \tag{3.3}$$

where *x* is the series of acquired data, *min* and *max* are minimum and maximum values in the data set.

3.1.3 Empirical Mode Decomposition

The signal from the bearings can be decomposed using EMD technique to segregate multi-tone signal to monotone signals i.e. finite set of intrinsic mode functions (IMFs) based on local minima and maxima. The decomposition of the real-time data *x*(*t*) is as follows and shown in Fig. 3.1 [177].

1. Acquire the vibration signal with the sampling rate needed for the applications.
2. Identify the extrema ($e_{max}[n]$ and minima ($e_{min}[n]$) for the sampled data points $x[n]$.
3. Generate upper and lower envelope i.e., $e_{max}[n]$ and $e_{min}[n]$ using cubic spline (CS) interpolation.
4. Calculate the mean $m[n]$ from the upper and lower envelope using (3.4);

$$m[n] = e_{max}[n] + \left(\frac{e_{max}[n] + e_{min}[n]}{2}\right) \tag{3.4}$$

5. Extract the mean from enveloped discrete time series, and obtain the difference signal from the previous signal i.e. $h[n] = x[n] - m[n]$
6. Check the properties of $h[n]$. If standard deviation (SD) is greater than 0.3, repeat steps 2-5 (shifting process) until the residual satisfies the stopping criterion as in (3.5) [178]. Generally, the preferred value of SD can be set between 0.1 and 0.3; however, it can be smaller than the prescribed value only when there is a necessity to extract every individual signal present in the acquired data [179].

$$SD = \sum_{n=1}^{N} \frac{(prev(h[n]) - h[n])^2}{prev(h[n])^2} \tag{3.5}$$

7. In the end the signal $x[n]$ can be represented as in (3.6).

$$x[n] = \sum_{i=1}^{n} c_i[n] + r_n[n] \tag{3.6}$$

where c_i and r_n are decomposed and residual modes extracted from the actual signal.

Shifting	IMF_1	IMF_2	.....	IMF_n
	$x[n]\|_L$	$r_1[n]\|_L=x[n]-c_1[n]$	.	$r_{n-1}[n]\|_L=r_{n-2}[n]-c_{n-1}[n]$
	P=CS(x[n]$\|_{minima})\|_L$	P=CS($r_1[n]\|_{minima})\|_L$	.	P=CS($r_{n-1}[n]\|_{minima})\|_L$
	Q=CS($x[n]\|_{maxima})\|_L$	Q=CS($r_1[n]\|_{maxima})\|_L$	.	Q=CS($r_{n-1}[n]\|_{maxima})\|_L$
	$m_{11}[n]=(P+Q)/2$	$m_{21}[n]=(P+Q)/2$	.	$m_{n1}[n]=(P+Q)/2$
1	$h_{11}[n]=x[n]-m_{11}[n]$	$h_{21}[n]= r_1[n]-m_{21}[n]$	.	$h_{n1}[n]= r_{n-1}[n]-m_{n1}[n]$
	$\frac{sqr(x[n]-h11[n])}{sqr(x[n])} > 0.3$	$\frac{sqr(r_1[n]-h21[n])}{sqr(r_1[n])} > 0.3$	.	$\frac{sqr(r_{n-1}[n]-hn1[n])}{sqr(r_{n-1}[n])} > 0.3$
	Y N	Y N		Y N
	P=CS($h_{11}[n]\|_{minima})\|_L$	P=CS($h_{21}[n]\|_{minima})\|_L$	.	P=CS($h_{n1}[n]\|_{minima})\|_L$
	Q=CS($h_{11}[n]\|_{maxima})\|_L$	Q=CS($h_{21}[n]\|_{maxima})\|_L$	.	Q=CS($h_{21}[n]\|_{maxima})\|_L$
	$m_{12}[n]=(P+Q)/2$	$m_{22}[n]=(P+Q)/2$	.	$m_{n2}[n]=(P+Q)/2$
2	$h_{12}[n]=h_{11}[n]-m_{12}[n]$	$h_{22}[n]= h_{21}[n]-m_{22}[n]$	.	$h_{n2}[n]= h_{n1}[n]-m_{n2}[n]$
.	.	.	.	.
.	.	.	.	.
.	.	.	.	.
k	$h_{1k}[n]=h_{1(k-1)}[n]-m_{1k}[n]$	$h_{2k}[n]=h_{2(k-1)}[n]-m_{2k}[n]$	.....	$h_{nk}[n]=h_{n(k-1)}[n]-m_{nk}[n]$
	$c_1[n]=h_{1k}[n]$	$c_2[n]=h_{2k}[n]$	.....	$r_n[n]=h_{nk}[n]$

Figure 3.1 EMD decomposition flow

3.1.4 Principal Component Analysis

Principal component analysis was introduced by Pearson and Hotelling to describe the variation in a set of multivariate data in terms of a set of uncorrelated variables [180]. It is generally used to de-correlate the cross-correlated signals and can be used for dimensional reduction. During data acquisitions, variables like acceleration or sound pressure etc. will have different scale, under these circumstances; the variable with higher scale will be dominant. Therefore, it is recommended that the signals should be standardized prior to the PCA [181].

Steps involved in PCA calculations are as follows;

1. The signals s of $(n \times p)$ dimensions are standardized using (3.7).

$$x_{ni} = \frac{(s_{ni} - \bar{s}_{ni})}{\sigma_{s_{ni}}} \tag{3.7}$$

where $\boldsymbol{x}$ is the standardized signal of dimension $(n \times p)$, i=1, 2…p.

2. Covariance matrix $\mathbf{C}$ of dimensions $(p \times p)$ is obtained from x using (3.8).

$$\mathbf{C} = \begin{pmatrix} v(x_{n1}) & c(x_{n1}\, x_{n2}) \ldots\ldots & c(x_{n1}\, x_{np}) \\ c(x_{n2}\, x_{n1}) & v(x_{n2}) & \ldots\ldots & c(x_{n2}\, x_{np}) \\ c(x_{np} x_{n1}) & c(x_{np}\, x_{n2}) \ldots\ldots & v(x_{np}) \end{pmatrix} \tag{3.8}$$

3. The Eigen values (λ_i) are calculated from the covariance matrix using (3.9),

$$\mathbf{C} - \lambda_i \mathbf{I} = 0 \tag{3.9}$$

where $\mathbf{I}$ is the identity matrix of dimension $(p \times p)$ and λ_i is the eigenvalues and

4. Evaluate the eigenvectors $\mathbf{Z}$ for different Eigen values using (3.10).

$$(\mathbf{C} - \lambda_i \mathbf{I})\mathbf{Z} = 0 \tag{3.10}$$

5. Finally, multiply the transpose of the eigenvectors obtained using (3.10) with that of the standardized signal $\boldsymbol{x}$ in (3.7) to obtain principal components. Finally, the variance for each of these PCs are calculated.

3.1.5 Hilbert Transform

The natural signal or the wave emanating from the SUT depends on the coupling, misalignment, imbalance or bearing faults etc. The wave and its propagation purely depend on the medium of transmission or the transfer function (TF) of the system till it reaches the sensors. The TF acts like a non-linear system or as a non-linear mathematical operator to the signals. The change in the behavior of the TF creates harmonic distortion in signals and results in frequency, phase and amplitude distortions. Frequency distortion occurs, if the system to be observed has different amplification or attenuation at different frequencies, whereas, phase distortion occurs due to the presence of energy storing elements. In case of phase distortion, the signals of different frequencies get shifted by different phase angles as the medium of propagation changes. Finally, the presence of harmonics or the mathematical non-linearity creates amplitude distortions. In bearings, inter-modulations occur when the resonating frequencies due to transient get coupled with the fault and the shaft rotating frequencies simultaneously. This section focuses on the amplitude demodulation using Hilbert transform and its impact on different test signals.

For segregations of the signal from the carrier, Hilbert transform is used to demodulate the signals. The envelope detection can be carried out using LPF or using

Hilbert transform method, but signal extraction using LPF produces more ripple and distortion compared to Hilbert. Therefore, Hilbert transform is generally applied to amplitude modulated signals with significant side band and carrier present in the signal. The amplitude modulated signal with transmitted carrier can be expressed using (3.11) [182].

$$x(t) = A_c[1 + k_a m(t)\,]cos(2\pi f_c t) \tag{3.11}$$

where $x(t)$ is the amplitude modulated signal, $m(t)$ message signal or the fault signal and f_c is the modulated carrier, k_a is the modulation index, A_c is the amplitude of carrier [36].

The signals generated from the bearing are AM-FM signals with multiple resonating frequencies present in the frequency spectrum. These types of signals have prominent side band frequencies (lower and upper side bands about the resonating frequencies) when the signal is least corrupted by noise. The Hilbert transform is the fastest non-coherent (the information related to the carrier is unknown) demodulation method adopted to extract the lower frequency (message signal) contents present in the signal. To estimate the lower frequency or the message signal, an analytical signal is formulated using the Hilbert transform as represented in (3.12) [183].

$$\begin{aligned} x(t) \overset{H}{\rightarrow} x_{\dagger}(t) = A_c[1 + k_a m(t)]\, cos(2\pi f_c t) \\ + jA_c[1 + k_a m(t)]\, sin(2\pi f_c t) \end{aligned} \tag{3.12}$$

where $x_{\dagger}(t) = A_c[1 + k_a m(t)]e^{j2\pi f_c t}$

To observe the effect of envelope detection using Hilbert transform; seven different synthetic signals are generated i.e. periodic, square wave signal, quasi-periodic, transient signal, amplitude modulated, frequency modulated and amplitude-frequency modulated as expressed in (3.13-3.19) respectively.

$$x_{PS} = A_m sin(2\pi f_m t) \tag{3.13}$$

$$x_{PH} = \frac{2}{j\pi} \sum_{m=-\infty}^{\infty} \frac{1}{2m+1} e^{j(2m+1)2\pi f_m t} \tag{3.14}$$

$$x_{QP} = A_m sin(2\pi f_m t) + A_c sin(\sqrt{2}.2\pi f_c) \tag{3.15}$$

$$x_{TS} = A_m e^{-\lambda t} sin(2\pi f_c t) \tag{3.16}$$

$$x_{AM} = (1 + (A_m/A_c)cos(2\pi f_m t))cos(2\pi f_c t + (\Delta f/f_m)cos(2\pi f_m t))|_{\Delta f=0} \quad (3.17)$$

$$x_{FM} = cos(2\pi f_c t + (\Delta f/f_m)cos(2\pi f_m t))|_{\Delta f=50} \quad (3.18)$$

$$x_{AM\_FM} = (1 + (A_m/A_c)cos(2\pi f_m t))cos(2\pi f_c t + (\Delta f/f_m)cos(2\pi f_m t)) \quad (3.19)$$

where the assumed damping factor λ is 0.8, sampling rate F_s is 12000 samples per sec, amplitude of the message signal A_m is 2, amplitude of the modulated signal A_c is 2, frequency of the message signal $f_m$is 5 Hz, frequency of the carrier f_c is 35 Hz, assumed duty cycle is 50%, frequency deviation Δf is $k_f A_m$, and modulation index $k_f|_{FM}$ for FM is 50, and frequency deviation $k_f|_{AM-FM}$ for AM-FM is 20 respectively.

a) Effect of Hilbert Transform on Periodic Signal

The periodic signal (PS) is shown in the Fig. 3.2(a) and its respective spectrum and spectral envelope are shown in Figs. 3.2(b) and (c) respectively. It is observed that the actual frequency of the message signal (or the fault signal in the bearing) is recovered significantly as in Fig. 3.2(b). But, if the signal characteristic is not known and the Hilbert transform is applied, then the spectral envelope detects mixed signals of different frequencies as shown in the Fig. 3.2(c) (even though the amplitudes are too low). Analytically, one can justify the results by looking at the amplitudes in both the cases and can decide the effectiveness of Hilbert transform accordingly.

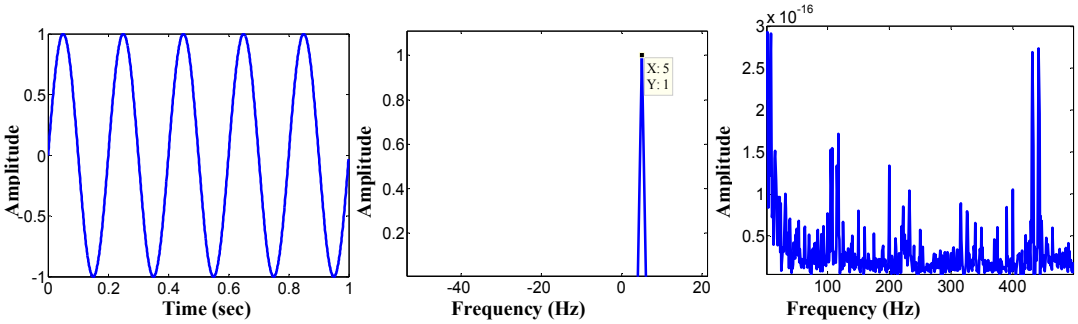

Figure 3.2 Periodic signal (a) time (b) spectrum (c) spectral envelope

b) Effect of Hilbert Transform on Periodic Harmonics

The periodic harmonic (PH) signal with odd harmonics is generated with 50% duty cycle and is shown in Fig. 3.3(a). It is observed from Fig. 3.3(b) that Hilbert transform effectively

extracts the signal frequency of 5 Hz using FFT. But, the frequencies in spectral envelope get shifted by the message signal frequency as shown in Fig. 3.3(c). It is inferred that the Hilbert transform on PH signal can mislead the information if it is applied blindly without analyzing much about the true form of the signals.

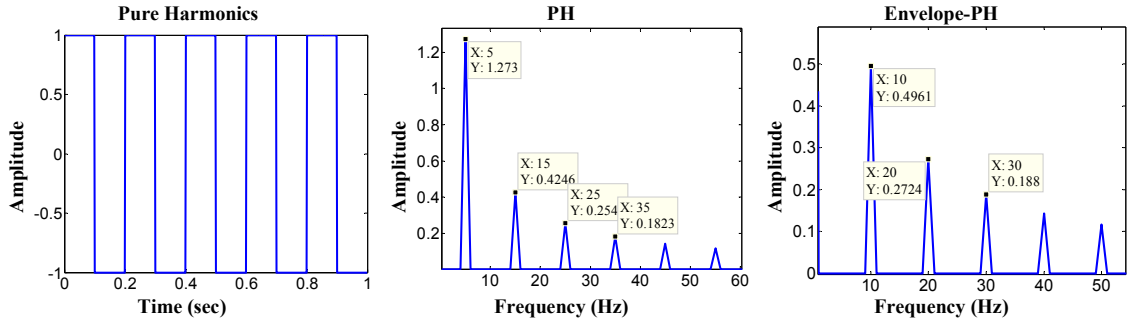

Figure 3.3 Periodic signal (a) time (b) spectrum (c) spectral envelope

c) Effect of Hilbert Transform on Quasi-Periodic Signal

The quasi-periodic signal (QP) generated using Equation (3.14) is shown in Fig. 3.4(a). The spectrum analysis in Fig. 3.4(b) extracts the information related to message signals correctly as there is no nonlinearity present. As the Hilbert transform is applied, it is observed that the frequency gets shifted to a lower band by 5 Hz and the harmonics are generated corresponding to 44.5 Hz as shown in Fig. 3.4(c). It shows that the envelope detection drifts the frequencies to lower value and creates harmonic pattern in the frequency spectrum.

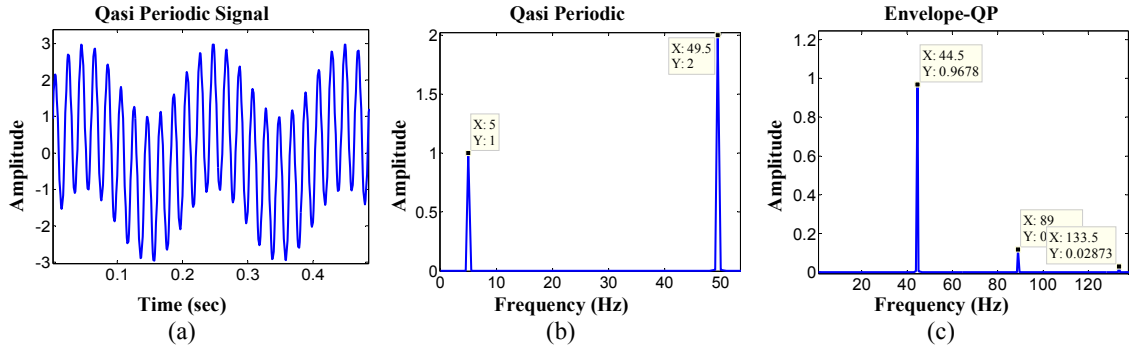

Figure 3.4 Quasi-periodic signal (a) time (b) spectrum (c) spectral envelope

d) Effect of Hilbert Transform on Transient Signal

The signal generated by the actual bearing creates an impulsive signal that decays down with the damping factor associated with the bearing. To analyze the effect of transient on the

envelope, the time series signal is generated as shown in Fig. 3.5(a). Fig. 3.5(b) clearly detects the carrier signal, but Fig. 3.5(c) anticipates no frequency in the signal. It means the Hilbert transform has no impact on the damping parameter of the system.

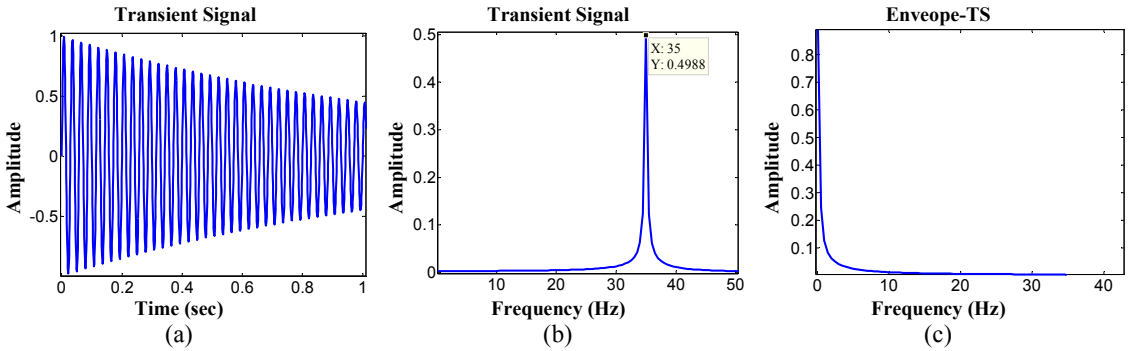

Figure 3.5 Transient signal (a) time (b) spectrum (c) spectral envelope

e) Effect of Hilbert Transform on AM Signal

The effect of Hilbert transform on amplitude modulated signal is verified and is shown in Fig. 3.6(a). It is observed from Fig. 3.6(b) that the carrier and the sidebands ($f_c \pm f_{AM}$) are extracted properly by spectrum analysis method. However, to mitigate the effect of modulation, the non-coherent Hilbert transform is used to decipher the actual signal from the carrier as shown in Fig. 3.6(c). Even though, the envelope could trace the fault, but in a real scenario the complexity is too high if the signal is corrupted by noise.

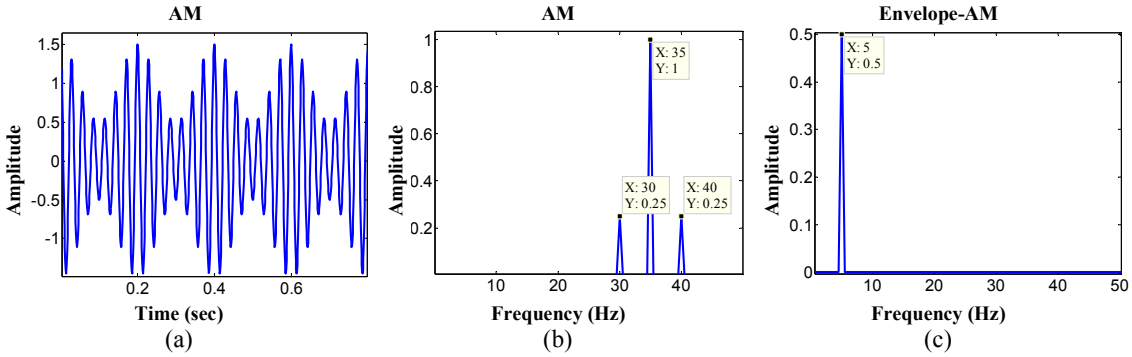

Figure 3.6 AM signal (a) time (b) spectrum (c) spectral envelope

f) Effect of Hilbert Transform on FM Signal

The frequency modulated signal generated using (3.17) is shown in Fig. 3.7(a). It is observed that apart from the message and carrier frequencies, some other dominating frequencies are appearing in Fig. 3.7(b). The reason behind the effect is the modulation

index (df/f_{FM}), which changes with change in environmental state, thereby, complicating the signal analysis process. Fig. 3.7(c) shows the presence of multiple frequencies in the spectrum due to shifting and deviation of one frequency from another. It suggests that prior to Hilbert transform the signal must be linearized to minimize the effect of side bands.

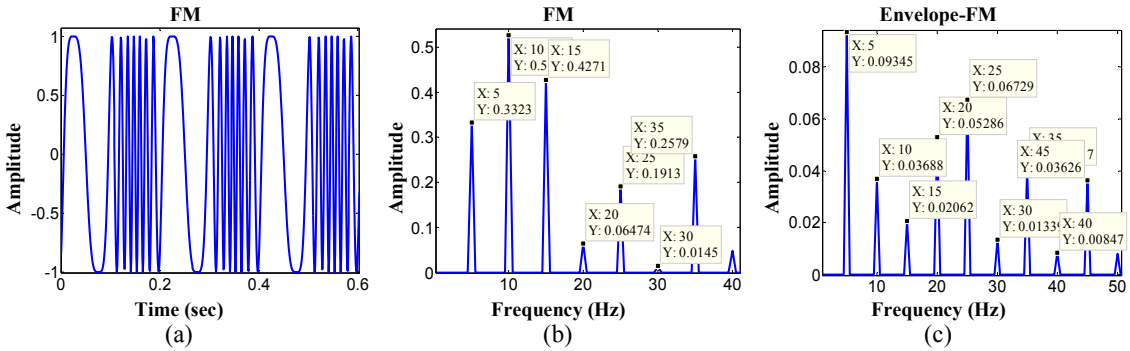

Figure 3.7 FM signal (a) time (b) spectrum (c) spectral envelope

g) Effect of Hilbert Transform on AM-FM Signal

Fig 3.8(a) shows the amplitude and frequency modulated signal generated using (3.18). It is observed from Fig. 3.8(b) that FFT predicts the presence of message as well as the carrier, but anticipates other frequency components in the spectrum. To intercept the actual signal present, envelope transform is applied as shown in Fig. 3.8(c).

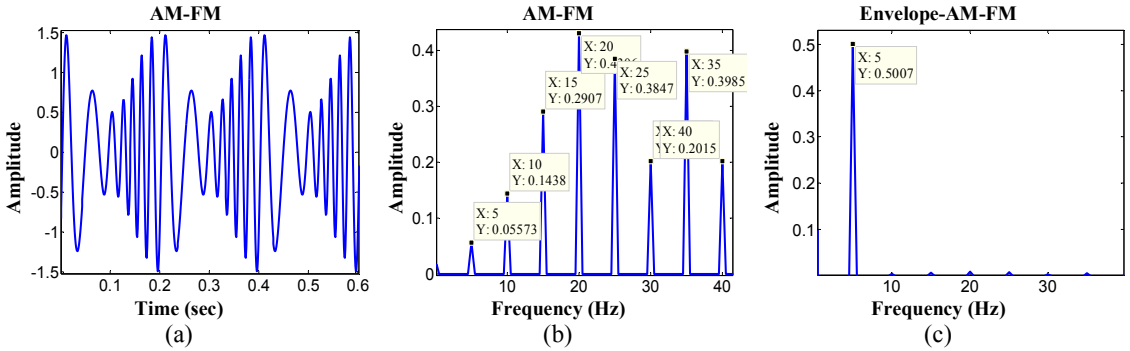

Figure 3.8 AM-FM signal (a) time (b) spectrum (c) spectral envelope

It is observed from the synthetic signals that the true analogy of the modulation is too tough to predict if the system behavior is not properly known. Therefore, the concerned system and the desired frequencies must be known mathematically prior to the use of any of the signal processing techniques. After verification of Hilbert transform on test signals, the proposed method is tested on the real-time experimental data set of CWRU.

3.2 Experimental Test Bench

The detailed experimental setup and vibration signals are taken from the Case Western Reserve University bearing data center is shown in Fig. 3.9 [184]. The experiment test bench consists of a 2 hp motor, a torque transducer/encoder, a dynamometer and a 6205-2RS deep groove ball bearing. In this experimentation different faults of diameters 0.007", 0.014", and 0.021" respectively are created in inner race, outer race and on the ball using electro-discharge machining (EDM). Drive end vibration data of the bearing are collected using accelerometers mounted on a magnetic base at 6 o'clock positions. The vibration signals are collected at a sampling rate of 12000 samples per sec using a 16 channel data acquisition card. Tables 3.1 and 3.2 represent the bearing configuration and the fault frequencies at 1797 rpm.

Table 3.1 Ball bearing configuration

Bearing Type	Pitch Dia. (in)	Rolling Element Dia. (in)	No. of Rolling Elements
6205-2RS, JEM SKF (DGBB)	1.537	0.3125	9

Table 3.2 Ball bearing frequencies

Shaft Speed (RPM)	BPFI (Hz)	BPFO (Hz)	BSF (Hz)	FTF (Hz)	RDF (Hz)
1797/29.95	162.177	107.373	70.608	11.930	141.217

*BPFI (Ball Pass Frequency Inner Race), BPFO (Ball Pass Frequency Outer Race), Ball Spin Frequency (BSF), Cage Defect Frequency (FTF) and Rolling Element Defect Frequency (RDF)

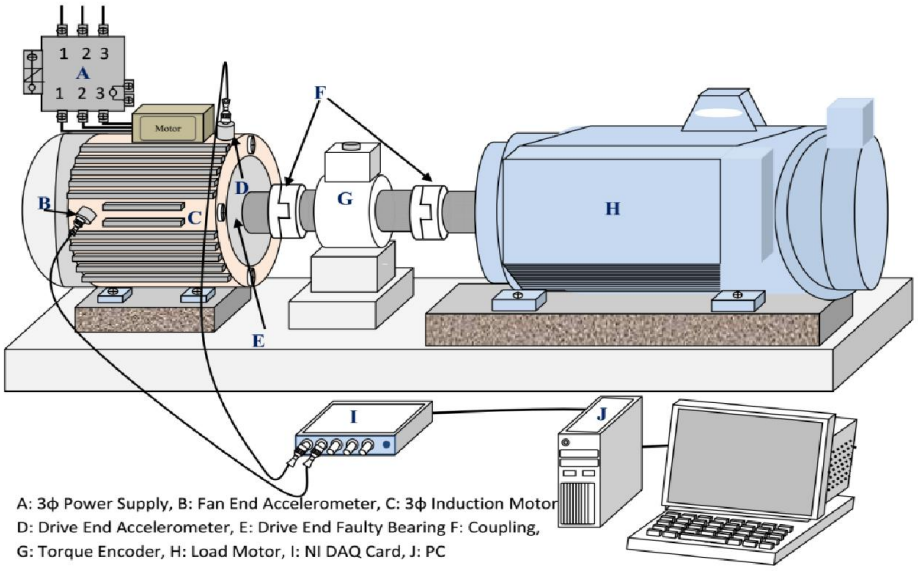

Figure 3.9 Schematic representation of sensors and DAQ in CWRU experimental test bench

3.3 Proposed Signal Extraction Techniques

Even though there are ample signal processing techniques present to diagnose the faults, however, the main objective of this chapter is to decode the information adaptively without prior filtration or resonance frequency identification techniques. Moreover, the analysis and identification of faults in the frequency domain is a typical task as compared to discrimination methods (PCA, SVM, ICA etc.). However, the frequency analysis method gives insights about the shaft frequency, fault frequencies and their harmonics. This method also clarifies the different types of modulation that occurred during the operation of the SUT. Even though, state of the bearings can be classified using discrimination techniques like PCA, SVM, however, the insight picture related to the frequencies is missing. Therefore, in this chapter three different approaches are adopted for fault identification and the process flow used is stated below. The overall processes followed to analyze and compare different algorithms are shown in Fig. 3.10.

a) Initially, the vibration signals acquired from the bearings are standardized (STD), non-standardized (NSTD, no preprocessing), and normalized (N) and later on these signals are compared based on their statistical parameters i.e. variance, standard deviation, peak value, crest factor, skewness, kurtosis, clearance factor, impulse factor etc. The best pre-processing method is further used for analysis of the faults in the bearings.
b) In this section three standard algorithms; i.e. FFT, envelope, cepstrum and proposed cepstral envelope (FECCV) algorithms are applied on the STD, NSTD, N signals. The frequency domains of the STD, NSTD and N are compared to find the best out of the three. This section (b) is compared with the previous section (a) to conclude the best pre-processing method (It is observed that STD gives better results as compared to NSTD result and can be found in the later result sections). The proposed cepstral envelope algorithm applied on the signals is shown in Fig. 3.11 and as follows;

    Step 1: Process the signal using standardization or Z-score normalization using (3.2) and (3.3) to generate $x'[n]$.

    Step 2: Calculate the Fourier transform of the standardized message signal with no filtration and padding i.e. take 24000 sample points at a sampling rate of 12000 sample per sec; $X(w) = \text{FFT}(x'[n])$

    Step 3: Take the *log* of the signal i.e. $D = log|X(w)|$

Step 4: Calculate the Fourier transform of step 3 i.e. $m = \text{FFT}(D)$

Step 5: Calculate the Hilbert envelope of step 4 i.e. $z = \text{HT}(m)$

Step 6: Finally, calculate the Fourier transform of step 5 i.e. $X'(w) = \text{FFT}(z)$

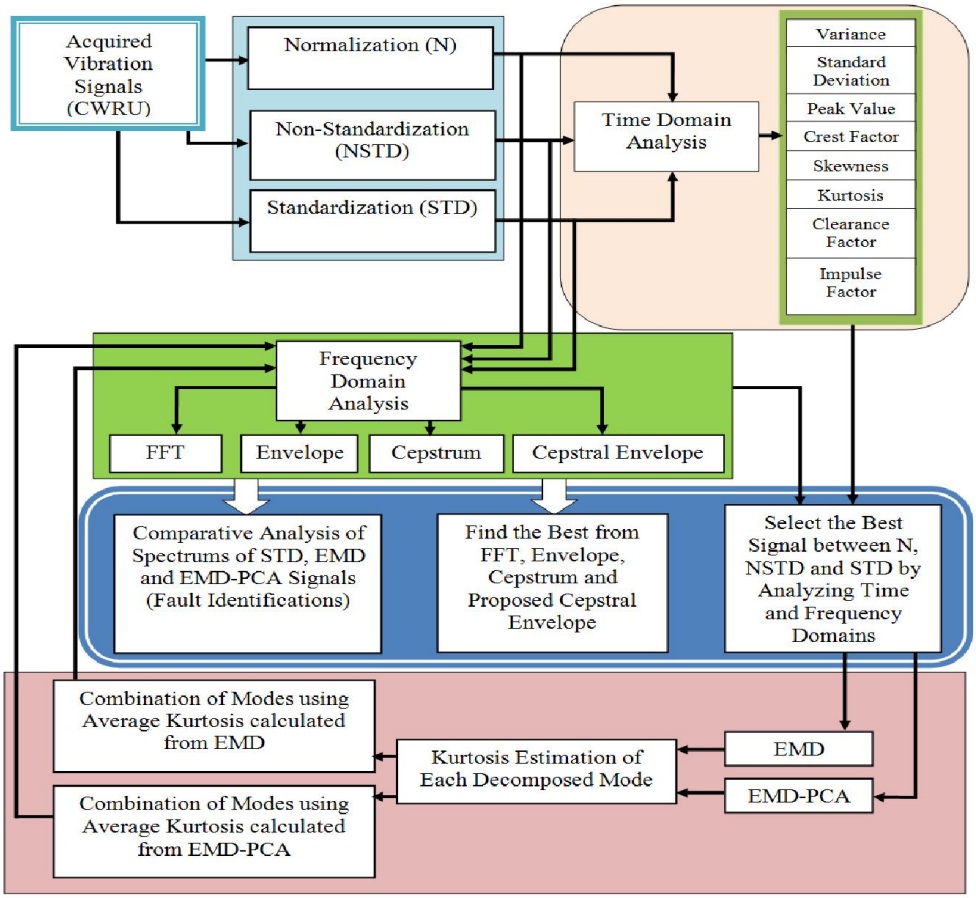

Figure 3.10 Overall analysis flow adopted for the current chapter

(c) In this approach standardized EMD-PCA/EMD based decomposition, and recombinations using average kurtosis are detailed as follows;

Step 1: Acquire the vibration data $x[n]$ at a sampling rate of 12000 samples per sec.

Step 2: Use data sample length of at least two times the sampling rate to avoid padding.

Step 3: Process the signal using standardization or Z-score normalization i.e. $x'[n] = (x - \mu)/\sigma$.

Step 4: Decompose the standardized signal using EMD i.e. $IMF_{1,2\ldots n}$; where n is an integer.

Step 5: The algorithm uses the divide and conquer approach through EMD-PCA based average kurtosis technique. All the decomposed IMFs are de-correlated using PCA to avoid mode mixing problem and finally the extracted principal components i.e. $PC_{1,2\ldots n}$ are selected based on average kurtosis as follows:

a. Calculate the kurtosis of the all the PCs (principal components) i.e. $K|_{PC1,PC2\ldots PCn}$, and obtain the average values i.e. $K|_{PCavg} = \frac{1}{n}\sum_{i=1}^{n} K_{PCi}$; where i is $1, 2\ldots, n$.

b. Select the mode/PCs that are above the average kurtosis and eliminate all other PCs i.e. $K_{PCi} \geq K|_{PCavg}$

c. Recombine the selected PCs to create a new signal; i.e. $y[n_l] = \sum_{i=1}^{l} PC_i$; where $l < n$ and it is an integer.

Step 6: Repeat the step 5 without using PCA

Finally, $x'[n]$ and $y[n_l]$ (time domain signal generated from step (b) and (c)) are analysed and compared to find their effectiveness in identification of faults. The extraction and analysis are carried out systematically using the flowchart given in the Fig 3.12.

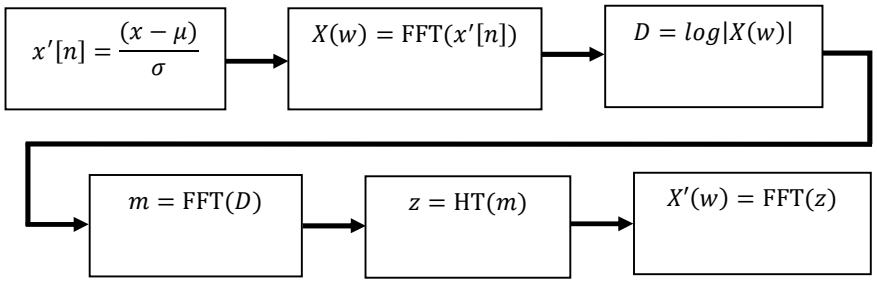

Figure 3.11 Cepstral envelope analysis

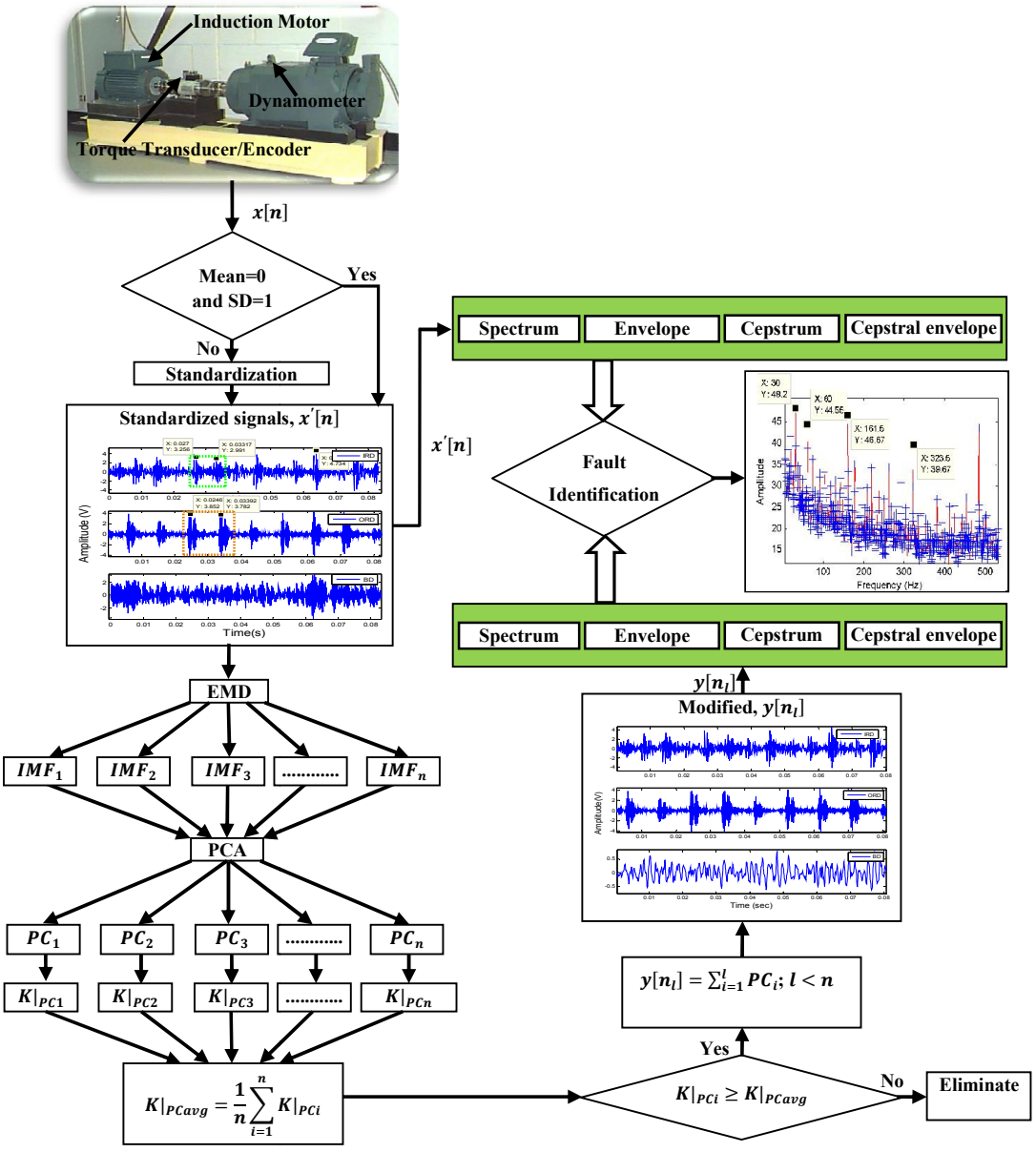

Figure 3.12 Proposed method for fault identification

3.4 Results and Discussion

These analyses are carried out for inner race defect (IRD), outer race defect (ORD) and ball defects (BD) for a minimal fault dimension of 0.1778mm. It is observed from Fig. 3.13 that the IRD and ORD defects (marked in rectangular boxes) can be calculated to a certain extent from their impulses in the time domain. But, it is tough to calculate the BD, as the impact is least acknowledged in the time series. In general, it is difficult to locate the exact time window in case of BD that truly reciprocates the fault frequency. Therefore, there is a need of an analytical technique which can be used to anticipate the information for all three defects.

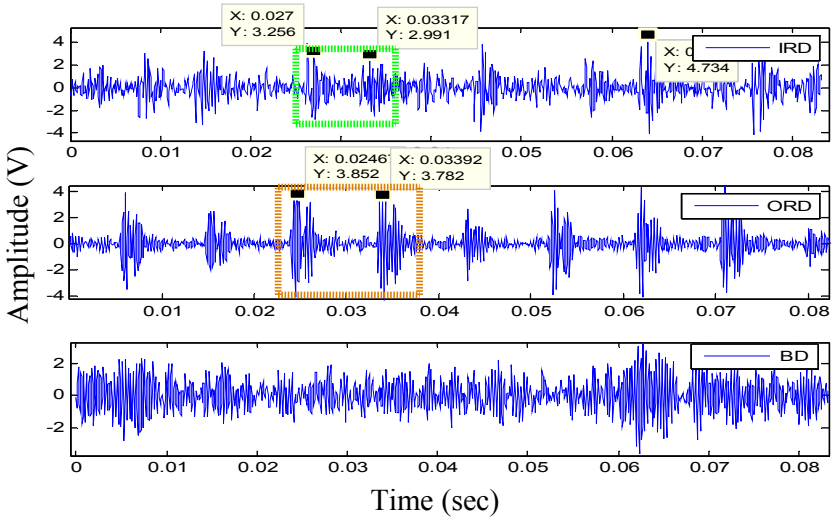

Figure 3.13 Time representation of IRD, ORD, and BD

3.4.1 Standardized Envelope and Cepstral Envelope Analysis

The effects of standardization (STD), normalization and non-standardization (NSTD) on different statistical parameters are listed in Table 3.3. It is observed that the mean and variance for the different faults after standardization are close to Gaussian with least shift in the kurtosis. But, there is an improvement in the peak value for all the three defects. The mean has shifted close to zero where as the variance and standard deviation approaches towards unity. Whereas, normalization has no effect on kurtosis, but the peak value and the clearance factor decrease as compared to the standardized results. It is observed that out of all these three analysis methods, standardization performs better in anticipating information as compared to NSTD and normalization.

Table 3.3 Statistical results with and without standardization and normalization for IRD, ORD, BD

	data	Mean	RMS	Var	SD	PV	CF	SK	KS	CLF	IF
IRD	Without STD	0.014	0.28	0.08	0.28	1.39	4.83	0.13	5.38	32.44	6.73
	With normalization	0.43	0.45	0.01	0.10	0.50	1.10	0.001	5.38	2.59	1.13
	With STD	-3.7e-13	0.99	0.99	0.99	4.83	4.83	0.13	5.38	09.38	6.73
ORD	Without STD	0.032	0.66	0.43	0.66	3.38	5.10	0.06	7.55	20.80	8.39
	With normalization	0.47	0.48	0.009	0.09	0.50	1.02	0.00	7.55	2.17	1.04
	With STD	-8.3e-13	1.00	1.00	1.00	5.11	5.11	0.06	7.55	13.87	8.42
BD	Without STD	0.015	0.13	0.01	0.13	0.54	3.93	-0.02	2.95	44.65	4.91
	With normalization	0.52	0.54	0.01	0.121	0.50	0.91	-0.00	2.95	1.78	0.94
	With STD	4.16e-13	1.00	1.00	1.00	3.95	3.95	-0.02	2.95	6.18	4.95

*Var: Variance, SD: Standard Deviation, PV: Peak Value, CF: Crest Factor, SK: Skewness, KS: Kurtosis, CLF: Clearance Factor, IF: Impulse Factor

The effects of STD, normalization and NSTD on the behavior of the signals are as shown in Figs. 3.14, 3.15 and 3.16 respectively. It is difficult to anticipate any information from Figs. 3.14(a), 3.15(a) and 3.16(a) as the signals are modulated by higher order resonating frequencies. It is observed from the Fig. 3.14(b) that the fault frequency and the intensity for IRD are 161.5 Hz and 0.1596 respectively. With normalization, the intensity in Fig. 3.15(b) is 0.01296, and it is not the only significant peak present in the signal. It can be concluded that the preprocessing with normalization decreases the signal intensity. However, with standardization in Fig. 3.16(b), the amplitude has increased from 0.1596 to 0.5516. The increments in values are observed for the harmonics corresponding to the fault frequency, and the second harmonics of shaft speed. It is observed that the detection sensitivity of simple cepstrum analysis is too low, as shown in Figs. 3.14(c) and 3.16(c) respectively. Therefore, to enhance the signal, cepstral envelope based analysis can be used as shown in Fig. 3.14(d). It is observed that the frequency of rotation is least significant for the envelope analysis, but is prominent in cepstral envelope, as shown in Figs. 3.14(d) and 3.16(d). The rotating and fault frequencies in Fig. 3.13(d) are 30 Hz and 161.5 Hz, with amplitudes of 40.99 and 40.96 respectively. The cepstral envelope in Fig. 3.16(d) depicts the rotating and fault frequency amplitudes of 48.2 and 46.67 respectively. It is observed, by standardization, the amplitudes have increased drastically without much change in the kurtosis. It can be concluded that the kurtosis is independent of amplitude; rather it depends on shape

parameter (distribution). The standardized results for the ORD for different spectrums are shown in Fig. 3.17. Figs 3.17(b) and (d) clearly depict the fault frequency of 107.5 Hz and shaft rotating frequency significantly, but the cepstrum analysis is less significant in detecting faults as shown in Fig. 3.17(c). This analysis clearly depicts that the fault frequencies can be detected significantly even without the use of complex algorithms. The significant improvement is contributed by the sample length chosen for the analysis and these results can be compared with that of morphological analysis performed in [159].

Even though the IRD and ORD are detected significantly, but the complexity lies in the detection of ball defect in the bearing. The random motion of balls is least known by the engineers as it is more erratic than certain, compared to the IRD and ORD. Fig. 3.18(a) shows the spectral plot of standardized BD signal and depicts nothing significant related to the fault, apart from the center frequencies (marked in rectangular dashed box). Without much analysis of the filtering operation, if the signal is inferred using envelope and cepstral analysis, then nothing is clearly observed about the fault, as shown in Figs. 3.18(b) & (c) respectively. However, Fig. 3.18(d) for the cepstral envelope detects the rotating frequency significantly with a least significant peak at 149.5 Hz. The deviation in the BD frequency is reported by one of the researchers in their signal analysis using morphological operators [159].

The main advantages of this technique are standardization, higher sample length selection rather than padded bits, and no filtration process prior to cepstrum analysis, as adopted by conventional techniques. The limitation is that even if the BD is appearing in the cepstral envelope, the intensity is not at par with the amplitude of rotation.

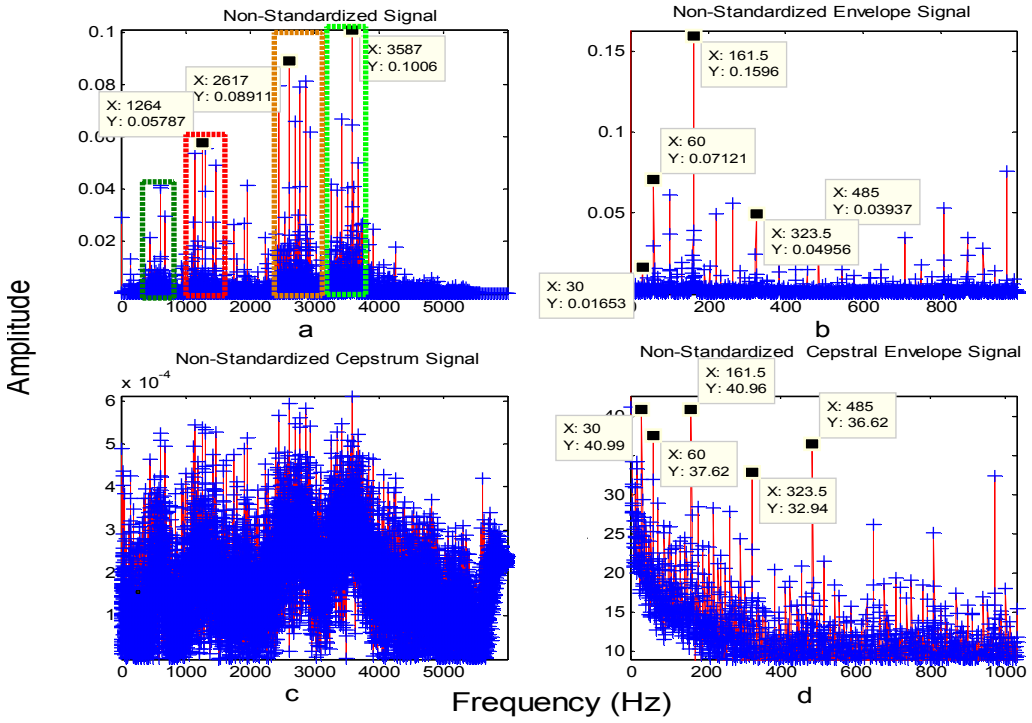

Figure 3.14 NSTD IRD spectrums for (a) actual (b) envelope (c) cepstral (d) cepstral envelope signals

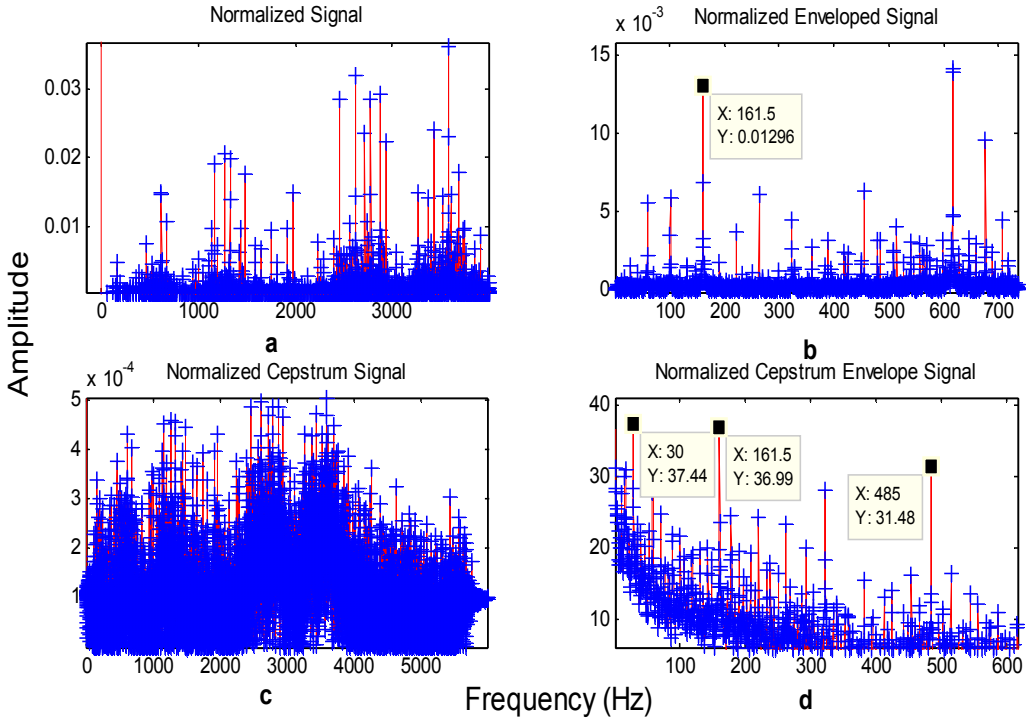

Figure 3.15 Normalized IRD spectrums for (a) actual (b) envelope (c) cepstral (d) cepstral envelope signals

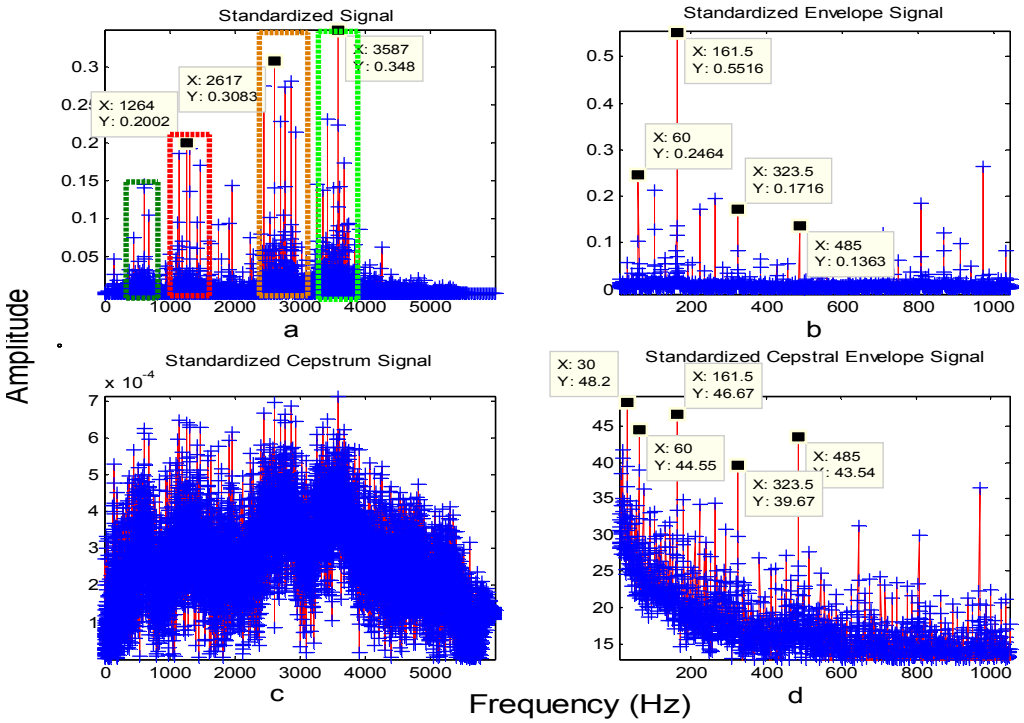

Figure 3.16 STD IRD spectrums for (a) actual (b) envelope (c) cepstral (d) cepstral envelope signals

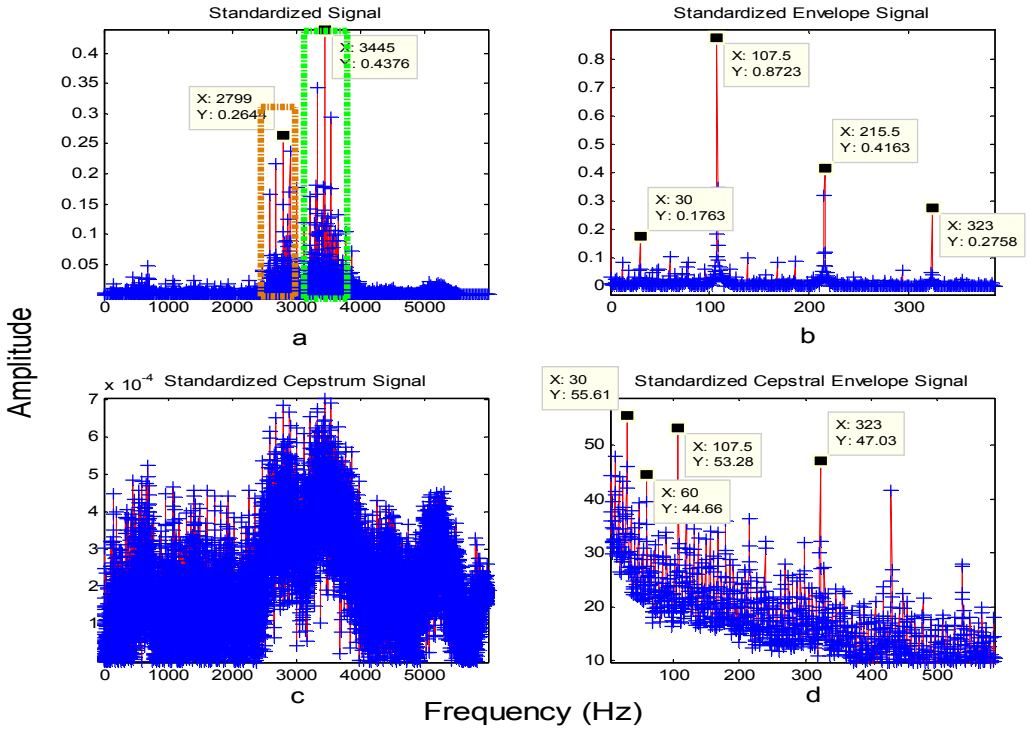

Figure 3.17 STD spectrums for ORD (a) actual (b) envelope (c) cepstral (d) cepstral envelope signals

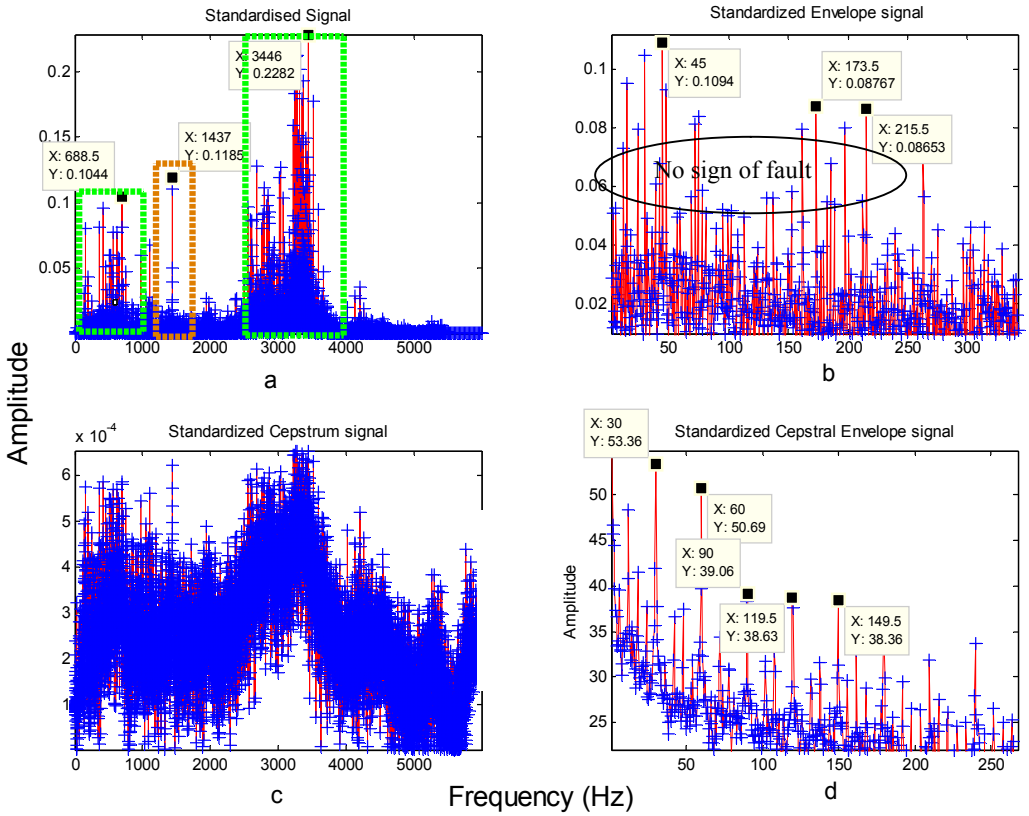

Figure 3.18 STD spectrums for BD (a) actual (b) envelope (c) cepstral (d) cepstral envelope signals

3.4.2 EMD in Fault Detection

As observed from the above analysis that, even though the faults can be identified easily without much computation complexity, the noise present in the signals is still persistent. For better detection and adaptive analysis of non-linear and non-stationary signals, EMD is used to decompose the signal into a number of IMFs and the extracted modes for the IRD, ORD and BD are shown in the Figs. 3.19, 3.20 and 3.21 respectively. Figs. 3.19(a) and (b) show the decomposed IMFs and the corresponding envelope spectrum. It is observed from Figs. 3.19(a) that it has multiple center frequencies spreading from IMF1 to IMF4 i.e. 3587 Hz, 1264 Hz, 1162 Hz and 615.5 Hz etc. But, the actual fault and shaft rotating frequencies are present at IMF6 and IMF8 respectively. Though, the envelope spectrum depicts the fault frequencies at multiple IMFs (IMFs 1-3), but, the frequency of rotation is not clearly visible in any of the IMFs.

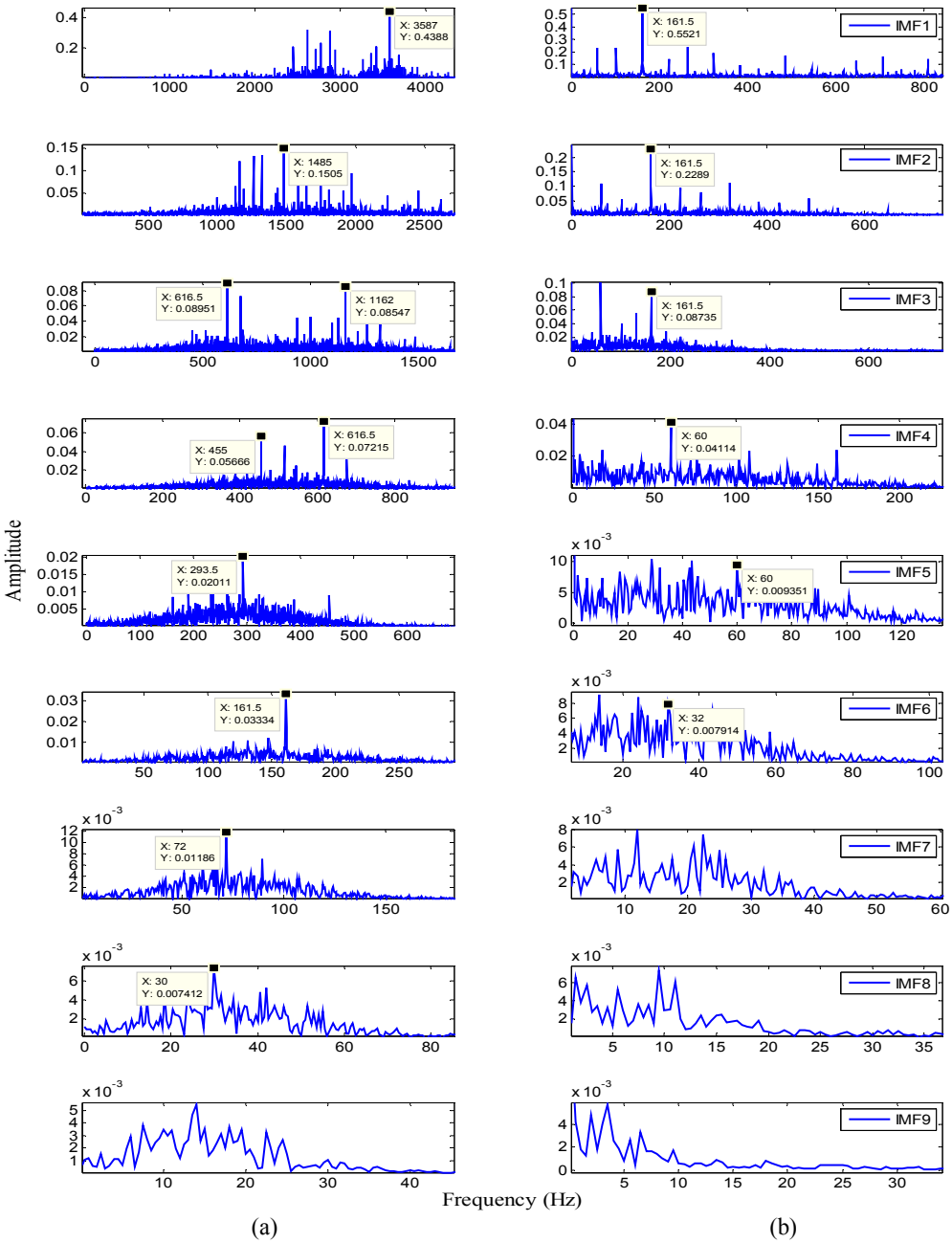

Figure 3.19 (a) Spectrum of decomposed IMFs (b) envelope for IRD

Similarly, the observation is further carried out to detect ORD, and the corresponding spectrum and spectral envelope are shown in Fig. 3.20. It is observed that the spectrum in 3.20(a) clearly does not show the presence of ORD fault in any of the IMFs, but detects its presence in spectral envelope plots in 3.20(b). The fault frequency of 107.5 Hz is detected at multiple IMFs i.e. IMF2, IMF3, and IMF4 respectively, and the shaft rotating frequency is

observed at IMF4. It is observed, if the true nature of the fault is not known, then FFT for time series may predict the ORD as IRD (IMF5).

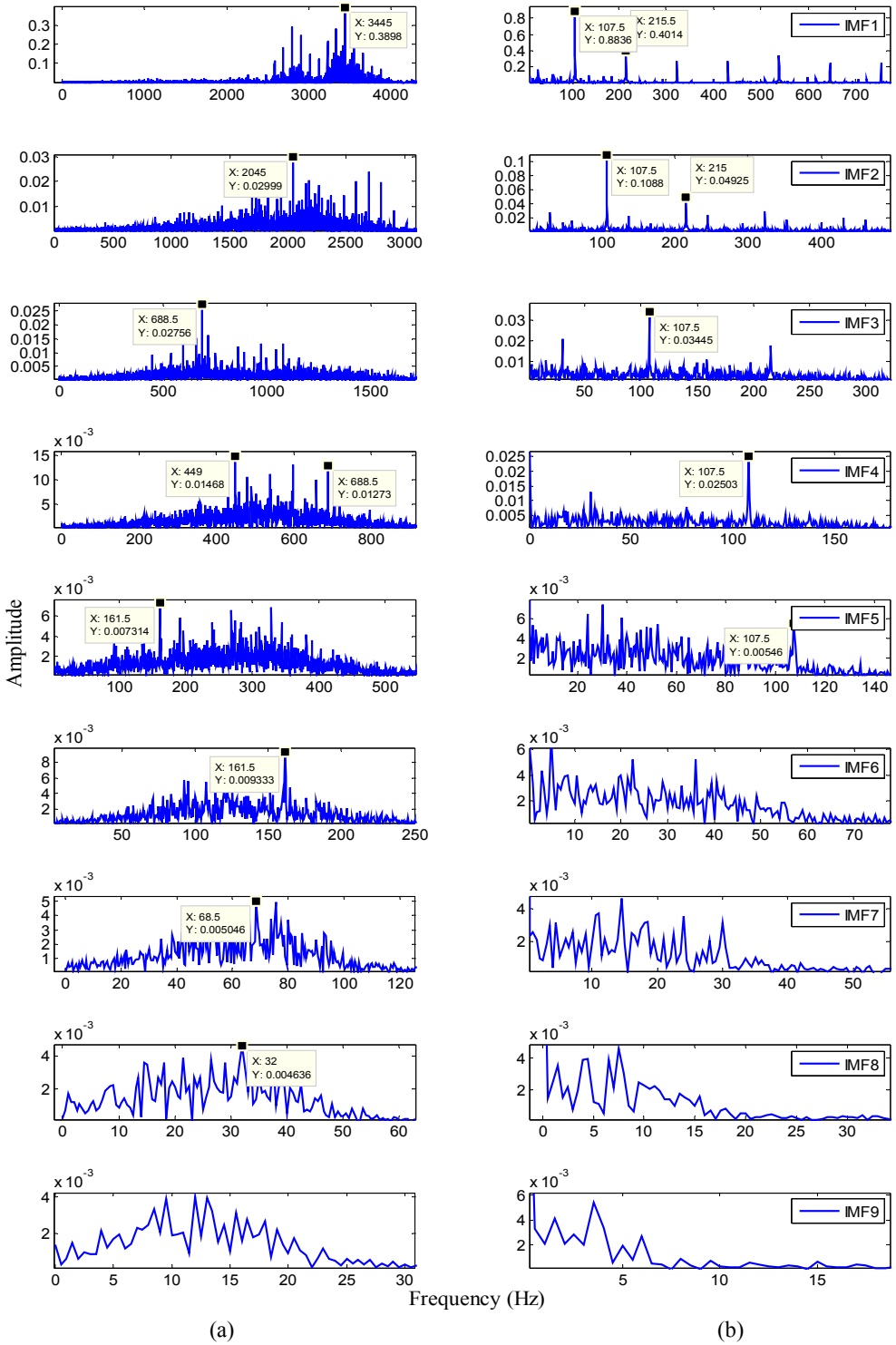

Figure 3.20 (a) Spectrum of decomposed IMFs (b) envelope for ORD

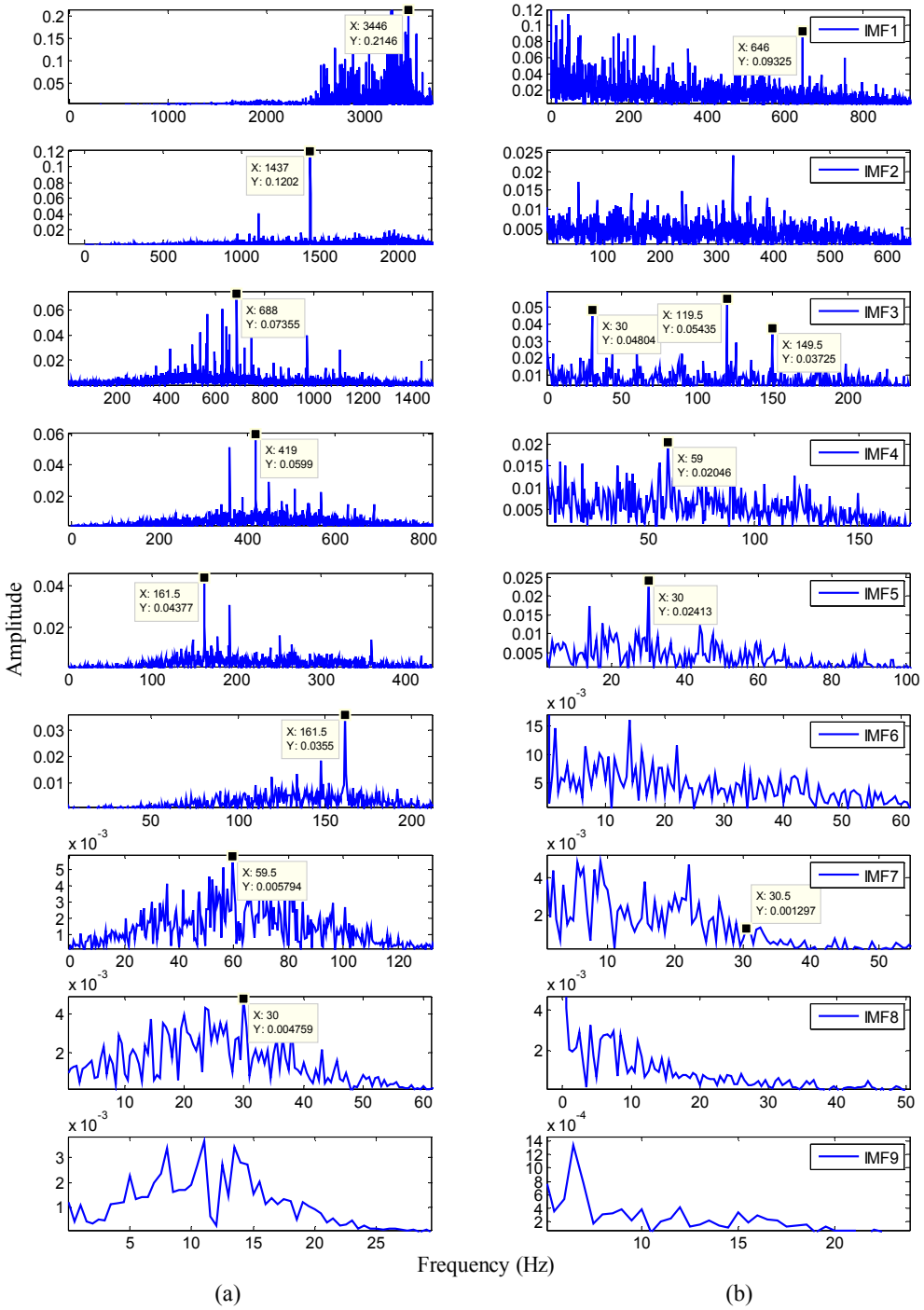

Figure 3.21 (a) Spectrum of decomposed IMFs (b) envelope for BD

Finally, the standardized decomposed result for the BD is shown in the Fig. 3.21. The center frequencies of 3446 Hz, 1437 Hz, and 688.5 Hz are apparent in the first three IMFs as

shown in Fig. 3.21(a). The signal also replicates a frequency of 161.5 Hz (IRD) at IMF5 and IMF6 respectively. This again increases the complexity in identifying the fault, whether it is inner or ball defect. But, when we look into the envelope spectrum in Fig. 3.21(b), fault is partially depicted at IMF3 and the shaft rotation at IMF5. The perplexity in identifying the fault from decomposed IMFs and envelope spectrum clearly denies the presence of BD fault, giving a rather false indication of IRD. Therefore, the divide and conquer rule by EMD is not sufficient enough in identifying the faults. To analyze the faults more accurately, a combinational approach is developed that divides and conquers using the average kurtosis technique.

3.4.3 EMD-PCA based average kurtosis

The process flow for the combinational method is shown in Fig. 3.12. Here, the significant IMFs are selected by de-correlating the modes using PCA, and later evaluating the kurtosis over the entire decomposed PCs. To reduce the computational overload of the large sample length signal, the decompositions are carried out using 'R-3.2.2 and Matlab-2014a' concurrently. The kurtosis of each decomposed IMFs are calculated with and without PCA are listed in Table 3.4. To avoid the mode mixing in each of the IMFs, the correlated signals are uncorrelated using PCA. The individual and average kurtosis for all the eleven PCs (principal components) are calculated, (threshold tolerance of -5% is accounted to limit the PCs) to set a limiting threshold. It can be observed from the Fig. 3.22(a) that, even after a combination of the PCs 1, 2, 3, 4, 7 and 8, the resulting center frequencies are in congruence with that of Fig. 3.16(a). However, it is observed from Figs. 3.22(b) and (d) that the intensities for the envelope and the cepstral envelope have increased to a higher value as compared to the standardized results. For envelope detection in Fig. 3.22(b), the amplitudes for the shaft rotation and inner race defect have increased to 0.06 and 0.57 respectively, as compared to 0.05 and 0.55, shown in Fig. 3.16. It is observed that the intensities are significant for the cepstral envelope method with the shaft and fault amplitudes of 49.44 and 48.78 respectively, as shown in Fig. 3.22(d). The harmonics related to the IRD are clearly visible in the cepstral envelope as compared to the envelope spectrum.

Table 3.4 Kurtosis evaluated from decomposed modes using EMD and EMD-PCA

Kurtosis						
IMFs	IR		OR		BD	
	EMD	EMD-PCA	EMD	EMD-PCA	EMD	EMD-PCA
1	4.55	4.54	6.70	6.70	2.68	2.68
2	4.76	4.75	7.13	7.13	2.59	3.17
3	3.36	3.38	4.28	4.29	3.25	2.66
4	3.11	3.11	3.60	3.59	2.84	2.85
5	2.89	2.89	3.56	3.56	2.59	2.60
6	2.54	2.54	3.19	3.16	3.25	3.27
7	3.19	3.20	2.89	2.92	3.22	3.22
8	3.50	3.51	2.79	2.87	2.60	2.66
9	2.94	2.90	3.73	3.66	2.82	2.91
10	2.26	2.56	3.16	2.03	4.56	2.68
11	2.20	2.31	1.64	3.15	0.67	2.73
Average	35.3/11=3.20	35.69=3.24	42.67/11=3.87	43.06/11=3.91	31.07/11=2.82	31.43/11=2.85

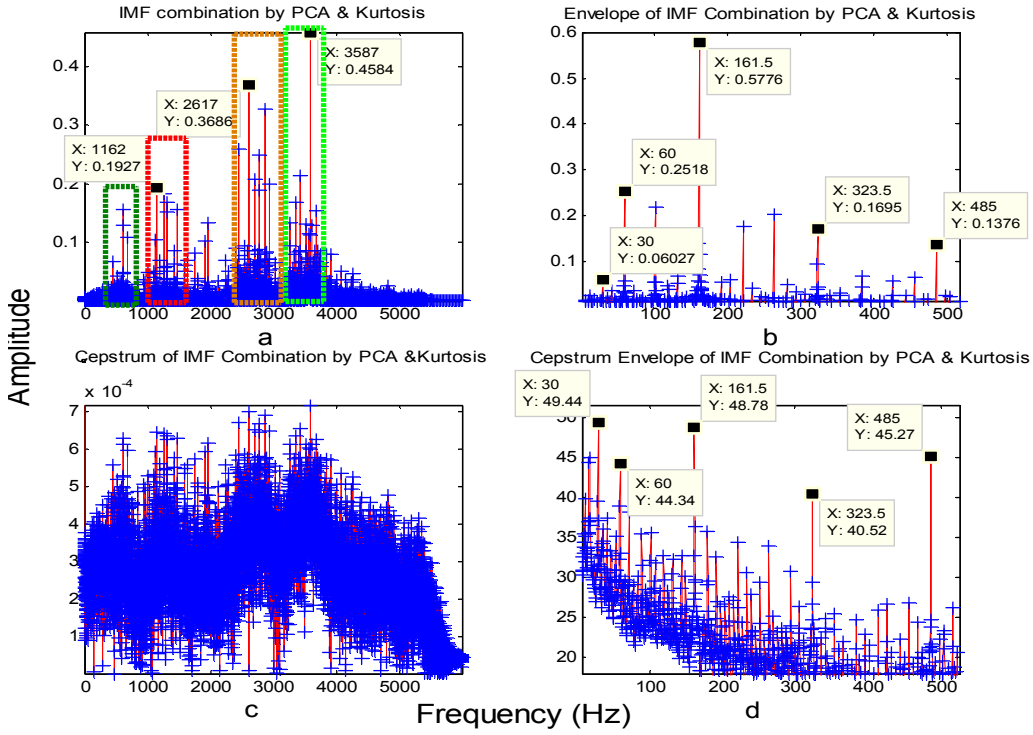

Figure 3.22 EMD-PCA based average kurtosis spectrums for IRD (a) actual (b) envelope (c) cepstral (d) cepstral envelope signals

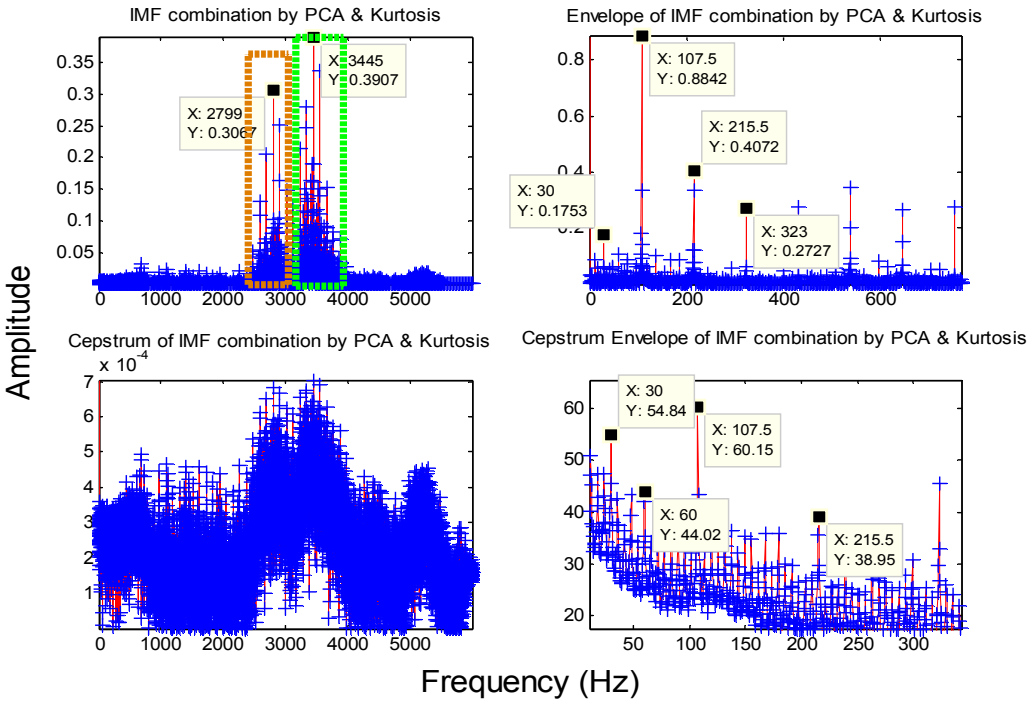

Figure 3.23 EMD-PCA based average kurtosis spectrums for ORD (a) actual (b) envelope (c) cepstral (d) cepstral envelope signals

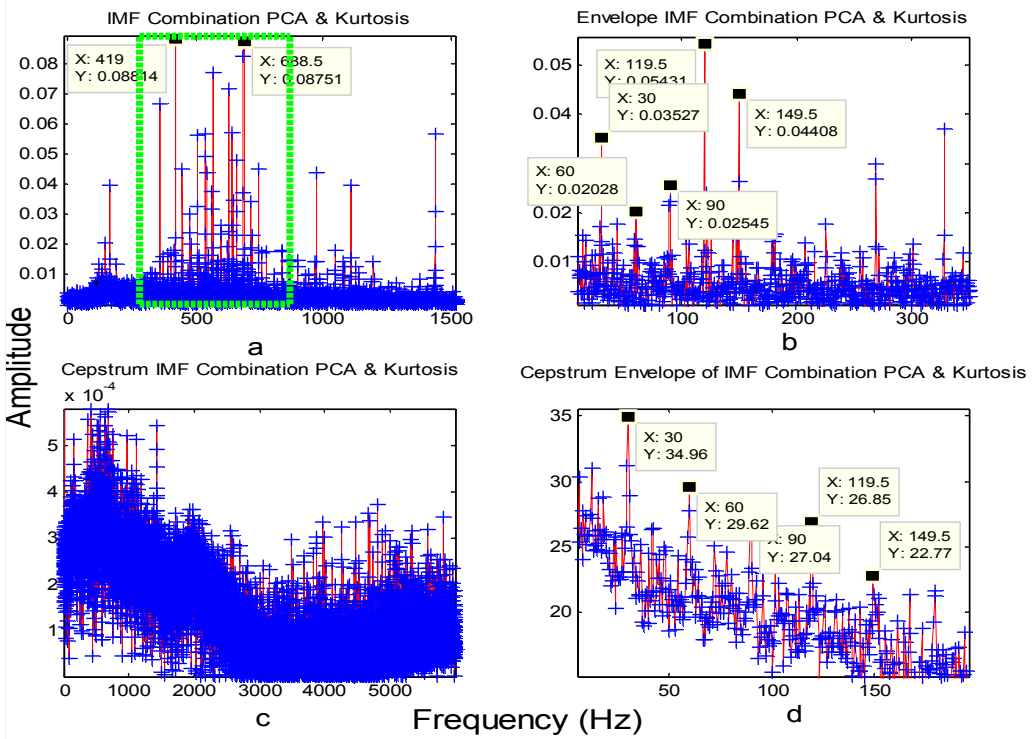

Figure 3.24 EMD-PCA based average kurtosis spectrums for BD (a) actual (b) envelope (c) cepstral (d) cepstral envelope signals

The analysis is further carried out to identify ORD and the corresponding results are shown in Fig. 3.23. Fig. 3.23(a) shows the time series spectrum and the related center frequencies at 3445 and 2799 Hz respectively. To extract the fault, envelope analysis is performed over the time series and is shown in Fig. 3.23(b). It clearly predicts the presence of the fault, and its harmonics related to ORD, even though the shaft rotation is least significant. The spectrum in Fig. 3.23(c) shows no sign of the ORD, further, to modify the signal property and minimize the effect of nonlinearity in sideband; cepstral envelope analysis is performed as shown in Fig. 3.23(d). This analysis clearly detects the presence of faults and shaft rotating frequency significantly, as compared to the envelope detection methods. Finally, it is observed that the Fig. 3.24(a) for BD depicts the center frequency around 688.5 Hz and we can effectively utilize this band to diagnose the fault much better as compared to Fig. 3.18(a). This method traces the center frequency adaptively without the use any pre-filtering or wavelet methods. The standardized results for the envelope detection could not classify the ball defect, whereas, the EMD-PCA method is able to diagnose and trace the shaft and fault frequencies effectively, as shown in Fig. 3.24(b). The cepstrum analysis shows no sign of defect apart from energy concentrated near the center frequency as shown in Fig. 3.24(c). In Fig. 3.24(d), the cepstral envelope diagnoses the fault and shaft frequency effectively, but the intensities are lower than those in Fig. 3.18(d). There are two possible reasons that can be concluded from the envelope and cepstral envelope analysis; 1). If the exact center frequency is identified through kurtosis, then the performance of the envelope detection is better than the cepstral envelope. But, most of the time it is very difficult to identify the center frequency. In those cases, the cepstral envelope can take the lead in identifying the faults as can be observed in the IRD and ORD analysis. 2). The reduction of amplitude in the cepstral envelope may occur sometimes due to the elimination of some of the center frequencies that might be contributing certain energy related to the fault.

It is observed, that the combinational approach, along with the envelope and cepstral envelope based analysis, can be used effectively for identifying the faults. Sometimes, envelope analysis is sufficient in detecting the fault using threshold based combinational approach, but most of the time for a clear visualization of fault and shaft speed the cepstral based envelope analysis can be used, as it works almost all the time irrespective of the nature

of the signals i.e. IRD, ORD, and BD. Table 3.5 shows the impact of different processing techniques on the signal intensities.

Table 3.5 Fault frequencies, shaft speed and the number of IMFs used in different methods

Signals RPM/Fault		Standardized signal		EMD based average kurtosis		EMD-PCA based average kurtosis	
		Envelope	Cepstral Envelope	Envelope	Cepstral Envelope	Envelope	Cepstral Envelope
IRD 0.007"	Speed	***30*** 0.05	***30*** 48.2	***30*** 0.05	***30*** 48.53	***30*** 0.06	***30*** 49.44
	Fault	***161.5*** 0.55	***161.5*** 46.67	***161.5*** 0.56	***161.5*** 49.44	***161.5*** 0.57	***161.5*** 48.78
IMFs used		11	11	6	6	6	6
ORD 0.007"	Speed	***30*** 0.17	***30*** 55.61	***30*** 0.17	***30*** 54.29	***30*** 0.17	***30*** 54.84
	Fault	***107.5*** 0.87	***107.5*** 53.28	***107.5*** 0.88	***107.5*** 59.5	***107.5*** 0.88	***107.5*** 60.15
IMFs used		11	11	4	4	3	3
BD 0.007"	Speed	NS	***30*** 53.36	***30*** 0.03	***30*** 28.95	***30*** 0.03	***30*** 34.96
	Fault	NS	***149.5*** 38.86	***149.5*** 0.04	***149.5*** 21.85	***149.5*** 0.04	***149.5*** 22.77
IMFs used		11	11	6	6	5	5

**Frequencies are represented in bold-italic and amplitudes are in non-italic, NA: not available*

Advantages and Limitations: The main advantage of this technique is that, IRD can be detected by using only six IMFs (with and without PCA), as compared to standardized results that use eleven IMFs. Fault analysis for ORD shows that the combinational approach removes unwanted noise components present in the signal, thereby improving the detection sensitivity of the fault in the spectrum. It is observed from the analysis that even if standardized EMD based technique can be used to identify three different faults, however, the same results can be achieved with fewer IMFs using standardized EMD-PCA based method. The BD defect for the standardized cepstral envelope is significant, but the rpm and the fault frequency are not parred, and also the envelope detection cannot trace the fault. But, by kurtosis based combination approach, the fault frequency is clearly detected in envelope spectrum as compared to the simple standardized cepstral envelope method. The

combinational approach shows significant results when used with the envelope and cepstral envelope techniques.

Limitation: It is observed, the intensity of the cepstral envelope is lower than that of standardized cepstral envelope only when the -5% of the threshold is assumed for BD fault. If kurtosis threshold is close to -10% of the average kurtosis, then the intensity increases to 39.22 at 149.5 Hz, but the envelope performance decreases. However, the dominance of the fault frequency is apparent with -5% of threshold in the combinational approach envelope spectrum as compared to standardized cepstral envelope technique.

3.5 Conclusion

- The fault analysis using both standardized cepstral envelope analysis and standardized EMD-PCA based average kurtosis techniques are useful in tracing the fault significantly.
- For faster detection of the fault, more intuitively, standardized cepstral envelope can be used. But, to clearly visualize the spectrum and significantly identify fault par with the rotation of the shaft, EMD-PCA based kurtosis approach can be adapted.
- Standardization helped to improve the intensity of the signal with least change in the kurtosis and decode the un-correlated effect of amplitude on shape parameters. However, it is observed that the normalization deteriorates the signal extraction process as compared to STD and NSTD methods.
- This approach is improved by the kurtosis selection method applied on IMFs based PCA. The number of IMFs required to reconstruct the signal is lower using EMD-PCA based method as compared to standardized EMD. The fault analysis using adaptive EMD-PCA based method is helpful in identifying the nature of the fault and clearly differentiates the faults and the shaft frequency effectively as well as their harmonics.
- Finally, it is observed from the experimental results that the envelope detection is more susceptible to noise as compared to the cepstral envelope analysis.

CHAPTER 4
Fault Identifications Using Unitary Sliding PDFs

The signals emanating from the bearings are complex and contribute various distributions. The distribution function and the underlying mathematical operations inherited by the signals during propagation have significant effect on statistical moments. This chapter analyzes the effect of various mathematical functions like shifting and shape functions on statistical properties of the signals related to bearings. Initially, the distribution function for healthy, inner race defect (IRD), outer race defect (ORD), and ball defects (BD) are tested using Kolmogorov-Smirnov test (KS- test) to identify the nature of the distribution. After successful investigation of the distribution functions, two different probability density functions i.e. Laplacian and rectangular functions are generated. This is done by formulating the boundary value from the sampling rate, impulse generated by any particular defects and the shaft rotation frequency. These probability density functions are used as unitary sample shifted sliding window over the faulty signals to generate frame based crest factor (FCF), frame based kurtosis (FKS) and frame based energy (FE) time series signals. It is observed that these proposed framing sequence methods effectively identify the faults in the bearings without the use of envelope detection method. Finally, it is concluded that the boundary limit and the probability density function have significant importance in detecting signals related to fault, however, if the boundary is not chosen properly then it may dilute the information content in the signals.

Results! Why, man, I have gotten a lot of results. I know several thousand things that won't work.

-Thomas Alva Edison

4.1 Introduction

Fault detection using vibration is the classical method to intercept incipient faults in bearings. The signals emanating from the bearings are basically nonlinear and non-stationary. The non-linearity along with the non-stationarity can alter the probability density function (pdf). In practical cases, the signal may converge to one or many distributions based on the sampling rate and sample length chosen for the analysis [185]. The probability density

function also depends on the sample length and the sampling rate of the data acquisition device [186,187]. The analysis of probability density function can be carried out using different testing methods like Kolmogorov-Smirnov test (KS-test), Anderson Darlington test (A-D test), Chi- Square test, Shapiro-Wilk normality test etc. [188,189]. The distribution function and the fourth order moment i.e. kurtosis have significant impact in differentiating the state of the bearings. Once the signals are decoded to a particular distribution, the fault can be extracted easily, even if the signals are buried in noise. Even though it seems to be the solution to many problems, still the ambiguity in the extraction persists due to ignorance and lack of understanding about the signal enhancement and extraction process. Therefore, the vital part in signal analysis lies in the study of the behavior of the signal rather than simply extracting information. Similar to the use of distribution functions, the fault can also be addressed using different flavors of kurtosis. This can be calculated in the time domain, frequency domain, and time-frequency domain [190,191]. The kurtosis and distribution functions have significant impact on time series signal and they are influenced by the different mathematical operators used in the demodulation steps [192,193]. Few mathematical operators that can be included to demodulate the signals are envelope detection and cepstrum analysis technique. In bearing fault analysis, envelope detection using Hilbert transform finds wide usage to demodulate the modulated signals [194,195,196]. Therefore, without Hilbert, it is very difficult to identify the lower defect frequency from the modulated signal.

This chapter uses the same setup as that of the previous chapter, but a new algorithm is proposed which can be used to suppress the higher order resonating frequency automatically without using Hilbert transform. The literature discussed above in this chapter uses Hilbert transform to decode the fault in the bearing. However, in this chapter, a unitary sample shifted Laplacian and rectangular probability density functions are proposed to detect and demodulate the defect frequency.

4.2 Kolmogorov Smirnov Testing

Initially, the Kolmogorov Smirnov test (KS-Test) is used to identify the probability density function of different faults related to bearings (CWRU data sets). This test is performed to estimate whether the data sample belongs to particular distribution functions or not. In this approach, the goodness of fit (GOF) test is used to measure the compatibility of a random sample with a theoretical probability distribution function and it works based on the

principle of empirical cumulative distribution function (ECDF). Here, the analysis is carried out using Easyfit to estimate the GOF. For the practicality of the observation the GOF is limited to normal and Laplacian distribution. The ranking is decided based on KS test performed using easyfit, where the best distribution is given a higher rank for a lower statistic; for an example distribution with test statistic 0.01 gets higher rank than that of 0.02. The goodness of fit is measured using distance (test statistics) and threshold value (critical value, 0.05 and 0.01). In this case, initially the distance between distributions and test signal is calculated and finally compared with a threshold value either to select or reject the distribution.

Initially, the distribution functions for ORD and IRD (0.007") are tested using KS test. It is observed from Fig. 4.1(a) that the IRD is closer to Laplacian distribution rather than normal distribution and the pdf is found to be 0.48 approximately. It is observed from Fig. 4.1(b) that the probability density function for ORD increases to 0.48 as compared to the IRD, and the distribution is close to Laplacian. When the KS test is conducted on BD, it is observed that the signal seems to be normally distributed rather than Laplacian, as shown in Fig. 4.1(c). Similarly, when the KS test is performed on higher fault dimension (0.021"), it is observed that the limiting value of the signal and its pdf start increasing drastically. The limiting value for IRD is found to be $-3.2<x<3.2$ for higher dimensional fault, whereas it is $-1.2<x<1.5$ for lower dimension faults; the detailed distributions are shown in Figs. 4.1(d) and (a). Similarly, the probability density function for ORD is observed to be approximately 0.88 with boundary value ranging between $-6<x<6$ for higher dimension fault as compared to $-3.2<x<3.3$ for lower dimensional fault and the details are shown in Figs. 4.1(e) and (b). The above analysis suggests that these distributions for IRD and ORD rather fall in the Laplacian category than in the normal. The same analysis when applied to BD, the distribution function approaches to normal as shown in Fig. 4.1(f). It can be concluded that the ORD and IRD follow the Laplace distribution, whereas, BD follows the normal distributions irrespective of the fault sizes. It can be inferred from the analysis that the distribution of the signal can either be Gaussian or Laplacian or of mixed types (most likely rankings of the distributions are taken into account). The rank wise analysis shows that the BD and healthy bearings for 0.007" and 0.021" defects best fit the normal distribution than the Laplacian distributions, but the reverse is true for the IRD and ORD defects. This test is performed on global and local signals repetitively with variation in sample size to validate the repeatability of their distributions [197].

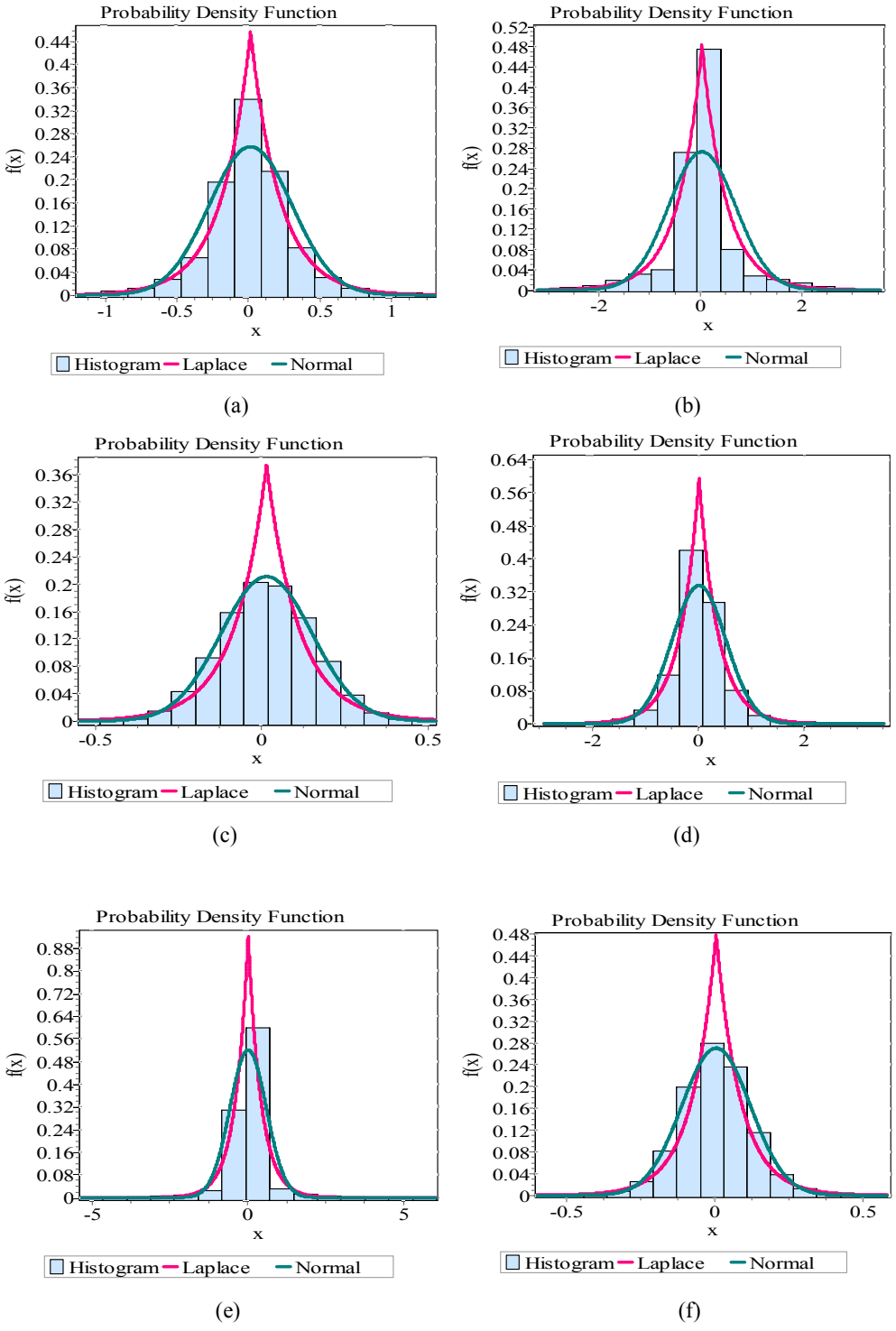

Figure 4.1 Probability density function (a) IRD, (b) ORD, (c) BD for 0.007" and (d) IRD, (e) ORD, (f) BD for 0.021"

4.3 Impact of Noise on Statistical Parameters

In this section, the effect of noises on the behavior of higher order statistics (HOS) i.e. kurtosis and crest factor (CF) are studied. The equations detailing the calculation of the different moments are detailed in Table 2.1. Initially, the faulty and healthy data sets of the bearings are taken as the reference and further different percentage of Gaussian and Laplacian noises are added to the signals as in (4.1).

$$\left.\begin{aligned} x_{nH} &= x_H + \delta x_{H|_{RMS}}.N_y(length(x_H)) \\ x_{nIRD} &= x_{IRD} + \delta x_{IRD|_{RMS}}.N_y(length(x_{IRD}) \\ x_{nORD} &= x_{ORD} + \delta x_{ORD|_{RMS}}.N_y(length(x_{ORD}) \\ x_{nBD} &= x_{BD} + \delta x_{BD|_{RMS}}.N_y(length(x_{BD}) \end{aligned}\right\} \tag{4.1}$$

where x_H, x_{IRD}, x_{ORD} and x_{BD} are the healhy, inner race, outer race and ball defect signals. x_{nH}, x_{nIRD}, x_{nORD} and x_{nBD} are the modified noisy signals for the healthy, inner, outer and ball defects. δ is 0, 0.2, 0.4, 0.6 and 0.8 respectively. $x_{H|_{RMS}}$, $x_{IRD|_{RMS}}$, $x_{ORD|_{RMS}}$, $x_{BD|_{RMS}}$ are the R.M.S value for the healthy, inner, outer and ball defect signals. N_y represents noise types i.e. Laplacian and Gaussian noises.

It can be observed from the Table 4.1 that after adding noise to the healthy bearing signals, the kurtosis started increasing from 2.802 to 2.915, and it indicates the change in the shape factor. The same rising pattern is observed for the ball defect i.e. the kurtosis increases from 2.952 to 3.037. But, dramatic changes are observed for IRD and ORD, i.e. the kurtosis started falling to a lower value due to the addition of Gaussian noise. The kurtosis decreased from 5.380 to 3.910 for IRD and 7.556 to 4.685 for ORD as shown in Fig. 4.2(a). It can be inferred that the vibration signals for healthy, BD, IRD and ORD exhibit different distributions. Similarly, the change in the kurtosis for different δ and for higher fault dimension is shown in Fig. 4.2(b).

Table 4.1 Statistical results for healthy, IRD, ORD and BD (0.007") for Gaussian noise

	P	Mean	RMS	Var	SD	PV	CF	SK	KS	CLF	IF	SF
Healthy	0	0.011	0.073	0.005	0.072	0.260	**3.534**	-0.076	**2.802**	74.106	4.394	1.243
	0.2	0.011	0.075	0.005	0.074	0.265	**3.533**	-0.074	**2.821**	72.775	4.395	1.243
	0.4	0.011	0.079	0.006	0.078	0.300	**3.785**	-0.066	**2.857**	73.881	4.710	1.244
	0.6	0.011	0.085	0.007	0.085	0.339	**3.949**	-0.058	**2.891**	71.230	4.916	1.244
	0.8	0.011	0.094	0.008	0.0939	0.378	**4.000**	-0.050	**2.915**	66.003	4.996	1.246
IRD	0	0.014	0.289	0.083	0.289	1.398	**4.832**	0.130	**5.380**	32.44	6.735	1.393
	0.2	0.014	0.294	0.0867	0.294	1.457	**4.941**	0.121	**5.212**	31.96	6.825	1.381
	0.4	0.014	0.311	0.096	0.310	1.552	**4.987**	0.099	**4.790**	29.216	6.735	1.350
	0.6	0.014	0.337	0.113	0.336	1.670	**4.954**	0.073	**4.312**	25.617	6.541	1.320
	0.8	0.014	0.370	0.136	0.369	1.810	**4.889**	0.049	**3.910**	22.241	6.345	1.297
ORD	0	0.032	0.661	0.436	0.660	3.380	**5.108**	0.064	**7.556**	20.844	8.393	0.032
	0.2	0.033	0.676	0.455	0.675	3.429	**5.073**	0.044	**7.214**	18.853	8.041	1.584
	0.4	0.034	0.715	0.510	0.714	3.600	**5.034**	0.023	**6.384**	15.524	7.476	1.484
	0.6	0.035	0.775	0.599	0.774	3.771	**4.864**	0.007	**5.458**	12.384	6.834	1.404
	0.8	0.036	0.851	0.724	0.851	3.965	**4.655**	-0.002	**4.685**	9.970	6.288	1.350
BD	0	0.015	0.137	0.018	0.136	0.541	**3.935**	-0.022	**2.952**	44.661	4.919	1.249
	0.2	0.014	0.140	0.019	0.139	0.568	**4.046**	-0.013	**2.979**	45.125	5.064	1.251
	0.4	0.014	0.148	0.0214	0.147	0.613	**4.135**	-0.005	**3.004**	43.807	5.185	1.253
	0.6	0.014	0.160	0.025	0.160	0.664	**4.134**	0.0007	**3.023**	40.475	5.188	1.254
	0.8	0.014	0.176	0.031	0.176	0.716	**4.052**	0.004	**3.037**	36.096	5.084	1.254

*Var:Variance,SD:Standard Deviation,PV: Peak Value, CF:Crest Factor,SK:Skewness, KS:Kurtosis, CLF:Clearance Factor, IF: Impulse Factor

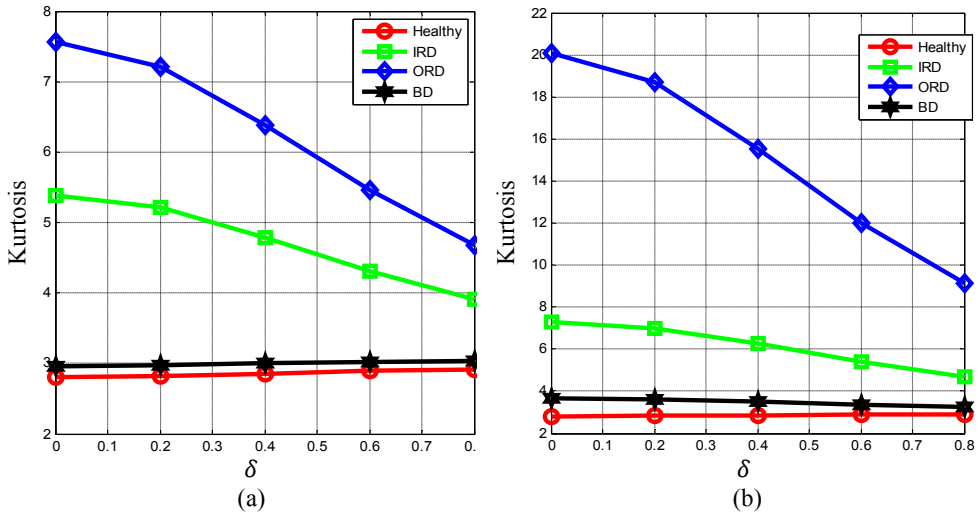

Figure 4.2 Impact of different level of noise on kurtosis of Healthy, IRD, ORD, BD (a) 0.007" (b) 0.021"

To infer more information, Laplacian noise is added to the signals as shown in Table 4.2. It is observed that the CF for the healthy, IRD, ORD, BD are ranging between 3.534-5.173, 4.832-5.470, 5.108 -5.147, and 3.935-5.090 respectively. It is depicted that CF increases for healthy, IRD and BD defects, whereas, it decreases for ORD. Data shows different behaviour in case of CF for variable noises. It is verified that due to the addition of Gaussian and Laplacian noises the skewness of the signals for IRD and ORD move towards zero i.e. from positive to zero. Whereas, the skewness for BD and healthy signals moves from negative to zero.

Table 4.2 Statistical results for healthy, IRD, ORD and BD (0.007") for Laplacian noise

	P	Mean	RMS	Var	SD	PV	CF	SK	KS	CLF	IF	SF
Healthy	0	0.011	0.073	0.005	0.072	0.260	**3.534**	-.076	**2.802**	74.106	4.394	1.243
	0.2	0.011	0.075	0.005	0.074	0.274	**3.650**	-.060	**2.840**	75.220	4.545	1.245
	0.4	0.011	0.079	0.006	0.078	0.342	**4.300**	-.041	**2.954**	84.477	5.375	1.250
	0.6	0.011	0.086	0.007	0.085	0.415	**4.826**	-.024	**3.166**	88.638	6.071	1.258
	0.8	0.011	0.094	0.008	0.093	0.489	**5.173**	-.012	**3.456**	88.151	6.570	1.270
IRD	0	0.014	0.289	0.083	0.289	1.398	**4.832**	0.130	**5.380**	32.443	6.735	1.393
	0.2	0.014	0.294	0.086	0.293	1.419	**4.824**	0.110	**5.210**	31.261	6.662	1.380
	0.4	0.014	0.310	0.095	0.309	1.562	**5.037**	0.083	**4.822**	29.930	6.838	1.357
	0.6	0.014	0.335	0.112	0.335	1.732	**5.165**	0.056	**4.479**	27.636	6.919	1.339

	0.8	0.013	0.367	0.135	0.367	2.013	**5.470**	0.036	**4.316**	26.340	7.282	1.331
ORD	0	0.032	0.661	0.436	0.660	3.380	**5.108**	0.064	**7.556**	20.844	8.393	1.643
	0.2	0.031	0.673	0.453	0.673	3.301	**4.898**	0.055	**7.170**	18.312	7.775	1.587
	0.4	0.031	0.711	0.504	0.710	3.555	**4.999**	0.046	**6.352**	15.912	7.521	1.504
	0.6	0.031	0.769	0.590	0.768	3.891	**5.058**	0.039	**5.542**	13.692	7.300	1.443
	0.8	0.031	0.844	0.712	0.843	4.347	**5.147**	0.036	**4.984**	12.037	7.234	1.405
BD	0	0.015	0.137	0.018	0.136	0.541	**3.935**	-.022	**2.952**	44.661	4.919	1.249
	0.2	0.015	0.140	0.019	0.139	0.543	**3.876**	-.020	**2.969**	43.220	4.847	1.250
	0.4	0.015	0.147	0.021	0.147	0.605	**4.094**	-.016	**3.035**	43.445	5.128	1.252
	0.6	0.015	0.159	0.025	0.159	0.745	**4.666**	-.010	**3.186**	46.251	5.873	1.258
	0.8	0.015	0.175	0.030	0.174	0.892	**5.090**	-.003	**3.412**	46.702	6.455	1.268

For more intuitive analysis, the signals generated using equation (4.1) are linearized using cepstrum analysis and later different concentration of noises are added by changing δ. It is observed from the Table 4.3 that the kurtosis and crest factor start falling with an increase in noise and these analyses are in congruence for healthy, IRD, ORD and BD faults. It is observed that the presence or absence of linearization has different impact on signals i.e. by slight modification in mathematical operators the statistical parameter of the faulty and healthy signals change drastically. The same observation is found for Laplacian linearized function as shown in Table 4.4. It is observed from the analysis that the complexity of the algorithms and mathematical operators used to extract the information can change the actual perception about signals.

Table 4.3 Linearized statistical results for healthy, IRD, ORD and BD (0.007") for Gaussian noise

	P	Mean	RMS	SD	PV	CF	SK	KS	CLF	IF
Healthy	0	0.0	0.010	0.010	0.580	**54.801**	49.403	**4318.580**	38550.638	149.632
	0.2	0.0	0.010	0.0108	0.581	**53.830**	46.569	**3992.466**	31917.735	136.261
	0.4	0.0	0.011	0.011	0.582	**51.046**	39.492	**3205.700**	21210.675	111.167
	0.6	0.0	0.012	0.012	0.583	**47.206**	31.059	**2328.327**	13698.351	89.408
	0.8	0.0	0.013	0.013	0.584	**43.041**	23.409	**1598.299**	9204.920	73.349
	0	0.0	0.014	0.014	1.209	**82.109**	78.295	**10626.825**	86345.023	323.195

IRD	0.2	0.0	0.015	0.015	1.212	**80.552**	73.284	**9760.121**	58095.537	265.374
	0.4	0.0	0.015	0.0159	1.214	**76.316**	61.773	**7796.688**	30731.249	193.204
	0.6	0.0	0.017	0.0172	1.217	**70.545**	48.362	**5644.635**	17588.253	146.310
	0.8	0.0	0.018	0.018	1.219	**64.323**	36.334	**3868.852**	11103.993	116.370
ORD	0	0.0	0.016	0.016	1.276	**77.925**	59.908	**7830.512**	91881.292	342.431
	0.2	0.0	0.016	0.016	1.279	**76.469**	56.009	**7185.243**	56603.469	269.087
	0.4	0.0	0.017	0.017	1.282	**72.463**	47.148	**5732.910**	27636.579	188.244
	0.6	0.0	0.019	0.019	1.285	**66.995**	36.861	**4145.177**	15324.069	140.338
	0.8	0.0	0.021	0.021	1.288	**61.097**	27.657	**2837.665**	9546.205	110.895
BD	0	0.0	0.011	0.011	0.791	**66.567**	1.048	**2456.814**	48311.326	195.595
	0.2	0.0	0.012	0.012	0.791	**65.272**	0.844	**2267.473**	38672.013	174.921
	0.4	0.0	0.012	0.012	0.790	**61.802**	0.595	**1819.458**	24503.344	139.177
	0.6	0.0	0.013	0.013	0.789	**57.065**	0.372	**1320.791**	15383.300	110.228
	0.8	0.0	0.015	0.015	0.789	**51.946**	0.208	**905.890**	10176.932	89.616

Table 4.4 Linearized statistical results for healthy, IRD, ORD and BD (0.007") for Laplacian noise

	P	Mean	RMS	SD	PV	CF	SK	KS	CLF	IF
Healthy	0	0.0	0.010	0.010	0.580	**54.801**	49.403	**4318.589**	38550.638	149.632
	0.2	0.0	0.010	0.010	0.582	**54.061**	46.654	**4006.960**	32664.777	137.954
	0.4	0.0	0.011	0.011	0.584	**51.550**	39.795	**3246.187**	22908.210	115.711
	0.6	0.0	0.012	0.012	0.586	**47.950**	31.510	**2381.720**	15602.555	95.644
	0.8	0.0	0.013	0.013	0.588	**43.955**	23.886	**1649.032**	10926.430	80.164
IRD	0	0.0	0.014	0.014	1.209	**82.109**	78.295	**10626.825**	86345.023	323.195
	0.2	0.0	0.014	0.014	1.209	**80.698**	73.802	**9841.920**	61223.681	272.113
	0.4	0.0	0.015	0.015	1.209	**76.668**	62.842	**7959.669**	34786.355	205.087
	0.6	0.0	0.0170	0.0170	1.208	**71.060**	49.684	**5831.048**	20874.202	158.848
	0.8	0.00	0.018	0.018	1.208	**64.913**	37.610	**4031.306**	13563.021	128.026
	0	0.0	0.016	0.016	1.276	**77.925**	59.908	**7830.512**	91881.292	342.431
	0.2	0.0	0.016	0.016	1.277	**76.540**	56.6157	**7262.094**	58302.682	272.881

ORD	0.4	0.00	0.017	0.017	1.278	**72.594**	48.175	**5855.359**	30787.520	198.375
	0.6	0.0	0.019	0.019	1.279	**67.146**	38.024	**4270.557**	17929.856	151.446
	0.8	0.0	0.020	0.020	1.280	**61.226**	28.757	**2942.178**	11488.822	121.276
BD	0	0.0	0.011	0.011	0.791	**66.567**	1.048	**2456.814**	48311.326	195.595
	0.2	0.0	0.012	0.012	0.791	**65.220**	1.110	**2264.157**	38891.130	175.438
	0.4	0.0	0.012	0.012	0.790	**61.721**	1.043	**1816.460**	25548.747	142.151
	0.6	0.0	0.013	0.013	0.790	**56.984**	0.898	**1320.416**	16742.957	115.039
	0.8	0.0	0.015	0.015	0.789	**51.880**	0.730	**908.097**	11457.353	95.134

In this chapter, rather than using complex mathematical operators or functions, the analysis is carried out by examining every bit of localized time domain samples. These analyses mainly concentrate on CF, KS, and Energy that are mostly influenced by the mathematical functions and produce significant patterns for different faults.

4.4 Proposed Signal Extraction Techniques

The signal emanating from the bearings are nonlinear and non-stationary in nature. There are no universal algorithms that can be used to depict all kinds of faults irrespective of the operating conditions. In this chapter, unitary sample shifted Laplacian and rectangular frame based kurtosis (FKS), frame based crest factor (FCF) and frame based energy (FE) time series signals are generated from the CWRU experimental data sets as shown in Fig. 4.3 [198]. In the past, kurtosis was used by many researchers both in time and frequency domains to identify the faults. Especially, the spectral kurtosis (SK) is used to select the energy band representing maximum kurtosis. The SK, even though promising, does not consider the ill effect of its sensitivity i.e. the effect of a unitary sample shift on the signals. Finally, it is observed from the literature that, SK and envelope techniques can be used to detect faults [199]. However, these methods do not consider the effect of even a unitary sample on the behavior of kurtosis and also on the resonating frequencies [200].

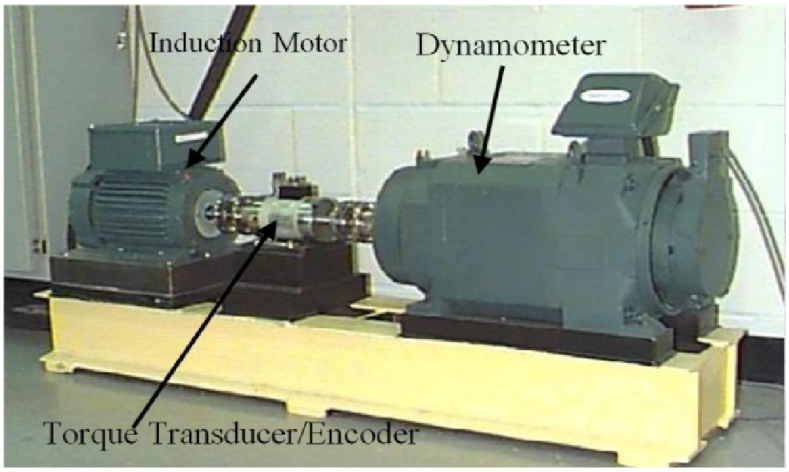

Figure 4.3 Experimental setup

In this chapter, a unitary sample shifted Laplacian and rectangular frame-based techniques are proposed to generate FCF, FKS and FE time series signals. These time series signals are generated for the IRD and ORD vibration signals. The main advantage of this proposed algorithm over other traditional techniques is that it can be used to suppress resonating frequency automatically by simply sliding the distribution window. This method does not need conventional Hilbert transform to extract the fault frequency. The steps adopted for signal extraction and analysis are mentioned below and shown in Fig. 4.4;

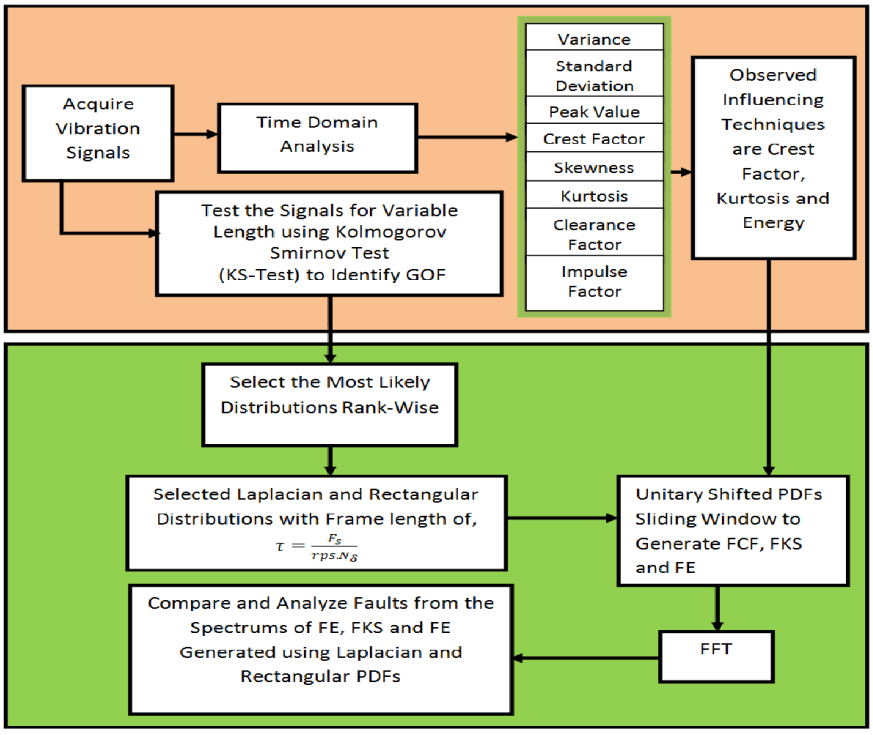

Figure 4.4 Overall process flow adapted in this chapter to anlyse the defects in the bearings

1. The vibration signals are acquired at a sampling rate of 12000 samples per sec.
2. For data analysis, 24000 samples are taken.
3. The different signals are segmented using the rectangular and Laplacian recursive unitary sample shifted sliding frame-based techniques.
4. The frame size τ is controlled by the sampling rate, rpm and the number of impulses generated for one complete shaft rotation and can be calculated as follows; $\tau = \frac{F_S}{rps.N_\delta}$.
5. FCF, FKS and FE time series signals are generated using frame-based techniques and the detail is given in Fig. 4.5.
6. The faults are identified from their spectrum and their effects are studied in detail.

Firstly, the rectangular frames are generated by recursive unitary frame shift technique using (4.2). FKS, FCF and FE time series are generated using rectangular unitary shifted frames as in (4.3), (4.4) and (4.5).

$$X_p = x[n](u[n-p] - u[n-\tau-p])|_{\tau=\frac{F_S}{rps.N_\delta}} \tag{4.2}$$

$$Y_{R|FKS}[p] = Kurt[X_p] = \frac{E[(X_p - \mu_{X_p})^4]}{(E[(X_p - \mu_{X_p})^2])^2} \tag{4.3}$$

$$Y_{R|FCF}[p] = CF[X_p] = \frac{0.5.(\max(X_p) - \min(X_p))}{\sqrt{\frac{1}{\tau}\sum_p^{\tau+p} {X_p}^2}} \tag{4.4}$$

$$Y_{R|FE}[p] = E[X_p] = \sum_p^{\tau+p} {X_p}^2 \tag{4.5}$$

The spectral analysis of the signals generated using rectangular frames is further verified using FFT (4.6).

$$X_{Y_R}(k) = \sum_{n=0}^{N-1} {Y'}_R[n].e^{-j2\pi kn/N} \tag{4.6}$$

where $p = 0, 1, 2 \ldots . N - \tau - 1$; and $n = k = 0, 1, 2, N-1$, F_s sampling rate, τ is frame length for single impulse and N_δ is the number of impulses generated for one complete rotation (depends on fault types) and X_p is the rectangular frame, $Y_R[p]|_{\text{FCF,FKS,FE}}$ are the time series generated using rectangular time shifted frames, $Y'_R[n]|_{\text{FCF,FKS,FE}}$ are the final time series after padding, and *rps* is the revolution of shaft per second.

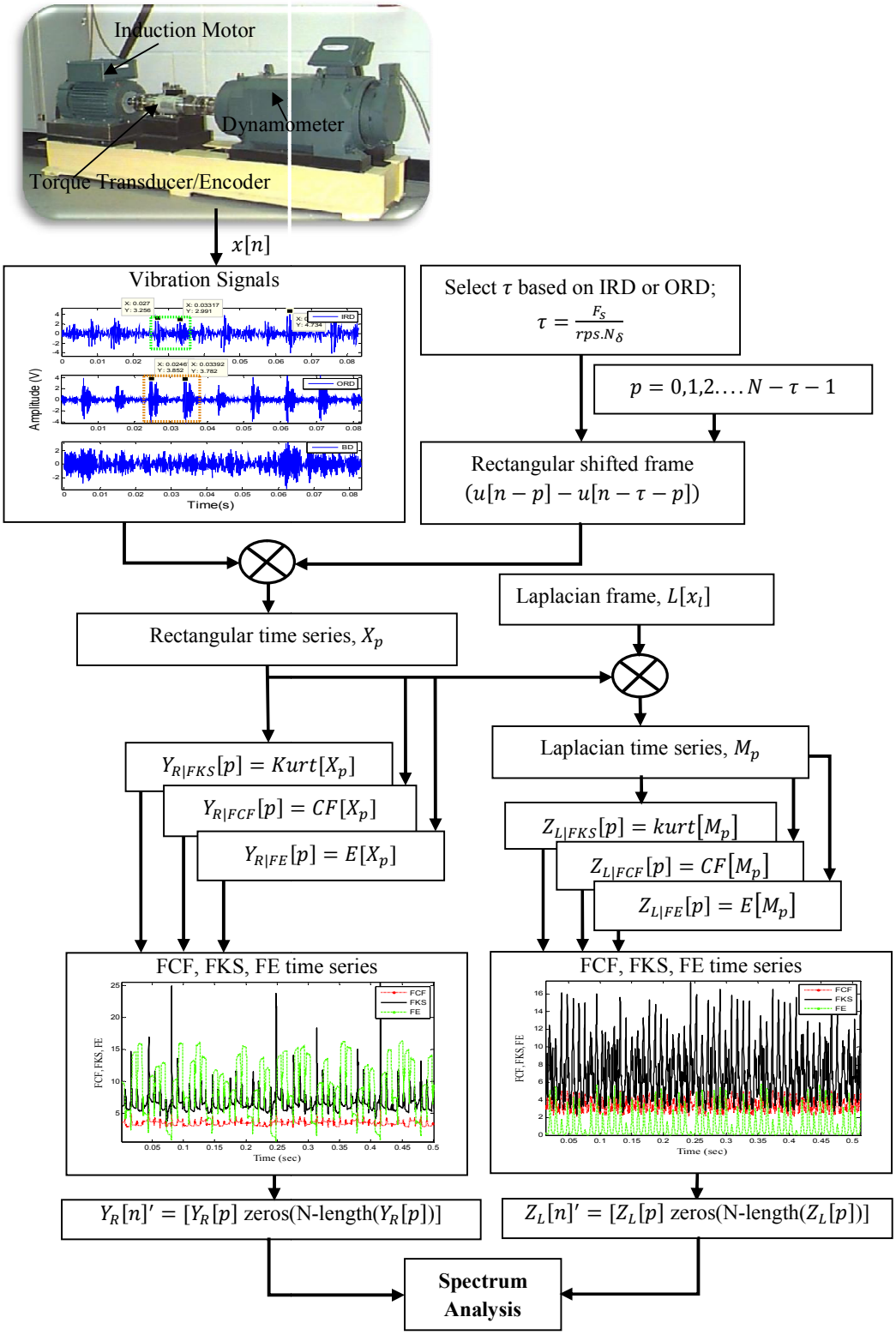

Figure 4.5 Proposed algorithm to generate FCF, FKS and FE using Laplacian and rectangular pdf

Secondly, Laplacian window function in (4.7) is applied over the rectangular frames in (4.2) to generate new shifted signals as in (4.8). Further, the generated signals are used to calculate the kurtosis, crest factor and energy as in (4.9), (4.10) and (4.11).

$$L[x_l] = \frac{1}{2b}\begin{cases} e^{\left(-\frac{\mu - x_l}{b}\right)} & if\ x_l < \mu \\ e^{\left(-\frac{x_l - \mu}{b}\right)} & if\ x_l \geq \mu \end{cases} x_l \in R\ \&\ b > 0 \tag{4.7}$$

where x_l is data sequence for the assumed boundary value of $x_l \in R$, μ is the location parameter or the mean, b is the diversity and assumed to be 1/2.

$$M_p = L[x_l]X_p \tag{4.8}$$

$$Z_{L|FKS}[p] = kurt[M_p] = \frac{E[(M_p - \mu_{M_p})^4]}{(E[(M_p - \mu_{M_p})^2])^2} \tag{4.9}$$

$$Z_{L|FCF}[p] = CF[M_p] = \frac{0.5.(\max(M_p) - \min(M_p))}{\sqrt{\frac{1}{\tau}\sum_p^{\tau+p} {M_p}^2}} \tag{4.10}$$

$$Z_{L|FE}[p] = E[M_p] = \sum_p^{\tau+p} {M_p}^2 \tag{4.11}$$

The spectral analysis of these signals generated using Laplacian frames are further analyzed using FFT in (4.12).

$$X_{Z_L}(k) = \sum_{n=0}^{N-1} {Z'}_L[n].e^{-j2\pi kn/N} \tag{4.12}$$

where $L[x_l]$ is the Laplacian frame, M_p is the Laplacian frame over the rectangular frames, $Z_L[p]|_{\text{FCF,FKS,FE}}$ are the time series generated using Laplacian time shifted frames, ${Z'}_L[n]|_{\text{FCF,FKS,FE}}$ are the final time series signals after padding.

The Laplacian distribution intensities for different values of x_l are shown in the Fig. 4.6. The boundary has tremendous impact on tail of the distribution and thereby improves or degrades the signal extraction. The constructions of the frames are interlinked and their properties are affected by the boundary conditions. Generally, the Laplacian distribution is having heavy tail, and can be divided into three different parts i.e. fat tail, long-tail and sub-exponential distributions. It is observed from the Fig. 4.6 that as x_l increases the signal approaches towards longer tail rather than fat tails i.e. maximum number of samples are in the tail end. For lower value of x_l, the distribution is flat and behaves like uniform distribution. Based on the type of the distribution and the range of kurtosis, the distribution

can be divided into three parts; mesokurtic, leptokurtic and platykurtic. The uniform distribution is regarded as platykurtic, Laplacian distribution is leptokurtic and normal distribution as mesokurtic. It is observed that the probability density function (pdf) has uniform values as x_l decreases. It means, the rectangular frame can be constructed from the Laplacian frame by changing the boundary value i.e. $-0.1 < x_l < 0.1$. The boundary value or limiting value of x_l for $b = 1$, creates variable property of the distribution i.e. the maximum number of zeros are placed at the tails for larger value of x_l. After significant validation, the optimal boundary range between $-3.2 < x_l < 3.3$ is achieved for the generation of Laplacian pdf with fat tail distribution.

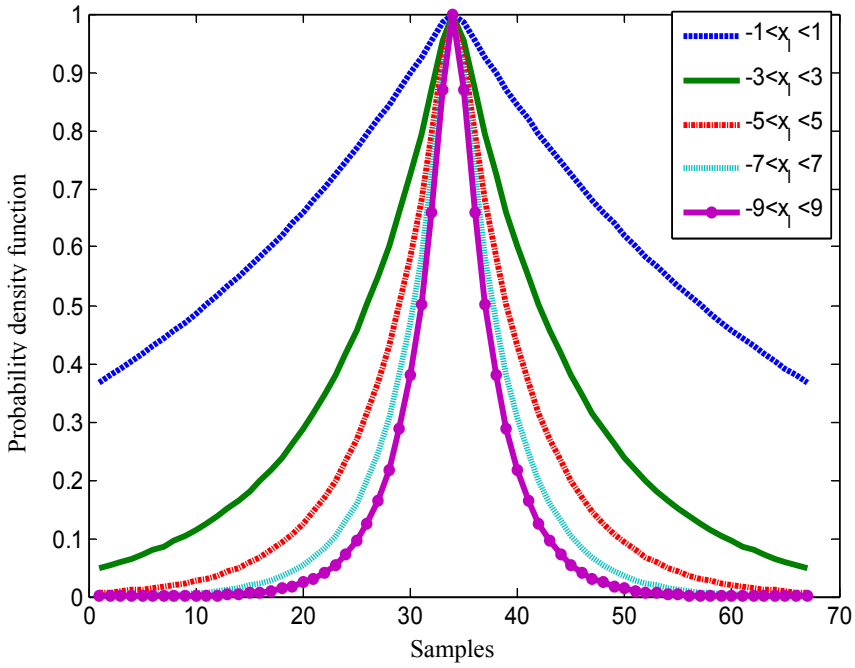

Figure 4.6 Laplacian pdf with different boundary values

4.5 Results and Analysis

This chapter concentrates on IRD and ORD analysis for two different fault sizes of 0.007" and 0.021" respectively. Initial analyses are carried out by using large sample length data and Hilbert transform is applied on these to demodulate the fault from higher order modulating carrier frequencies. Finally, the observation and analysis are carried out using the proposed technique to extract information without using Hilbert transform.

4.5.1 Case Study 1: Fault Identification Using Conventional Hilbert Spectral Analysis Techniques (IRD and ORD of 0.007")

The signals from the bearings are AM-FM in nature; therefore, for segregations of fault signals from the carrier, conventional Hilbert transform with a modified sample length is adapted to demodulate the signal. In [133], the center frequencies representing the maximum energy are filtered by band pass filter and then the envelope detector is used to identify the fault. But this analysis can be satisfied using padding free large sample length selection approach. In envelope detection, the modulated carrier signal can be transferred to the Hilbert domain using (3.12). Fig. 4.7 shows the IRD and ORD spectrums for the actual vibration and envelope signals. Fig. 4.7(a) shows the presence of multiple modulated center frequencies in the spectrum. Envelope spectra using Hilbert transform in 4.7(b) detects the second order harmonics of the rotational frequency i.e. 60 Hz and the IRD frequency of 161.5 Hz effectively. It is observed from the figures that the rotational frequency is least significant in the spectrum. Similarly, ORD in Fig. 4.7(c) shows no traces of the fault, rather it indicates the presence of significant intensity around 3445 Hz. Generally, for these types of modulated signals (high frequency signals), the SK techniques are used to trace the band depicting the actual energy band. Once the energy band is identified, then envelope detection is used to identify the faults. Fig. 4.7(d) shows the rotational frequency of 30 Hz and the fault frequency of 107 Hz after envelope detection.

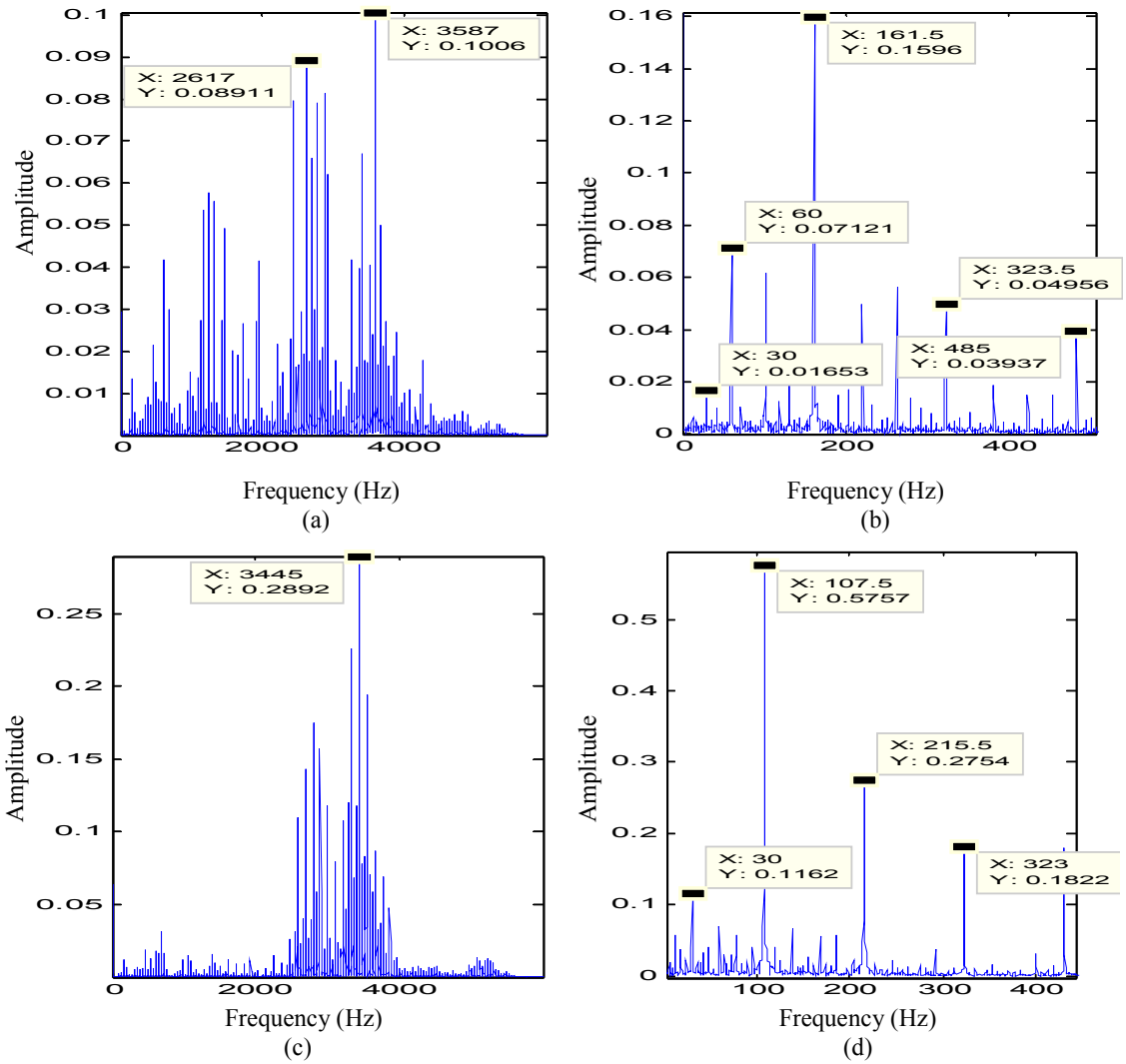

Figure 4.7 (a) spectrum (b) spectral envelope for IRD; (c) spectrum (d) spectral envelope for ORD

4.5.2 Case Study 2: Fault Identification Using Proposed Unitary Sample Shifted Rectangular Sliding Frames (IRD and ORD of 0.007")

The proposed technique does not perform any Hilbert transform to extract information from the signal; rather it automatically suppresses the center frequencies by unitary sample shifted method. Hence, it avoids the search for the center frequencies that represents the maximum kurtosis, as prevalently used in conventional SK analysis methods.

Fig. 4.8(a) shows the FCF, FKS and FE generated from the vibration signals using (4.3), (4.4) and (4.5) respectively. It shows that the FKS, FCF, and FE change suddenly from lower to higher values at certain sample points due to the iterative shifting of the rectangular frame. It is observed that the signals generated by FCF and FKS are loosely periodic impulses, whereas, it is rectangular for FE i.e. the energy remains stable for a certain time,

even after sliding of the frames. Therefore, signals generated using the framing methods are observed to be least corrupted by noise and the peaks are detected effectively. Thus it can be concluded that even a unitary sample shift can change the outlier of the signal and the distribution; this analysis is in congruence with the statement given by West fall on kurtosis [192]. Therefore, sliding the frame by even a unitary sample can change the distribution, and hence, thereby changing the kurtosis. It is observed that the defect signals may not be holding a single distribution, rather a mixed distribution, as the time and environmental state changes. Therefore, during operation of machineries, assuming a random frame or the window size can create disturbance in the signal analysis as well as on kurtosis estimation.

Fig. 4.8(b) shows that the FCF, FKS, and FE for ORD increase as compared to IRD. If the FE and FKS are calculated for the same time frame, it is observed from Figs. 4.8(a) and (b) that the FE is not significant when the kurtosis is high. Hence, the kurtosis does not suggest higher energy accumulation. Therefore, for better visualization of all these generated frames, FFT is used to construct the spectrum as shown in Fig. 4.9. It shows that the rotational (30 Hz) and the fault (161.5 Hz) frequencies are apparent without the use of Hilbert spectral analysis. The FKS and FE in Figs. 4.9(b) and (c) trace the rotational frequency and the IRD fault significantly. However, FCF depicts the rotational and the fault frequencies along with a spurious significant peak at 72 Hz respectively.

Fig. 4.10 shows the ORD spectral plots for the time series generated using FCF, FKS, and FE. Fig. 4.10(a) traces the fault frequency of 107.5 Hz with ease, but the rotational frequency is unnoticeable. Fig. 4.10(c) identifies the rotational and the fault frequencies effectively, but is diluted by other frequency components. It is also observed that the fault frequency is having lower intensity as compared to the rotational frequency. Similarly, FKS in Fig. 4.10(b) clearly depicts the presence of rotational and the fault frequencies effectively.

These three methods using rectangular sliding frames are significant in detecting the IRD and ORD faults and the rotational frequencies effectively. These proposed methods automatically suppress the presence of higher order resonating frequencies and thereby avoid the use of envelope technique. It is observed that this method acts as a filter for the higher order modulated frequency and helps in reducing the presence of sidebands.

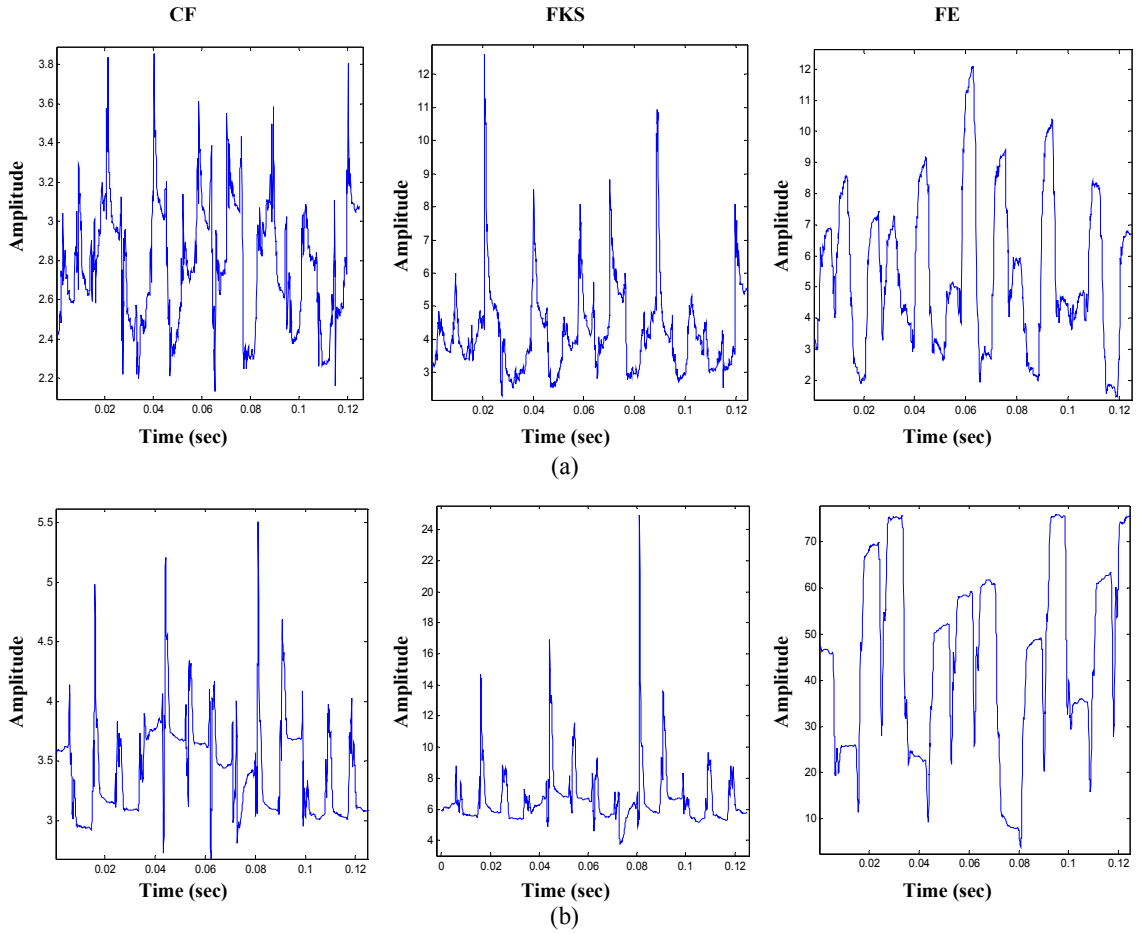

Figure 4.8 Rectangular time series FCF, FKS and FE (a) IRD (b) ORD for 0.007" fault

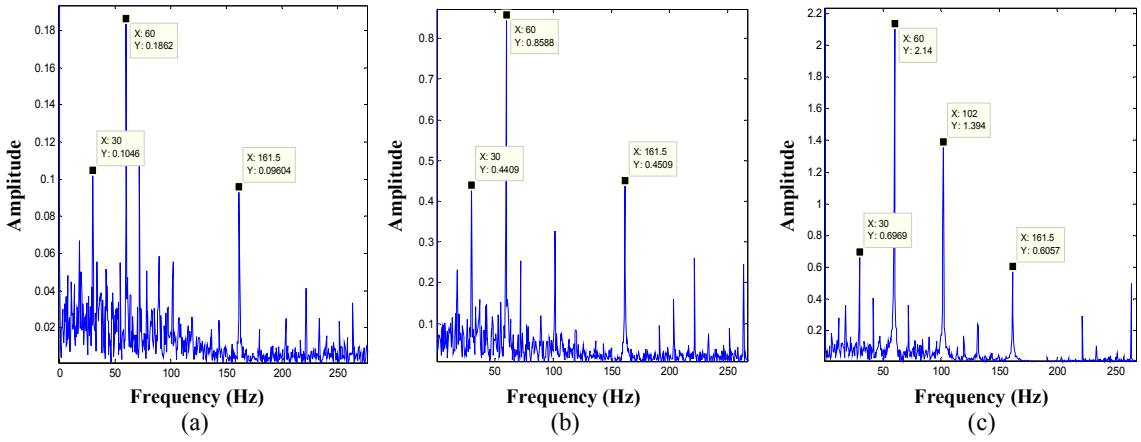

Figure 4.9 FFT of rectangular frames for IRD (a) FCF (b) FKS (c) FE for 0.007" fault

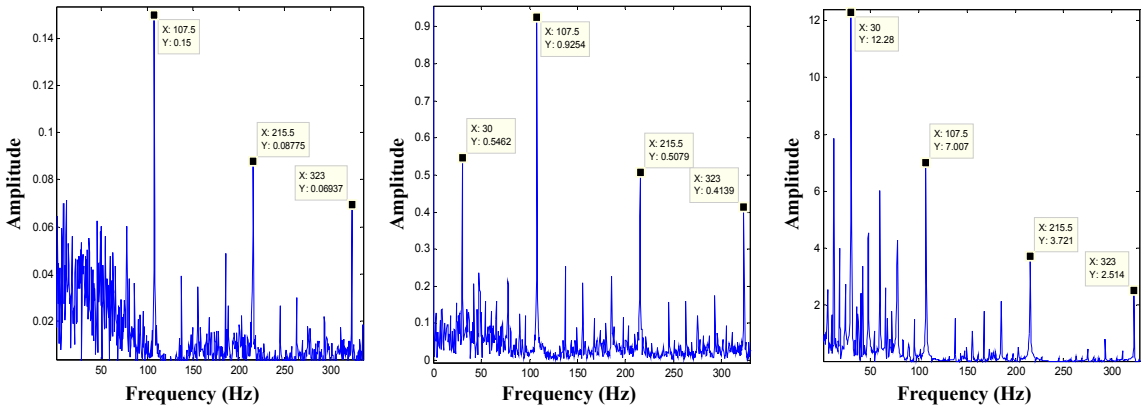

Figure 4.10 FFT of rectangular frames for ORD (a) FCF (b) FKS (c) FE for 0.007" fault

4.5.3 Case Study 3: Fault Identification Using Proposed Unitary Sample Shifted Laplacian Sliding Frames (IRD and ORD of 0.007")

In this section, the Laplacian fat tail distribution function is used to analyze the IRD and ORD signals. Figs. 4.11(a) and (b) show the FCF, FKS and FE time series generated using unitary time shifted Laplacian frame. It is observed that the impulses are nearer as compared to signals generated using the rectangular frame, as in Fig. 4.8. Frame-based time series in Fig. 4.11(a) shows that IRD detection using FE is of lower intensity than that of rectangular frame based method, but the intensity improved significantly for FKS. Fig. 4.11(b) for ORD shows that even though the intensity decreases, but the number of impulses increases for all these three analysis techniques. To more intuitively analyze the behavior, spectral analyses are used as shown in Figs. 4.12 and 4.13. Fig. 4.12 shows that the fault features are much more significant and the intensities are quite high for the IRD and this is true for all three methods. It is also observed that the second harmonic of the rotational frequency and the fault frequencies are apparent for all three methods as well. The fault intensities for FCF, FKS and FE have increased from 0.09604 to 0.2244, 0.4509 to 1.583, and 0.6057 to 0.6365 respectively, using Laplacian sliding frames as compared to the rectangular sliding frames.

Fig. 4.13 shows the ORD fault identified using the Laplacian sliding frame. Fig. 4.13(a) detects the rotational frequency, fault and its second harmonics effectively; whereas Fig. 4.13(b) shows the presence of significant intensities at fault and rotational frequencies. Fig. 4.13(c) detects the fault and the rotational frequency as well as the presence of other frequency components. Similarly, the ORD intensities in Fig. 4.13 increase from 0.15 to 0.5097, 0.9254 to 1.583, and 7.007 to 7.937 respectively, for FCF, FKS, and FE generated

using Laplacian shifted distribution function.

Conclusion from case study 2 and 3: The effect of rectangular and Laplacian frames are compared to identify IRD and ORD faults. It is observed that the performance of Laplacian distribution is better than rectangular distributions for all the three cases (FCF, FKS and FE) in terms of fault feature identifications. It is observed that the tail and the shape of the distribution have significant influence on identification and improvement of fault intensity; however, the length of the distributions affects the intensities the least. Therefore, it can be observed that, even though both the distributions are of same length, however, the performance of Laplacian window is better than that of rectangular. It can also be inferred that, not only kurtosis but also crest factor and energy can be used as indicators to identify faults in bearings. Finally, it can be concluded from the results that these techniques operate as a self-demodulation method and are free from envelope detection technique.

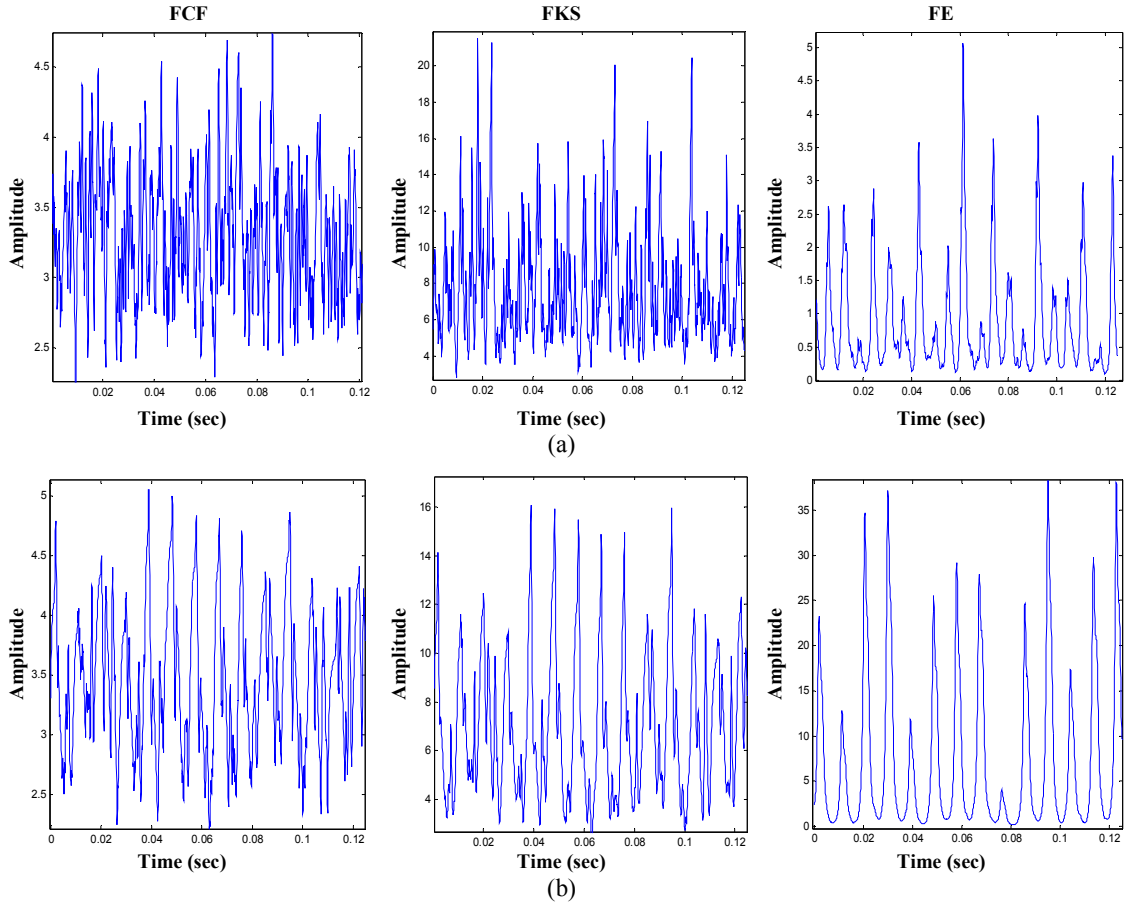

Figure 4.11 Laplacian time series FCF, FKS and FE (a) IRD (b) ORD for 0.007" fault

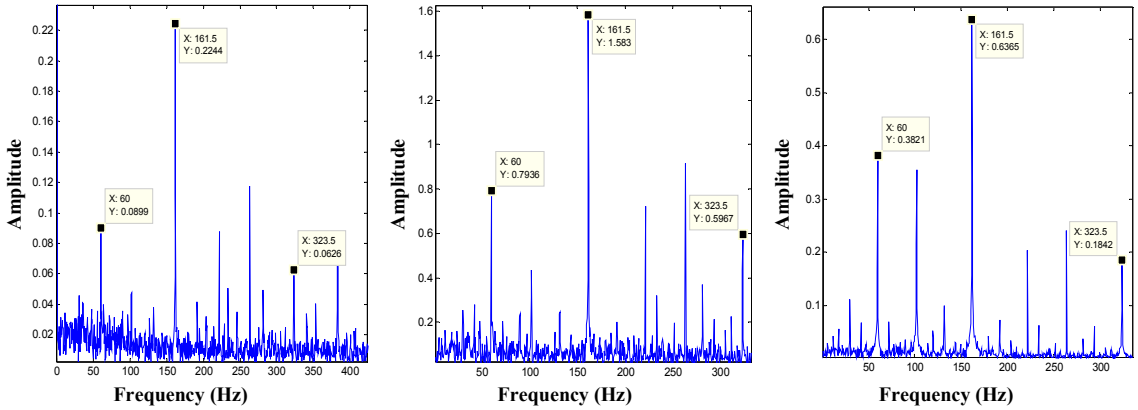

(a) (b) (c)

Figure 4.12 FFT of Laplacian frames for IRD (a) FCF (b) FKS (c) FE for 0.007" fault

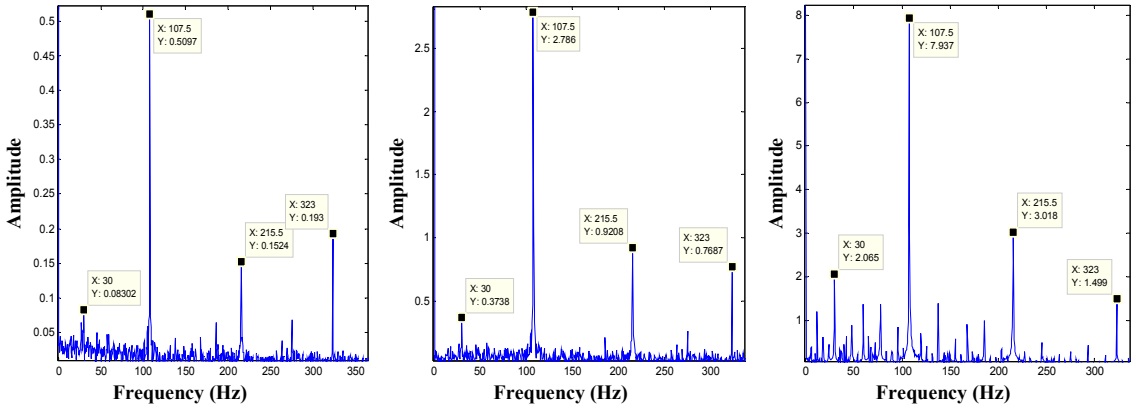

(a) (b) (c)

Figure 4.13 FFT of Laplacian frames for ORD (a) FCF (b) FKS (c) FE for 0.007" fault

4.5.4 Case Study 4: Fault Identification Using Proposed Unitary Sample Shifted Rectangular Sliding Frames (IRD and ORD of 0.021")

To more intuitively analyze the effectiveness of the proposed algorithm, investigations are carried out for a fault dimension of 0.021". Figs. 4.14(a) and (c) show that the performance of FCF is better in terms of fault detection, whereas, FE performs better in detecting shaft rotations. The kurtosis in Fig. 4.14(b) has a dominant peak at 132 Hz as compared to the expected frequency of 162 Hz. Similarly, it is observed from Fig. 4.15 that ORD is identified successively using FCF, FKS, FE methods. Fig. 4.15(a) and (b) detect the fault frequency and the revolution of the shaft, however, the shaft speed intensity dominates over the fault frequency. Similarly, Fig. 4.15(c) detects the revolution of the shaft better as compared to the fault frequency and it suggests that that the revolution of the shaft is more observable in the energy spectrum as compared to the kurtosis and crest factor spectrums.

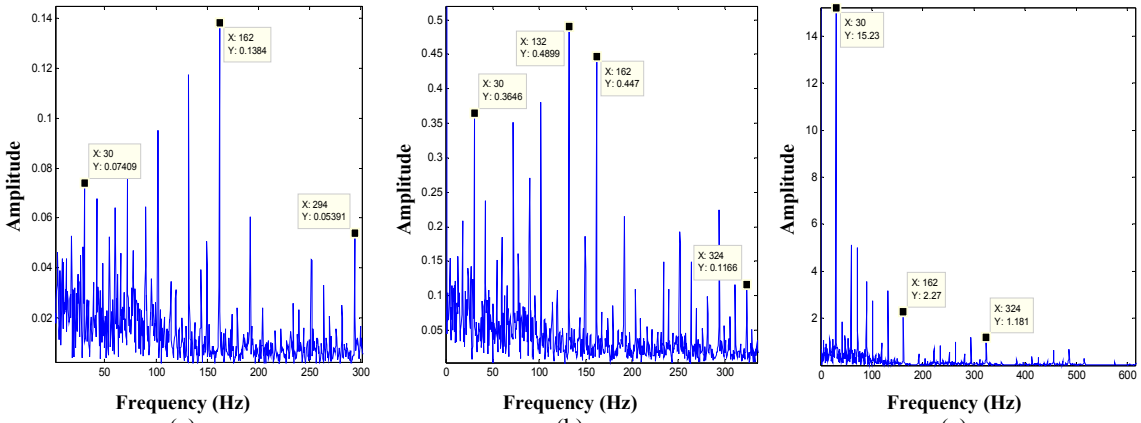

(a) (b) (c)

Figure 4.14 FFT of rectangular frames for IRD (a) FCF (b) FKS (c) FE for 0.021" fault

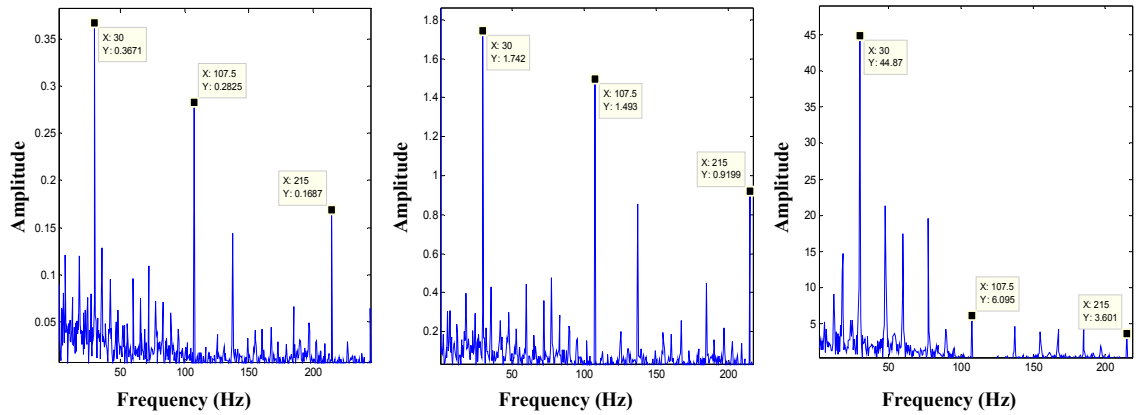

(a) (b) (c)

Figure 4.15 FFT of rectangular frames for ORD (a) FCF (b) FKS (c) FE for 0.021" fault

4.5.5 Case Study 5: Fault Identification Using Proposed Unitary Sample Shifted Laplacian Sliding Frames (IRD and ORD of 0.021")

In this case study, the effect of Laplacian distribution with a fat tail is used to test its effectiveness in detecting fault of 0.021". Figs. 4.16(a) and (b) show that the fault frequency of 162 Hz for IRD is detected faithfully by FCF and FKS generated using Laplacian method. The defect detected using FE time series method is shown in Fig. 4.16(c). The analysis for ORD in Figs. 4.17(a) and (b) shows that the fault frequency is significant with change in the distribution functions, whereas, the shaft rotating frequency is prominent in the energy spectrum as shown in Fig. 4.17(c).

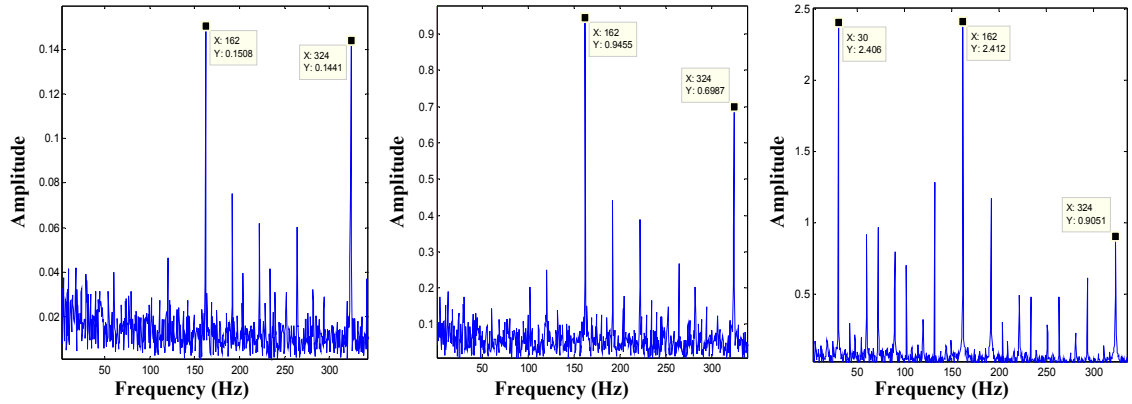

Figure 4.16 FFT of Laplacian frames for IRD (a) FCF (b) FKS (c) FE for 0.021" fault

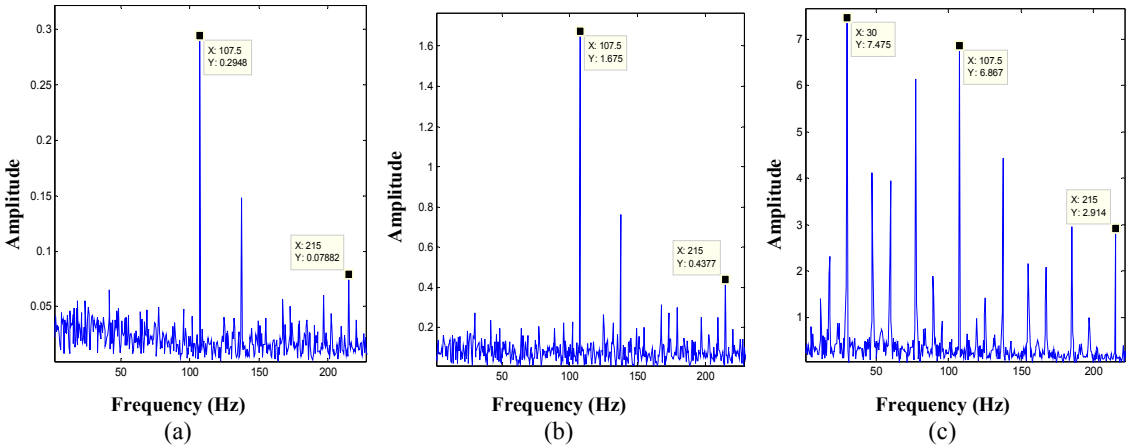

Figure 4.17 FFT of Laplacian frames for ORD (a) FCF (b) FKS (c) FE for 0.021" fault

Conclusion from Case Study 4 and 5: It is observed that the statistical techniques are useful in identifying faults in the bearing using the Laplacian method, and increase in the signal intensities are due to the accumulation of energy with change in the tail of the distributions.

4.5.6 Probability Density Functions and Their Effect

Analysis 1 for FCF: Table 4.5 shows the effect of different distribution functions on the FCF. It is observed that by Laplacian distribution function the fault intensity increases by 133.33% for IRD and 239.33% for ORD. The relative changes in intensity for IRD and ORD with the distributions (rectangular to Laplacian) are 8.695% and 4.25% respectively. It is also anticipated that the leakage of energy is more in case of rectangular distribution as compared to Laplacian distribution.

Analysis 2 for FKS: The effect of unitary sample shifted kurtosis on fault and shaft rotation intensities for various distribution functions are listed in Table 4.6. It is observed that the

change in fault intensities for IRD and ORD are significant for Laplacian distribution as compared to the rectangular distribution. The changes in fault intensities are reported to be 251.77%, 201.18%, 111.40% and 12.19% respectively. The intensities related to faults are clearly observed using the Laplacian method rather than using the rectangular sliding method.

Analysis 3 for FE: It is observed from Table 4.7 that even though FE detects fault by Laplacian, but the change in fault intensity is less competitive as compared to FCF and FKS techniques. However, the rotation of the shaft is detected prominently by FE, hence, the detection sensitivity for shaft rotation is significant for FE as compared to FCF and FKS methods.

Finally, it can be concluded that the effect of rectangular and Laplacian frames are competitive enough in identifying IRD and ORD faults. It is observed that the performance of Laplacian distribution is better than rectangular distributions for all the three cases (FCF, FKS, and FE) in terms of fault feature identifications. Even though, both the distributions are of the same length, but the performance of Laplacian window is better than rectangular. It is also verified that not only kurtosis, but also the crest factor and energy can be used to identify faults in the bearing without using envelope detection technique.

Table 4.5 Effect of rectangular and Laplacian pdf on FCF

	Rectangular fault intensity (r_{fi})	Laplacian fault intensity (l_{fi})	Change in % $\frac{(l_{fi}-r_{fi})}{r_{fi}}$	Rectangular rps intensity (r_{rpsi})	Laplacian rps intensity (l_{rpsi})	Change in rps intensity in % $\frac{(l_{rpsi}-r_{rpsi})}{r_{rpsi}}$
IRD (0.007")	0.096	0.224	133.33%	0.140	NA	NA
ORD (0.007")	0.150	0.509	239.33%	NA	0.083	NA
IRD (0.021")	0.138	0.150	8.69%	0.074	NA	NA
ORD (0.021")	0.282	0.294	4.25%	0.3671	NA	NA

Table 4.6 Effect of rectangular and Laplacian pdf on FKS

	Rectangular fault intensity (r_{fi})	Laplacian fault intensity (l_{fi})	Change in % $\frac{(l_{fi}-r_{fi})}{r_{fi}}$	Rectangular rps intensity (r_{rpsi})	Laplacian rps intensity (l_{rpsi})	Change in rps intensity in % $\frac{(l_{rpsi}-r_{rpsi})}{r_{rpsi}}$
IRD (0.007")	0.450	1.583	251.77%	0.440	NA	NA
ORD (0.007")	0.925	2.786	201.18%	0.546	0.373	-31.68%
IRD (0.021")	0.447	0.945	111.40%	0.364	NA	NA
ORD (0.021")	1.493	1.675	12.19%	1.742	NA	NA

Table 4.7 Effect of rectangular and Laplacian pdf on FE

	Rectangular fault intensity (r_{fi})	Laplacian fault intensity (l_{fi})	Change in % $\frac{(l_{fi}-r_{fi})}{r_{fi}}$	Rectangular rps intensity (r_{rpsi})	Laplacian rps intensity (l_{rpsi})	Change in rps intensity in % $\frac{(l_{rpsi}-r_{rpsi})}{r_{rpsi}}$
IRD (0.007")	0.605	0.636	5.12%	0.696	0.100	-85.63%
ORD (0.007")	7.007	7.937	13.27%	12.280	2.065	-83.18%
IRD (0.021")	2.270	2.412	6.25%	15.230	2.406	-84.20%
ORD (0.021")	6.095	6.867	12.66%	44.870	7.475	-83.34%

4.6 Conclusion

This chapter investigates and analyzes the effect of Laplacian and rectangular unitary time shifted framing methods to extract, demodulate and identify the bearing faults.

- This analysis shows that the performances of rectangular unitary time shifted frames are significant in detecting faults, as well as shaft rotating frequencies, from the FCF, FKS and FE time series.
- FKS for IRD and ORD are consistent in analyzing the fault frequencies, but FE performs better in the detection of shaft revolution. However, FCF can be used to identify faults, but the performance is not at par with that of FKS and FE.
- It is observed that the FCF, FKS, and FE analysis based on the Laplacian frames are significant in detecting the faults and can be used for noisy signals.
- The main advantages of proposed algorithms are the way the sliding based distribution functions suppress the modulated higher order harmonics and bring back the actual frequency components near the fault frequency bands, RPM, and their harmonics without the use of SK method and Hilbert transform. Finally, it is observed that the proposed

method behaves like a self-demodulating algorithm in fault feature extractions. This method is also tested on IRD and ORD faults under different loading conditions i.e. for 1hp, 2hp and 3hp for different fault sizes. The performance of the proposed method is observed to be efficient in detecting faults under different conditions as well.

CHAPTER 5
Vibro-Acoustic Signals in Fault Analysis

The sensing methods have significant impact on faithful signal acquisition from the real time environment. Therefore, the impact of vibration and acoustic based sensing methods are used in parallel for fault detection in the bearing. In this chapter, the vibro-acoustic features of the bearing are extracted using variational mode decomposition (VMD) and empirical mode decomposition (EMD) techniques. The extracted decomposed modes are selected using CC and log-variance based method to identify the actual mode depicting the fault frequency and the shaft rotation. The performance of VMD is observed to better for most of the cases with least spectral leakages, but at lower speed EMD performs better than VMD.

Each celestial body, in fact each and every atom, produces a particular sound on account of its movement, its rhythm or vibration. All these sounds and vibrations form a universal harmony in which each element, while having it's own function and character, contributes to the whole.
-Pythagoras (569-475 BC)

5.1 Introduction

The bearing fault can be addressed using various sensors as discussed in chapter 2, however, recently the research has paved the way to understand the effect of vibro-acoustic signals in fault identification. The vibro-acoustic been carried to study the relation between acoustic and vibration spectrum and their reliability in fault identifications. Recently, sound based analysis using microphone has gained importance with the change in its design, sensitivity, cost and the non-invasive process monitoring ability as compared to vibration sensors [201]. Eventually, the designers of pressure based microphone (Sanken CO-100K) have achieved frequencies close to 100 kHz that approximately match the ultrasonic range. But, the issues with the environmental noise have cut down the demand and usability of microphones in the past. Nowadays, researchers are focusing on microphones to analyze faults in the bearings and predicted their usability in advance fault detections [202]. In [203], the usability of AE, microphone, and vibration sensors are compared to detect faults in the journal bearing and rolling bearing of vessels. Similar experiments using these sensors were carried out by many researchers in the field of process control, pump and induction motors. These projected the capability of acoustics in fault detection [204,205,206].

Apart from these sensing techniques, some of the adaptive nonlinear and non-stationary signal processing techniques can be used intrinsically to decompose signal into modes. In the past fifteen years, EMD has strengthened the field of fault analysis in detecting nonlinear and non-stationary signals. Till date it has been modified into many forms like ensemble empirical mode decomposition (EEMD), complete ensemble EMD (CEMD) and Complete EEMD with adaptive noise (CEEDMAN) etc. [207,208]. To better analyze AM-FM signals simultaneously, EMD can be used as a better choice over other algorithms like wavelet and WVD [209]. But, EMD and its variants still suffer from mode mixing issues during signal reconstructions using Cubic Spline interpolation. More recently, variational mode decomposition (VMD) has gained advantage over EMD in extracting information from the bearing and is free from mode mixing issues [210,211]. Some of the researchers have used fusion of VMD along with detrend fluctuation analysis (DFA) to diagnose defects [212]. Similarly, many researchers have used EMD along with Hurst to diagnose fault in bearings. Generally, Hurst is used in differentiating signal from the noise and can be used as an indicator to select the actual mode from the decomposed modes based on coherency. Especially, these combinational approaches have a lot of applications in the areas of image processing, signal processing, mechanical engineering and financial stock market analysis etc. [213,214,215,216].

In this chapter, initially, the depths of modulation on the acquired vibro-acoustic signals are verified using FECCV method used in third and fourth chapters. This method is used to evaluate whether to follow the algorithms developed in chapters 3 & 4, or a new modification or approach needs to be carried out to analyze the signals. Moreover, this chapter focuses more on comparing two different sensors like accelerometer and pressure microphone, and two different algorithms like VMD and EMD in diagnosis of fault. Initially, VMD and EMD are concurrently used to decompose vibro-acoustic signals from the bearings, and the modes depicting the fault and the shaft rotation frequencies are extracted using correlation coefficient (CC) and log-variance approaches [217].

5.2 Variational Mode Decomposition

VMD decomposes the real-valued input signal $x(t)$ into a number of discrete sub-signals (modes), and has sparsity property while producing the decomposed signals [218]. The signal is decomposed into a number of modes u_k around the center frequency ω_k. The decomposition steps are as follows in (5.1),

$$\min_{\{u_k\}\ \{\omega_k\}}\left\{\sum_k \left\|\partial_t\left[\left(\delta(t)+\frac{j}{\pi t}\right)*u_k(t)\right]e^{-j\omega_k t}\right\|_2^2\right\} \tag{5.1}$$

where $x=\sum_k u_k$ and $\{u_k\}=\{u_1,\ldots\ldots\ldots u_k\}$ and $\{\omega_k\}:=\{\omega_1,\ldots\ldots\ldots,\omega_k\}$ are the set of nodes and their center frequencies.

The absolute integral property of the signal can be set using (5.2),

$$l(\{u_k\},\{\omega_k\},\lambda)=\alpha\sum_k\left\|\partial_t\left[\left(\delta(t)+\frac{j}{\pi t}\right)*u_k(t)\right]e^{-j\omega_k t}\right\|_2^2+ \\ \|x(t)\textstyle\sum_k u_k(t)\|_2^2+\langle\lambda(t),x(t)-\sum_k u_k(t)\rangle \tag{5.2}$$

This helps in subjecting ω_k at the center of gravity of the corresponding modes in the power spectrum, λ is the Lagrangian multiplier. Complete optimization of VMD is as follows;

1. Step 1: Initialize $\{\hat{u}_k^1\},\{\omega_k^1\},\hat{\lambda}^1,n\leftarrow 0$

   Repeat $n\leftarrow n+1$

   for $k=1{:}\,K$ do

   update $\hat{u}_k$ for all $\omega\geq 0$ using (5.3)

$$\hat{u}_k^{n+1}(\omega)\leftarrow\frac{\hat{x}(\omega)-\sum_{i<k}\hat{u}_i{}^{n+1}(\omega)-\sum_{i>k}\hat{u}_i{}^{n}(\omega)+\frac{\hat{\lambda}^n(\omega)}{2}}{1+2\alpha(\omega-\omega^n{}_k)^2} \tag{5.3}$$

2. Step 2: Update ω_k using (5.4)

$$\omega_k^{n+1}=\frac{\int_0^\infty\omega|\hat{u}_k(\omega)|^2\,d\omega}{\int_0^\infty|\hat{u}_k(\omega)|^2\,d\omega} \tag{5.4}$$

3. Step 3: dual ascent $\omega\geq 0$:

$$\hat{\lambda}^{n+1}(\omega)=\hat{\lambda}^n(\omega)+\tau\left(\hat{x}(\omega)-\sum_k\hat{u}_k^{n+1}(\omega)\right) \tag{5.5}$$

4. Finally, repeat the process till its convergence (5.6)

$$\sum_k\|\hat{u}_k^{n+1}-\hat{u}_k^n\|_2^2/\|\hat{u}_k^n\|_2^2<\epsilon \tag{5.6}$$

Once the modes are obtained, FFT is applied to the decomposed modes to get the frequency domain of the signals as defined in (5.7).

$$X(\tilde{k})=\sum_{n=0}^{N-1}u_k.e^{-j2\pi\tilde{k}n/N} \tag{5.7}$$

where *N* is number of discrete sample points.

5.3 Experimental Setup and Methodology

The schematic views of the fault analysis simulator and the actual test bed are shown in Figs. 5.1 & 5.2 respectively. Piezoelectric accelerometer and array microphone sensors are used to acquire the vibration and acoustic signals respectively. These sensors are interfaced with the 24 bit NI USB-4432 DAQ card to acquire the signals. The vibro-acoustic signals from the bearing are sampled simultaneously at a rate of 5120 samples per sec for duration of six seconds. Sampling rate of 5120 is chosen in reference to the frequency of IRD fault at 3000 RPM i.e. 270.747 Hz and the assumed sampling rate is ten times greater than what is desired in practical applications. The oversampling rate beyond desired sampling rate can increase the implementation costs in practical applications [219]. But, as far as data acquisition time is concerned, it can be of longer duration for better predictability of the signal. However, if meaningful information can be passed with least number of data samples, then utilization of resources can be minimized [220]. The vibro-acoustic signals are analyzed for a sample size of 10000 and processed using EMD and VMD to get monotonic signals. The large sample length is chosen to minimize the effect of noise on the signal [221].

For fault identification, SKF-6205 deep groove ball bearing (DGBB) is used. A fault of 0.5mm is created in the inner race using an electrical discharge machine (EDM) as shown in Fig. 5.2(d). For performance analysis, the bearing is rotated at variable speed starting from 1000 to 3000 revolutions per minutes (RPM) using variable frequency drive (VFD) as in Fig. 5.2. To avoid any drift in speed, torque and current, the induction motor is operated using space vector modulation (SVM) technique. Tables 5.1 and 5.2 represent the bearing configuration and the fault frequencies at various speeds of 3000, 2500, 2000, 1500 and 1000 RPM respectively.

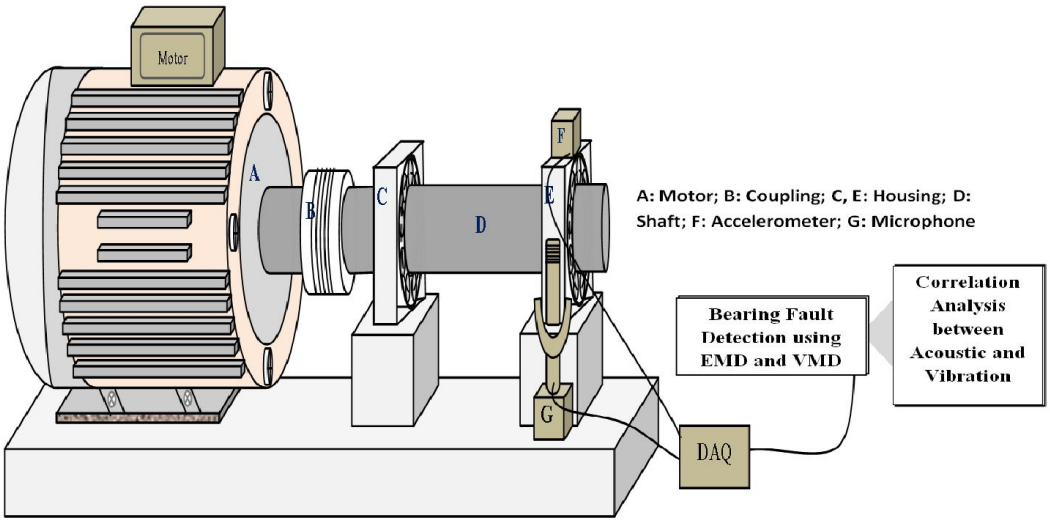

Figure 5.1 Bearing fault simulator schematic with sensor and data acquisition system

Figure 5.2 Experimental setup (a) 1-NI-USB DAQ , 2-Motor, 3-Signal conditioner (SC) (b) 4-Microphone, 5-Accelerometers, 6-Proximity sensor (c) 7-Variable frequency drive (d) 8-Electrical discharge machine, 9-IRD

Table 5.1 Ball bearing configuration

Bearing Type	Pitch diameter (inch)	Rolling element diameter (inch)	Number of rolling element
6205 (DGBB)	1.537	0.3125	9

Table 5.2 Ball bearing frequencies

Shaft Speed (RPM)	BPFI (Hz)	BPFO (Hz)	BSF (Hz)	FTF (Hz)	RDF (Hz)
3000 (50.00 Hz)	**270.747**	179.253	117.877	19.917	235.754
2500 (41.66 Hz)	**225.622**	149.378	98.231	16.598	196.462
2000 (33.33 Hz)	**180.498**	119.502	78.585	13.278	157.169
1500 (25.00 Hz)	**135.373**	86.627	58.939	9.959	117.877
1000 (16.66 Hz)	**90.249**	59.751	39.292	6.639	78.585

* ball pass frequency inner race (BPFI), ball pass frequency outer race (BPFO), ball spin frequency (BSF), cage defect frequency (FTF) and rolling element defect frequency (RDF)

5.4 Proposed Signal Extraction Techniques

The vibro-acoustic signals are decomposed and extracted using the following algorithms and the detail is shown in the Fig. 5.3.

1. Decompose the vibration and acoustic signals concurrently using EMD and VMD.
2. Analyze the extracted modes of VMD and EMD using FFT.
3. Extract the exact modes depicting the fault and shaft rotation frequencies using correlation coefficient (CC) and log-variance approach in (5.8) and (5.10) respectively. This approach identifies the exact mode depicting the fault frequency and shaft rotation irrespective of the maximum energy concentration at certain center frequencies.
4. The rising slopes and the highest peaks are used as an indicator to select the actual mode depicting the fault frequency and the rest are rejected.

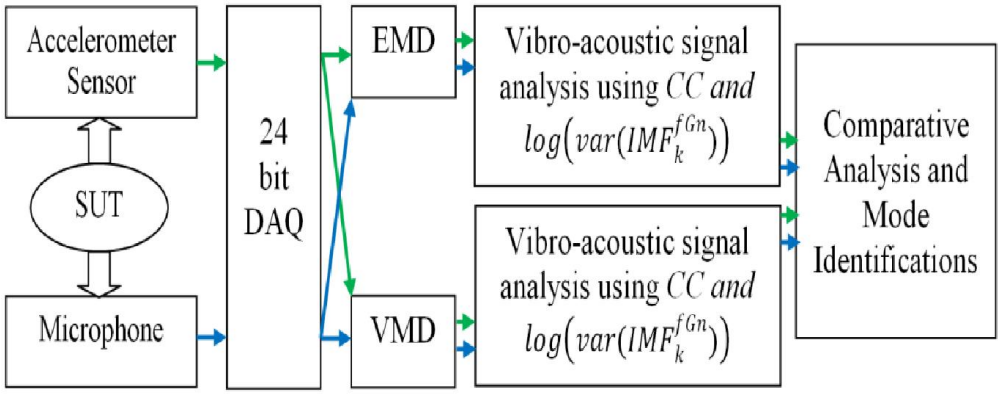

Figure 5.3 Comparative analysis of acoustic and vibration signals using EMD and VMD

The correlation coefficient (CC) can be expressed as in (5.8) [222].

$$CC(k) = \frac{\sum_{n=1}^{L} IMF_k[n].x[n]}{\sqrt{\sum_{n=1}^{L} IMF_k[n].IMF_k[n]}\ \sqrt{\sum_{n=1}^{L} x[n].x[n]}} \tag{5.8}$$

where $x[n]$ is the un-decomposed signal and k represents the mode, $k = 1, 2 \ldots 11$, $n = 1,2,3, \ldots L$ and L is sample size. The energy based empirical variance of the modes can be calculated using (5.9).

$$E[k] = \frac{1}{L}\sum_{n=1}^{L}(IMF_k[n])^2 \tag{5.9}$$

The variances of the modes are related to the mode indices through the relations (5.10) [223].

$$log\left(var(IMF_k^{fGn})\right) = 2Hlog(\tau_k) + log(C) \tag{5.10}$$

where C, k, H, fGn and τ_k are constant, the mode index, Hurst exponent, fractional Gaussian noise and periods of the signals respectively. The log-variance of negative slope is assumed to be noisy in nature based on the observation referred in [155]. It shows that the maximum value of log-variance energy is concentrated on a mode which corresponds to the coherent mode. The analysis looks for the coherent mode reflecting the maximum energy accumulation and is verified using the decomposed modes extracted using EMD and VMD.

5.5 Results and Discussion

The vibro-acoustic features of the bearing are analyzed using EMD and VMD. Since, the accelerometer and microphone behave as an impedance network to the system under test, the change in the characteristic of the fault will have different effects on both the sensors.

5.5.1 Verifications of Amplitude Modulation

This analysis is carried out to identify the effects of amplitude modulation in the experimental test signals [224, 147]. The modulation creates sidebands in the spectrum and can be recovered using envelope and cepstral analysis techniques [225]. This analysis is performed to verify the effect of envelope and cepstrum analysis on the observed frequency spectrum. It is observed from Fig. 5.4 that the standardized acoustic and vibration signals hardly indicate the presence of significant impulses. Therefore, to observe the effect of modulation, spectrum, envelope and cepstral-envelope are compared in the Fig. 5.5. It is

observed from acoustic signal FFT in Fig. 5.5(a) that the fault frequency of 270.3 Hz is clearly noticeable, whereas, envelope detects only the shaft rotating frequency of 50.18 Hz effectively, but fails to trace the defect. Similarly, cepstral envelope in Fig. 5.5(a) traces the fault, but the signals are buried in noise. Further, the analyses are carried out on vibration signal to identify defects in the signal. It is observed from Fig. 5.5(b) that the fault and the shaft rotating frequencies are detected from vibration signal FFT, whereas the envelope and cepstral-envelope methods fail to detect faults. It can be inferred that both acoustic and vibration signatures are in congruence for FFT rather than for envelope and cepstral-envelope methods. It can be concluded that prior to any processing, the effect of amplitude modulation needs to be tested using FECCV technique (discussed in chapter 4).

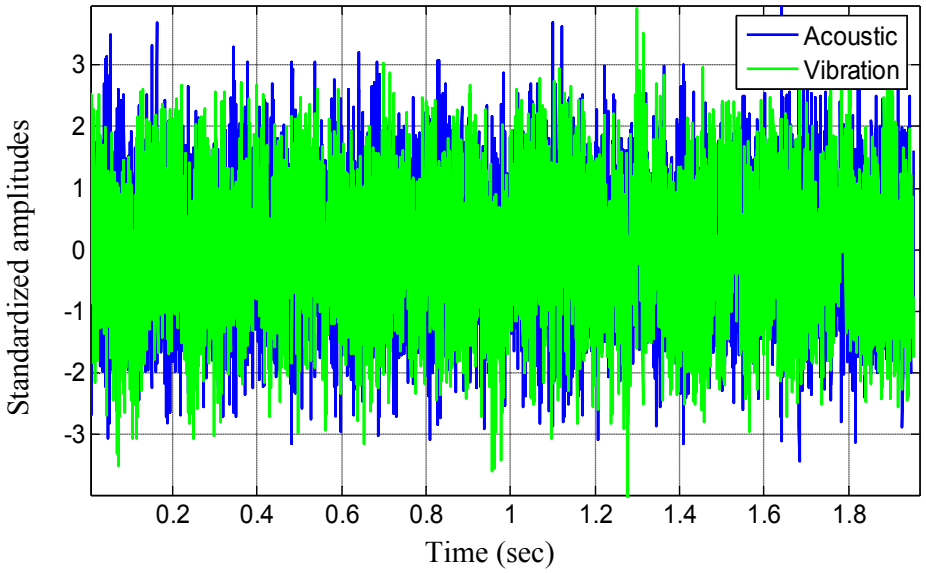

Figure 5.4 Time response of acoustic and vibration signals at 3000 RPM

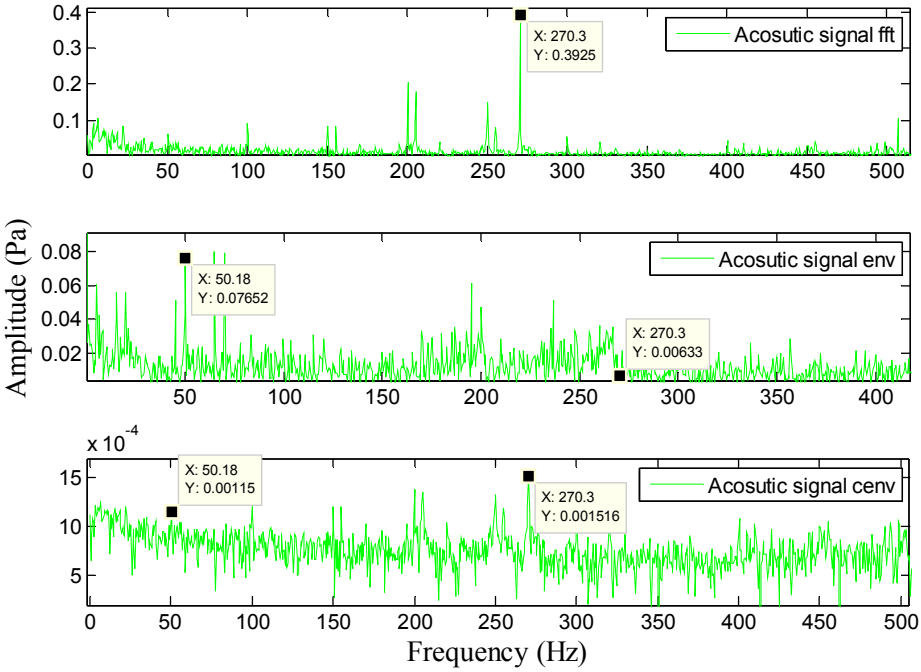

(a)

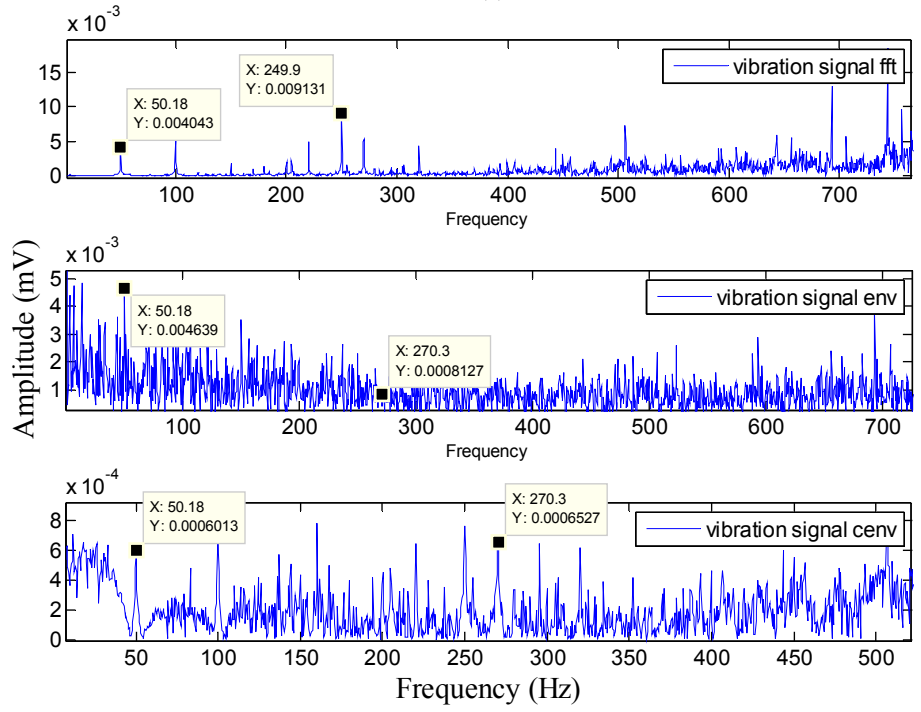

(b)

Figure 5.5 Spectrum using FFT, envelope and cepstral envelope at 3000 RPM (a) acoustic (b) vibration signals

5.5.2 Vibro-Acoustic Signals Decomposition using EMD

The vibro-acoustic fault signals are decomposed by EMD to obtain likely stationary modes from the signals. These signals are classified using CC and log-variance to identify the exact mode depicting the fault frequency.

Case Study 1: Vibro-Acoustic Signals Analysis at 3000 RPM

Initially, the analysis is carried out to identify the IRD defect using the acoustic signal. The extracted IMFs for acoustic signals are shown in Figs. 5.6(a) & (b). The acoustic signal is decomposed to its lowest frequency level as shown in Fig. 5.6(a). Here, the monotonic signal extraction is avoided to reduce the unwanted computational cost incurred for the calculation of maxima and minima. The time series signals extracted by mode decomposition techniques are further evaluated using FFT as shown in Fig. 5.6(b). It is observed that the intensity of the acoustic signal is significant at M3 and M4. The M5 and M6 have higher intensity next to the fault frequency of 270.3 Hz. The extracted fault frequency closely matches with that in Fig. 5.5(a). It is observed that the rotating frequency and their harmonics are deviating by very slight extent due to the mode mixing issues suffered by EMD. The approximate values of intensities obtained from Fig. 5.6(b) are listed in Table 5.3.

Similarly, the vibration signal for IRD is decomposed into modes using EMD, as shown in Fig. 5.7(a). The frequency spectrums extracted from the IMFs are shown in Fig. 5.7(b). It is observed from the spectrums that the intensity of vibration is significant for M1 and M2. These IMFs have higher intensity at 743.4 Hz for the M2 and the resultant intensities for all other modes are listed in Table 5.3. A false fault frequency is predicted at 743.4 Hz if the mathematical formulation is not referred in fault identification. However, the actual fault and shaft rotating frequencies can be traced using the mathematical formulation and observed for M3-M6. It is depicted from the vibro-acoustic results that EMD suffers from mode mixing issues and it is really difficult to trace the exact mode depicting the fault frequency. It can be concluded from the analysis that acoustic signals are significant in identifying the fault frequency as compared to the vibration signals, if the dominant peaks are considered for fault detection.

Table 5.3 Frequencies and Intensities of acoustic and vibration signals for EMD

Decomposed Signals	Acoustic signal		Vibration signal	
	Intensity (Pa)	Center Frequencies (Hz)	Intensity (mV)	Center Frequencies (Hz)
Mode1	0.064	1440	0.100	743.40
Mode2	0.045	743.40	0.070	743.40
Mode3	0.258	270.30	0.045, 0.030	250, 270.30
Mode4	0.119	270.30	0.030	249.90
Mode5	0.077	99.84	0.039	99.84
Mode6	0.041	50.18	0.027	50.18
Mode7	0.062	22.02	0.007	34.30
Mode8	0.080	10.00	0.006	18.00
Mode9	0.080	10.00	0.008	9.00
Mode10	0.080	3.00	0.005	5.00
Mode11	0.050	1.50	Nil	Nil

To infer the mode mixing issues, all the modes for acoustic and vibration signals are merged together, as shown in the Figs. 5.8(a) & (b). Fig. 5.8(a) shows that different modes are overlapping on one another for the acoustic EMD (Aemd), but the fault frequency is significant for M3 as compared to all other modes. Fig. 5.8(b) for vibration EMD (Vemd) has significant energy corresponding to higher frequencies (M1), even though the fault is traced at M3. For better segregation of signals, the analyses are further carried out using CC and log-variance slopes based on Hurst as an indicator to select mode depicting fault frequency. Fig. 5.8(c) shows that the fault frequency is observed for the M3 with CC of 0.45, but it is below 0.2 for shaft rotating frequency. Similarly, the acoustic signal in Fig. 5.8(d) has positive peak at 270.3 Hz, but vibration fails to predict the defect. This analysis shows that the M3 is the actual mode not M4 (Check Table 5.3), and this is validated using CC and log-variance methods.

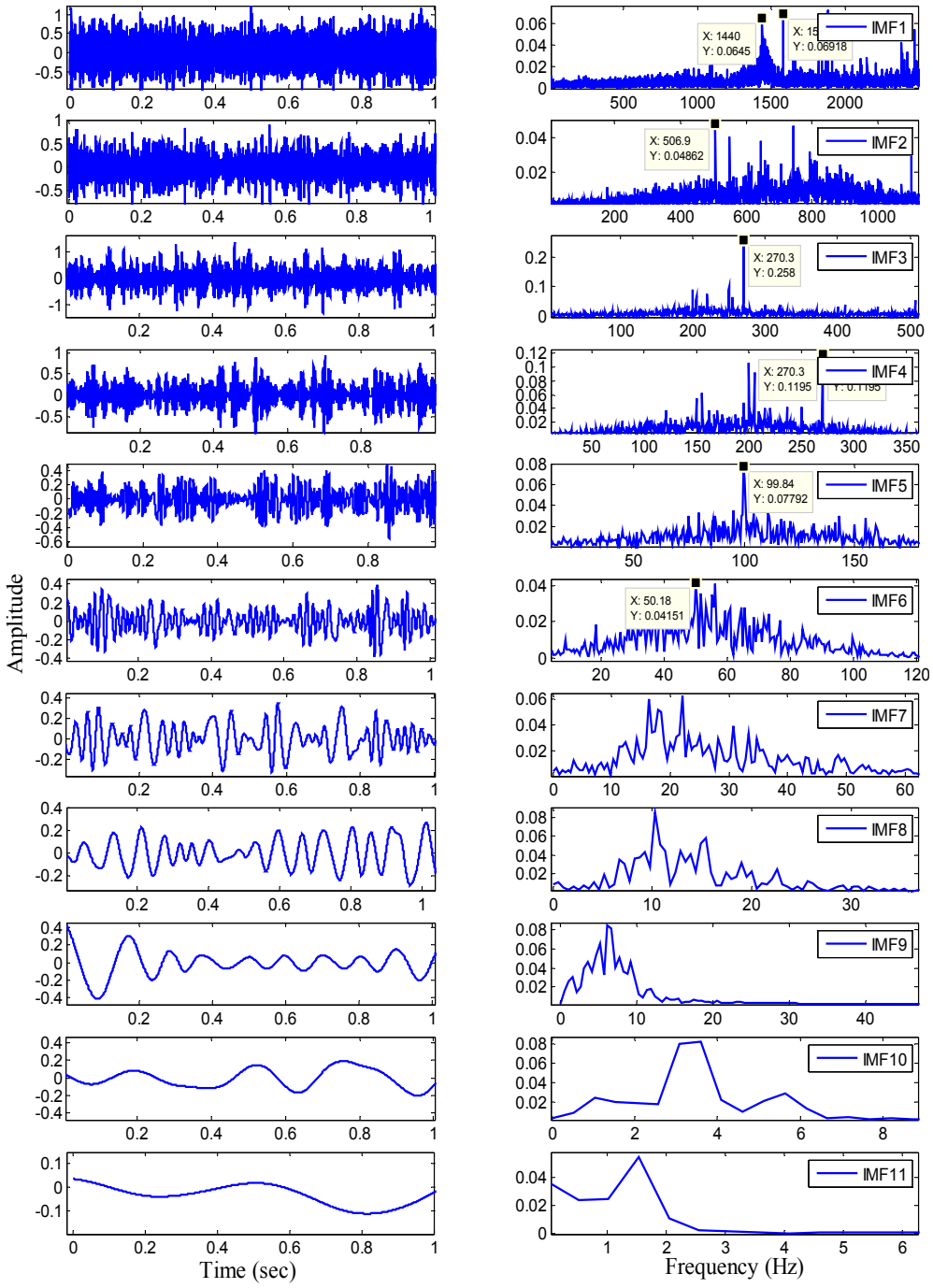

Figure 5.6 Aemd (a) Time domain (b) Frequency domain

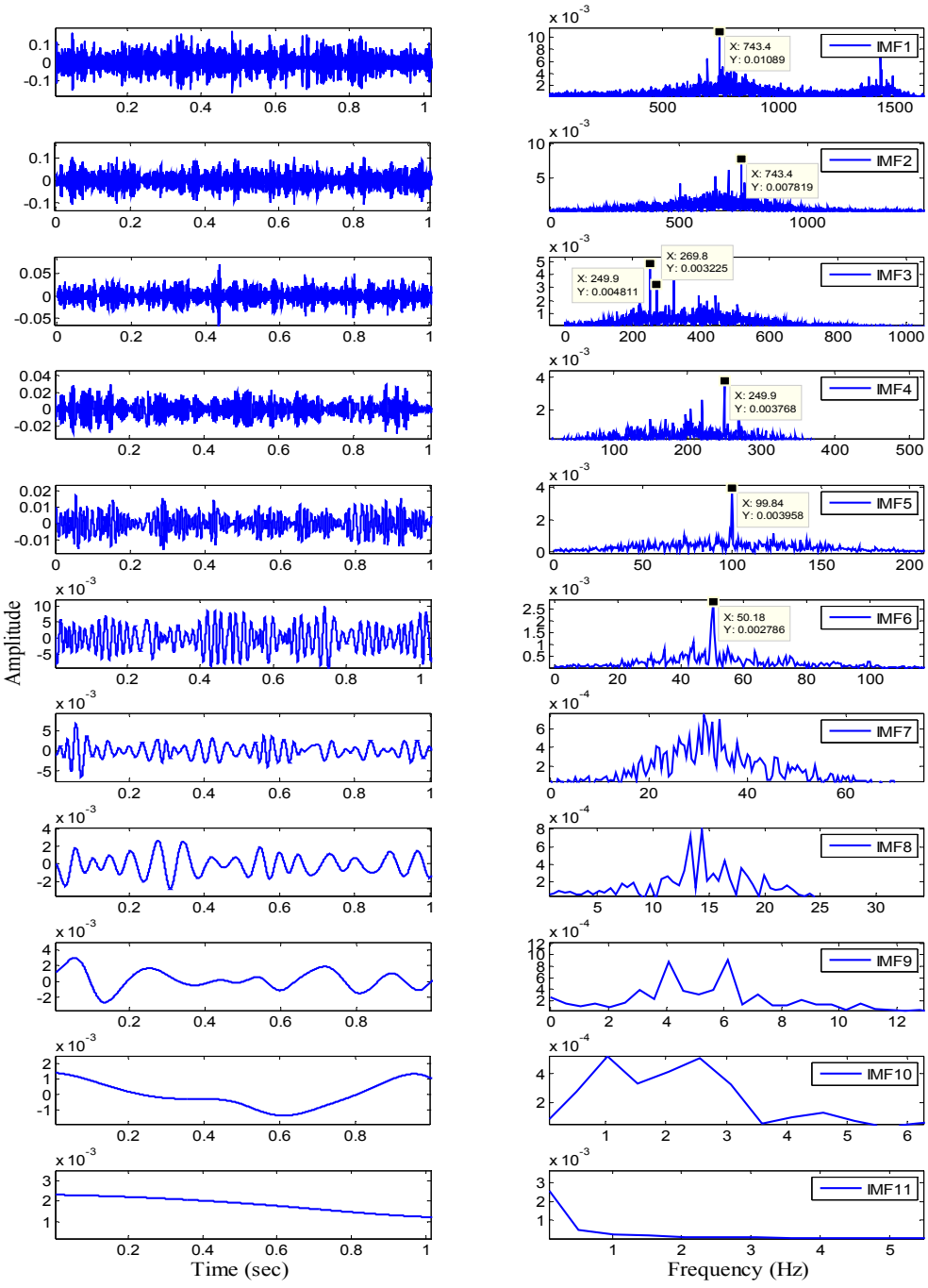

Figure 5.7 Vemd (a) Time domain (b) Frequency domain

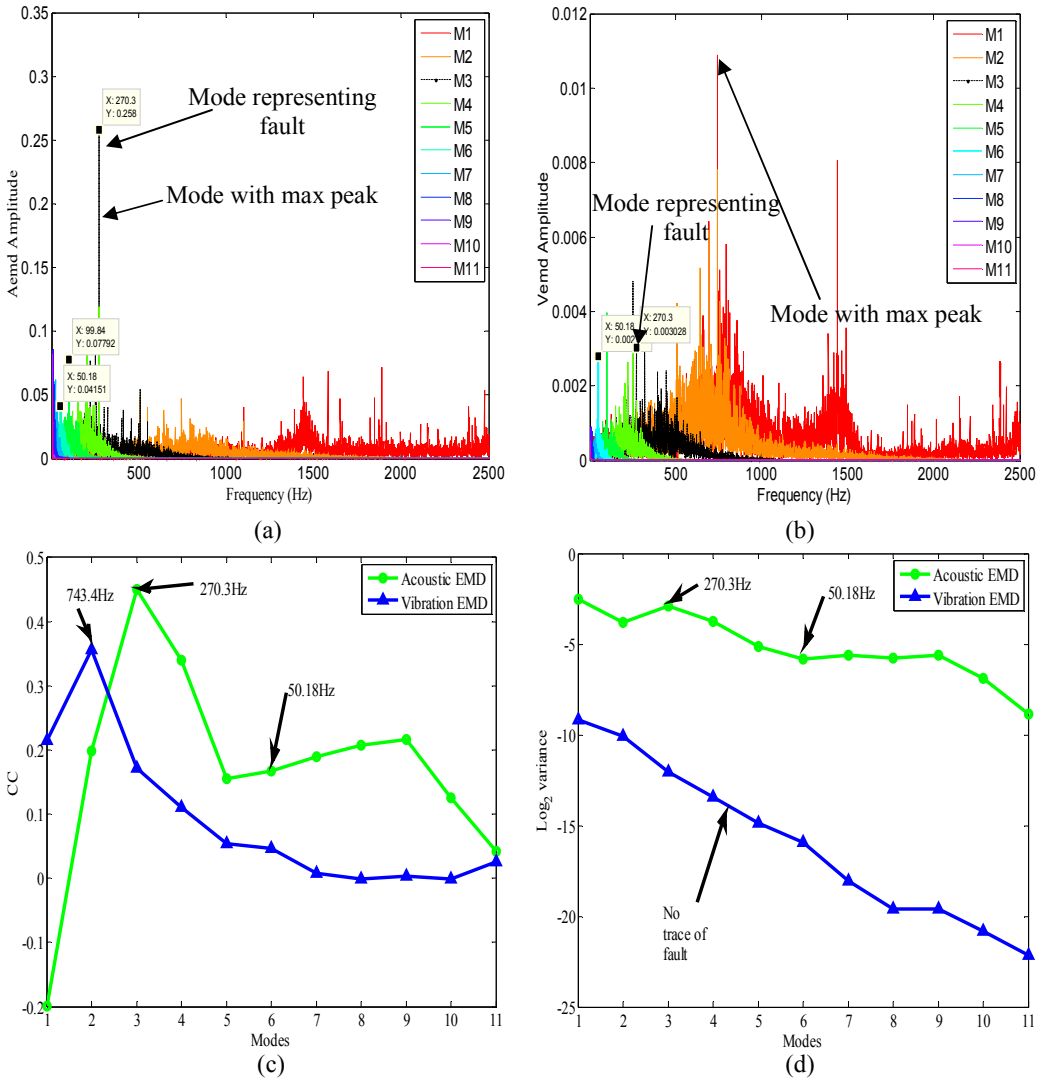

Figure 5.8 EMD modes at 3000 RPM (a) FFT acoustic signal (b) FFT vibration signal (c) $\boldsymbol{CC}$ (d) Log_2 (variance)

Case Study 2: Vibro-Acoustic Signals Analysis at 2500 RPM

It is observed from Figs. 5.9(a) and (b) that the M4 depicts the fault frequency of 224.8 Hz in the acoustic and vibration spectrums, even if the maximum energy is concentrated near M1 and M5 (acoustic and vibration). Vibro-acoustic spectrums also trace the shaft rotating frequency of 41.47 Hz which can be observed from the M7. Fig. 5.9(c) shows that the M4 and M7 in the acoustic spectrum clearly match to mode of CC indicating maximum correlation. The CC for vibration signal fails to predict the fault and the first harmonic of the rotating speed, but traces the second harmonic corresponding to the shaft rotation. It can be observed from Fig. 5.9(d) that the acoustic mode identification using log variance matches with the CC plot. Even though, the mode does not indicate maximum peak, however, in that case the rising slope can be presumed as an indicator of the actual signal rather than noise.

But all the falling slopes can be rejected as Hurst describes them as noise, and hold no congruence with the signal.

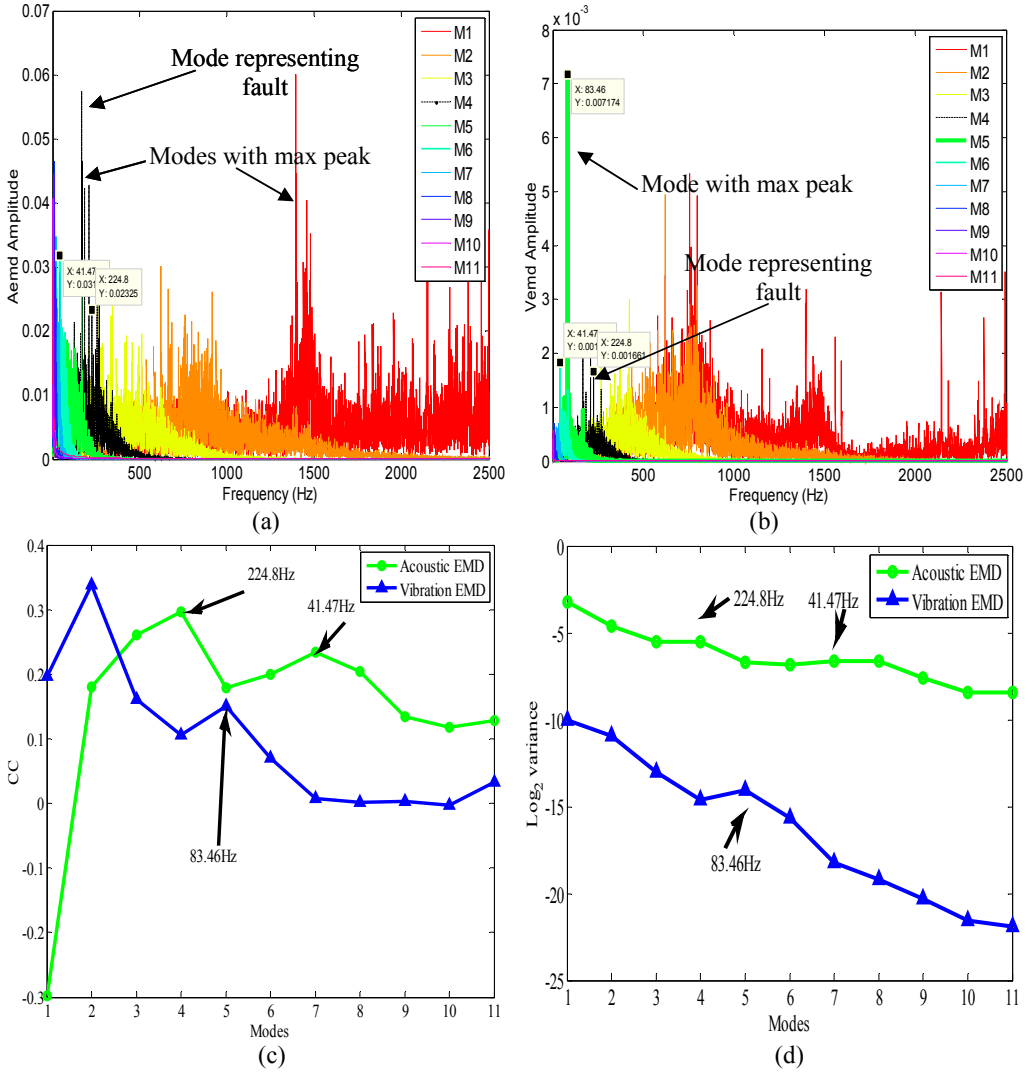

Figure 5.9 EMD modes at 2500 RPM (a) FFT acoustic signal (b) FFT vibration signal (c) $\boldsymbol{CC}$ (d) Log_2 (variance)

Case Study 3: Vibro-Acoustic Signals Analysis at 2000 RPM

The spectrums in Figs. 5.10(a) and (b) for both acoustic and vibration signals identify the M4 as the fault frequency band. The IRD frequency of 180.2 Hz is detected by EMD and matches with the calculated frequency in Table 5.2. The shaft rotating frequency of 33.33 Hz is observed for M7 and can be visualized in the vibro-acoustic spectrums. The CC for acoustic signal in Fig. 5.10(c) reflects M3 and M4 as the mode numbers corresponding to the fault. The acoustic spectrum fails to trace the shaft rotating frequency, whereas, the vibration spectrum identifies the M7 as the mode indicating the shaft speed. The log.variance for both acoustic and vibration signals are least significant in tracing the fault and the shaft rotating

frequencies, even though the slope is less at M4. It is observed the performance of CC is better compared to log_variance in identifying exact mode representing the fault and the shaft rotating frequencies.

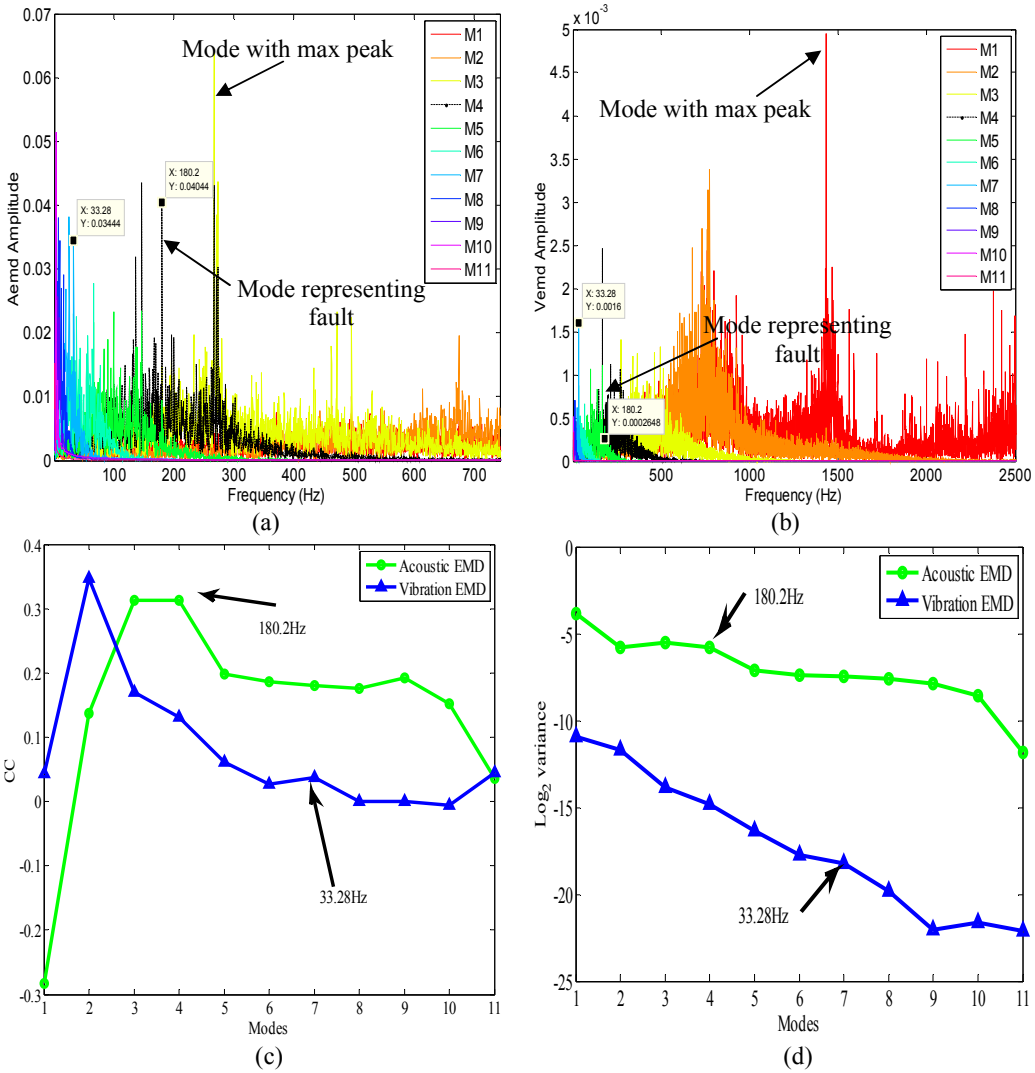

Figure 5.10 EMD modes at 2000 RPM (a) FFT acoustic signal (b) FFT vibration signal (c) CC (d) Log_2 (variance)

Case study 4: Vibro-Acoustic Signals Analysis at 1500 Rpm

It is observed from Figs. 5.11(a) and (b) that the fault frequency of 135.2 Hz is significant in the acoustic spectrum rather than in the vibration spectrum, even though it can be traced using mathematically calculated values, as shown in table 5.2. The spectrums in vibro-acoustic fail to indicate the shaft rotating frequency effectively and it might be buried in the noise. The acoustic signal is having maximum energy around the center frequency of 1500 Hz. Further, the analyses are carried out using CC and log_variance methods as shown in Figs. 5.11(c) and (d). It is observed that, CC for acoustic indicates M4 and M7 as fault and

shaft rotating frequencies respectively, even if the energy is low. But, the CC for vibration signal fails to represent any of the features. The log-variance indicates the fault frequency partially as the slope is low, but the shaft rotating frequency is predicted correctly. The CC for vibration signal could not able to trace the fault and shaft rotation from the extracted modes.

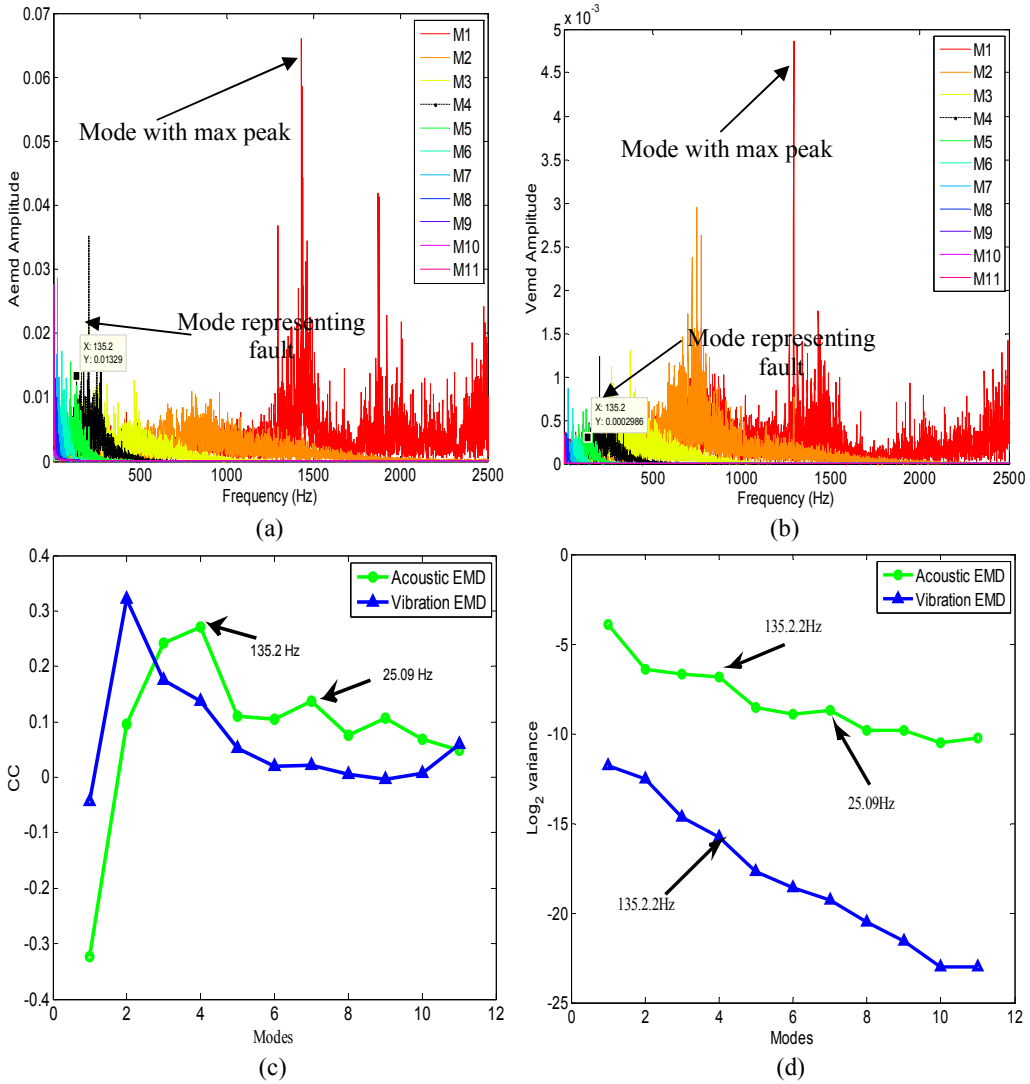

Figure 5.11 EMD modes at 1500 RPM (a) FFT acoustic signal (b) FFT vibration signal (c) CC (d) Log_2 (variance)

Case Study 5: Vibro-Acoustic Signals Analysis at 1000 RPM

Finally, the effects of lower speed on the behavior of vibro-acoustic signals are studied using EMD. It is observed from the acoustic spectrum in Fig. 5.12(a) that the fault and shaft rotating frequencies of the bearing are observed to a certain extent, but the vibration spectrum fails to depict the presence of fault as in Fig. 5.12(b). Similarly, the CC and Log.

variance in Figs. 5.12(c) and (d) misinterpret the mode, and fails to detect the presence of faults. It is observed as the speed reduces the detection sensitivity decreases with a lowering in the correlation between the modes and the actual signal.

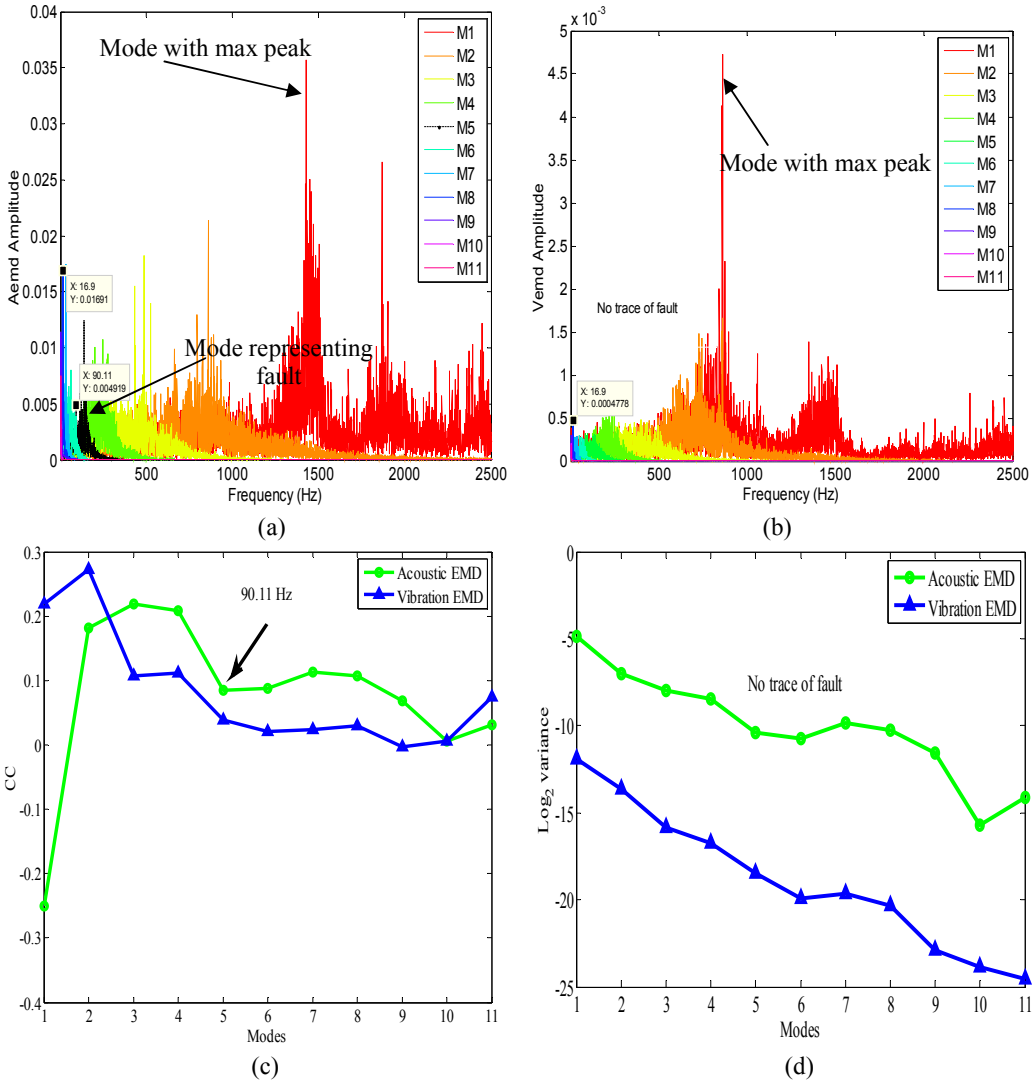

Figure 5.12 EMD modes at 1000 RPM (a) FFT acoustic signal (b) FFT vibration signal (c) $\boldsymbol{CC}$ (d) Log_2 (variance)

5.5.3 Vibro-Acoustic Signals Decomposition using VMD

After rigorous verification of EMD under variable speed, the process is repeated using VMD to analyze its effect on vibro-acoustic fault identification of bearings.

Case Study 6: Vibro-Acoustic Signals Analysis at 3000 RPM

Initial observations are carried out at 3000 RPM for vibro-acoustic signals, and the extracted modes are shown in Figs. 5.13 and 5.14. The acoustic time series and the frequency spectrums for the extracted modes using VMD (Avmd) are shown in Figs. 5.13(a) and (b). It

is observed from Fig. 5.13(b) that the modes extracted using VMD separate out signals into different bands based on the constraint bandwidth. The detailed intensities observed for these modes are listed in Table 5.4. The M10 and M11 are selected based on the mathematical fault frequencies obtained from Table 5.2. The selection of mode is very tough when the center frequencies based on Wiener filtering and shifting operations are used to extract the information. It shows a wider frequency extraction range as compared to EMD. It means both the algorithms are sensitive for different sensing technologies i.e. for acoustic and vibration sensing. The extracted intensity of the signal is higher for VMD as compared to EMD. It clarifies that for high noisy environment VMD can perform better than EMD. But as far the mode extraction is concerned; it cannot be used to predict the number of modes adaptively.

The extracted time series and spectral vibration of VMD based decomposed modes (Vvmd) are shown in Figs. 5.14(a) & (b). VMD extracts the vibration feature of the signal and depicts the actual speed of the shaft and its harmonics at M11 as in Table 5.4. The decision of the exact number of modes to extract monotonic signal is the limitation of VMD. It is observed from Fig. 5.14(b) that the intensity of vibration is significant at lower modes as compared to the higher modes. As far as the mode selections are concerned, the vibration data fails to predict the fault frequency without the help of mathematical formulations as in Table 5.2.

For clear visualization of the actual behavior of the vibro-acoustic modes, the signals are plotted in a single graphical window as shown in Figs. 5.15(a) and (b). It is observed from the acoustic modes in Fig. 5.15(a) that the modes are free from mode mixing problem encountered by EMD. The M10 represents the actual fault frequency, whereas the shaft rotating frequency is observed in M11. The observed patterns are also reflected for the equivalent modes for the vibration signal as shown in Fig. 5.15(b). The acoustic signal shows the M10 as the dominant mode, whereas the vibration shows the M7 as the dominant mode. For comprehensive analysis and the selection of modes, further, the analyses are carried out using CC and log_variance methods. It is observed from the Fig. 5.15(c) that the M10 for acoustic clearly represents IRD with CC of 0.6 and is much improved as compared to that in EMD. Vibration signal predicts the M7 as the dominant mode with a frequency of 743.7 Hz. It is observed that vibration fallshort in predicting actual fault frequency as compared to its acoustic counterpart. The fault frequency shows a maximum peak for the log_variance analysis and is in congruence with CC as shown in Fig. 5.15(d). Again the CC

and log.variance fail to detect the fault, even though it is detected by the vibration spectrums. It can be concluded that the vibration-acoustic signal pattern follows different characteristics i.e. the property (chaotic or random) distribution function for both the signal might be different as the TF of acquisition sensor changes (assuming housing as the transfer function (TF) for the vibration sensor and air medium as the channel/TF for acoustic sensors).

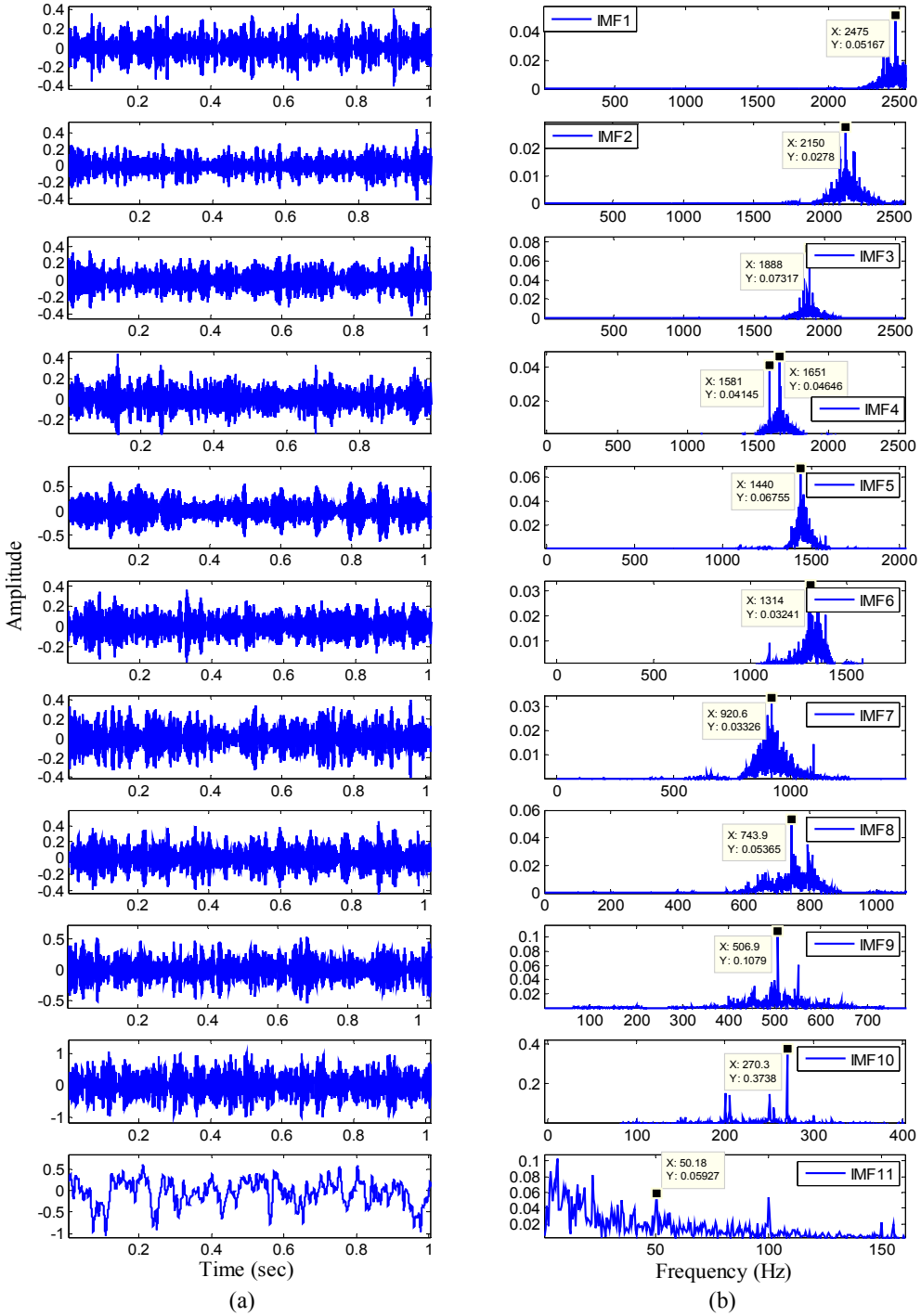

Figure 5.13 Avmd (a) Time domain (b) Frequency domain

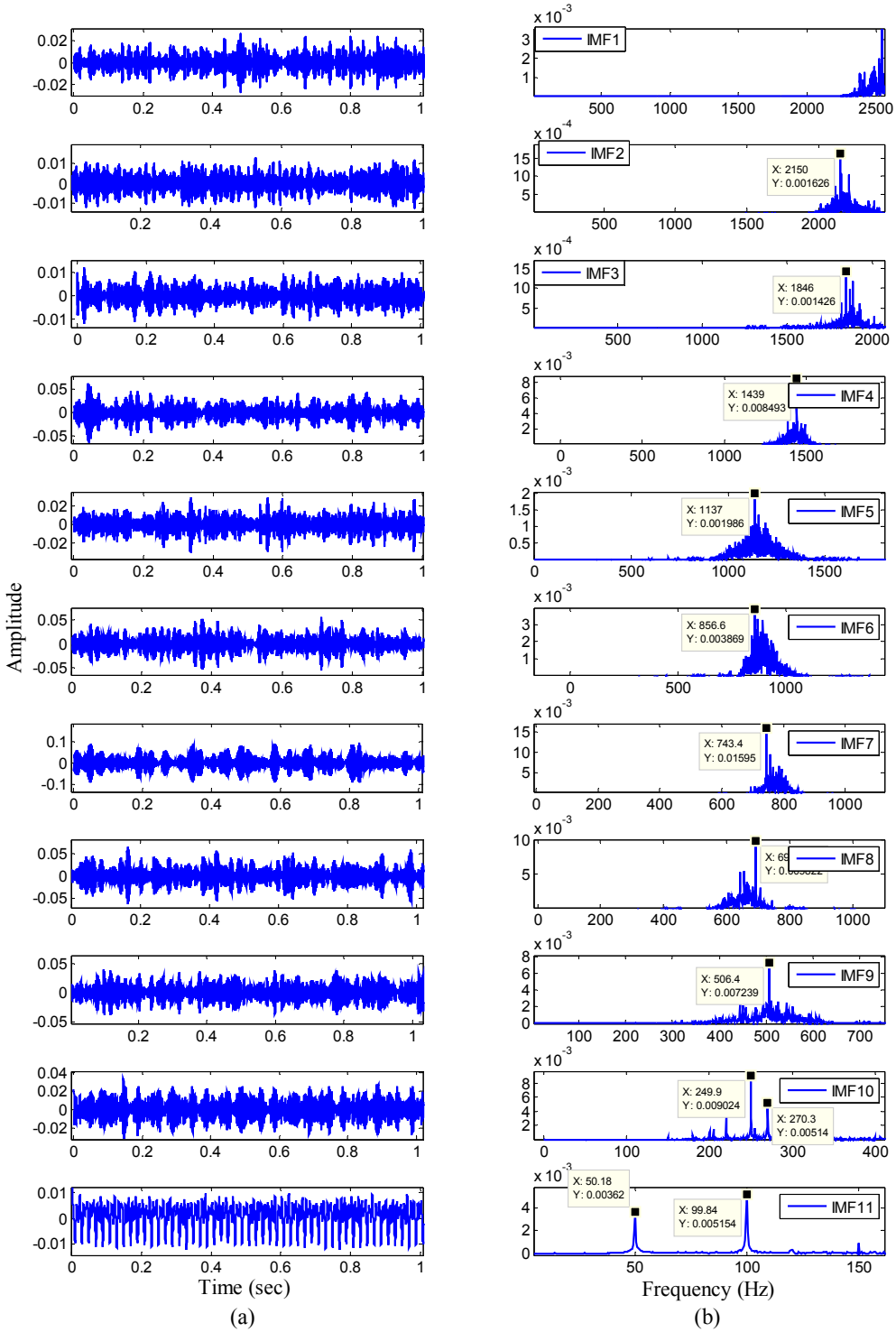

Figure 5.14 Vvmd (a) Time domain (b) Frequency domain

Table 5.4 Frequencies and Intensities of acoustic and vibration signals for VMD

Decomposed Signals	Acoustic signal		Vibration signal	
	Intensity (Pa)	Center Frequencies (Hz)	Intensity (mV)	Center Frequencies (Hz)
Mode 1	0.050	2475	0.030	2547
Mode 2	0.027	2140	0.016	2150
Mode 3	0.070	1888	0.010	1846
Mode 4	0.046	1651	0.080	1439
Mode 5	0.060	1440	0.010	1137
Mode 6	0.032	1314	0.030	856.6
Mode 7	0.033	920.6	0.159	743.4
Mode 8	0.050	743.9	0.098	693.2
Mode 9	0.107	506.9	0.072	506.4
Mode 10	0.373	270.3	0.085,0.05	250, 270.3
Mode 11	0.06, 0.054	50, 99.84	0.036, 0.051	50, 99.84

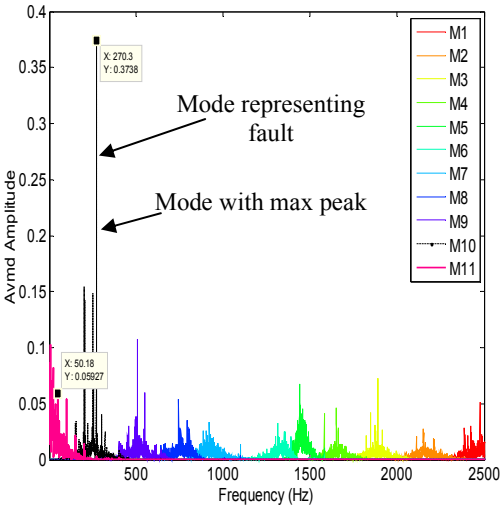

(a)

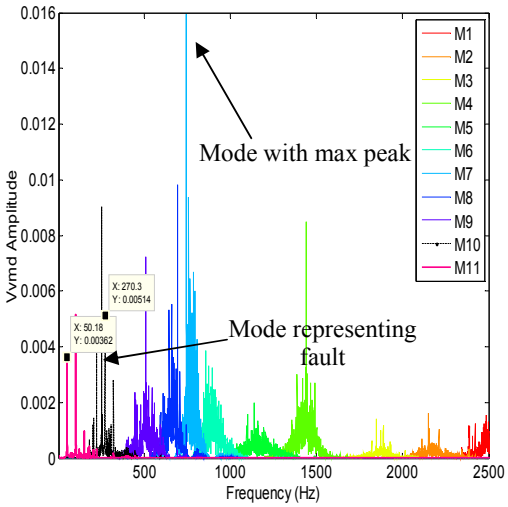

(b)

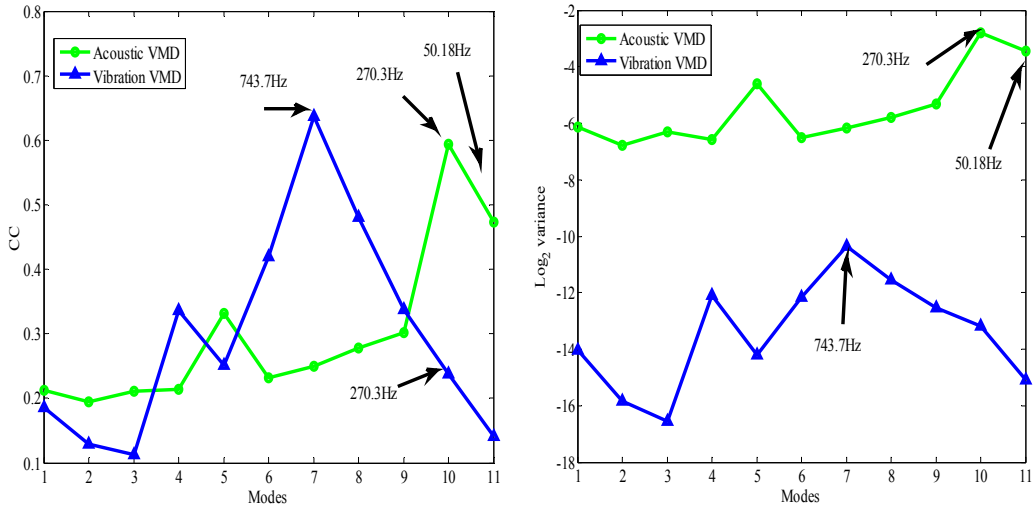

(c) (d)

Figure 5.15 VMD modes at 3000 rpm (a) FFT acoustic signal (b) FFT vibration signal (c) $\boldsymbol{CC}$ (d) Log_2 (variance)

Case Study 7: Vibro-Acoustic Signals Analysis at 2500 rpm

It is observed from the Fig. 5.16(a) that the fault and shaft rotating frequencies (224.8 Hz and 41.47 Hz) are present in M10 and M11 modes respectively. But, the M11 in Fig. 5.16(b) indicates both the frequencies (fault and shaft) without alteration in the modes. Fig. 5.16(c) depicts the fault and shaft rotation with CC of 0.4 and 0.45 approximately. The rising slopes are the indication of congruence of the modes with the actual signal. The log-variance also follows the same pattern as that of CC in identifying the fault and shaft rotating frequencies for acoustic signal, but fails to predict from vibration as shown in Fig. 5.16(d).

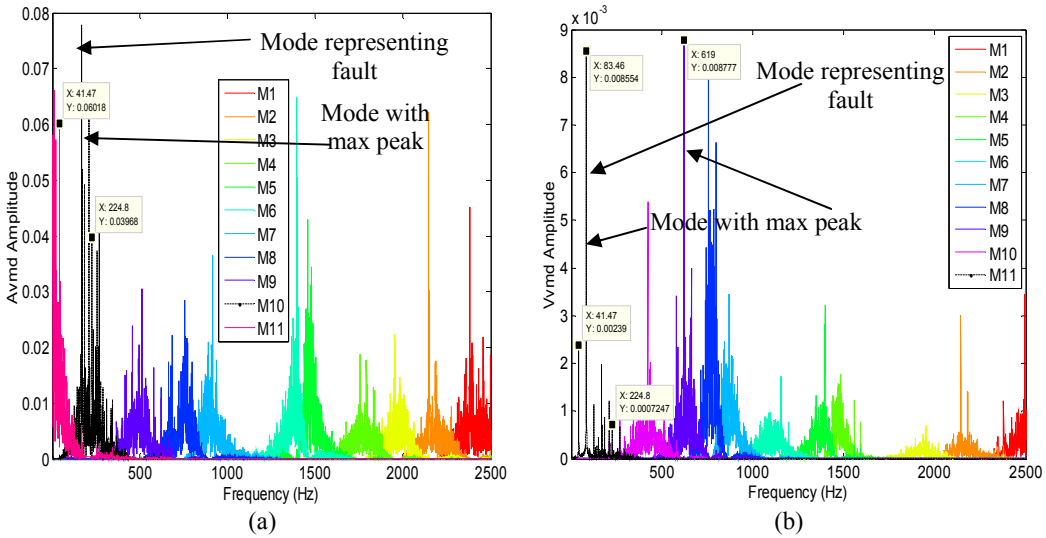

(a) (b)

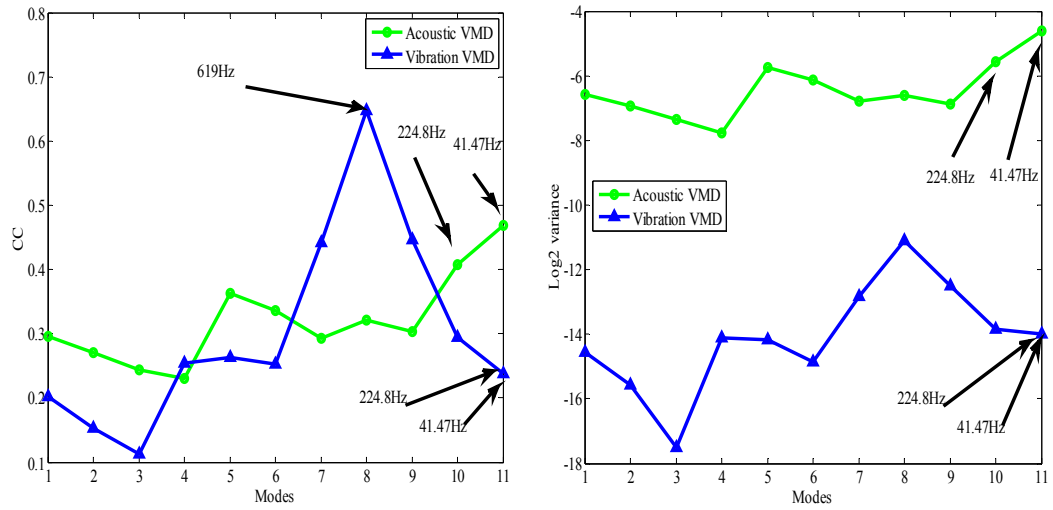

Figure 5.16 VMD modes at 2500 RPM (a) FFT acoustic signal (b) FFT vibration signal (c) $\boldsymbol{CC}$ (d) Log_2 (variance)

Case Study 8: Vibro-Acoustic Signals Analysis at 2000 RPM

It is observed from Fig. 5.17(a) that the fault and shaft rotating frequencies are present in the M10 and M11 modes respectively, and the intensity of the observed signal is found to be better than the extracted modes using EMD. It can be concluded that the spectral leakage for EMD is more compared to VMD. For competitive analysis, the observations are carried out for the vibration signal and the modes are presented in Fig. 5.17(b). The fault and shaft rotation are represented by the M10; it is observed from the mode that the signal intensities are too low compared to that of acoustic. Fig. 5.17(c) clearly shows maximum correlation at M10 and M11 with the varying CC of 0.5, and it matches to that of Fig. 5.17(a). The CC for vibration fails to depict the frequencies and is lacking in comparison to the acoustic in predicting fault. The log.variance analysis in Fig. 5.17(d) has a rising slope at M10 and M11, and represents the fault and shaft rotating frequencies of 180.2 Hz and 33.28 Hz respectively. The fault detections using vibration signals are observed to be poor performer compared to acoustic signals.

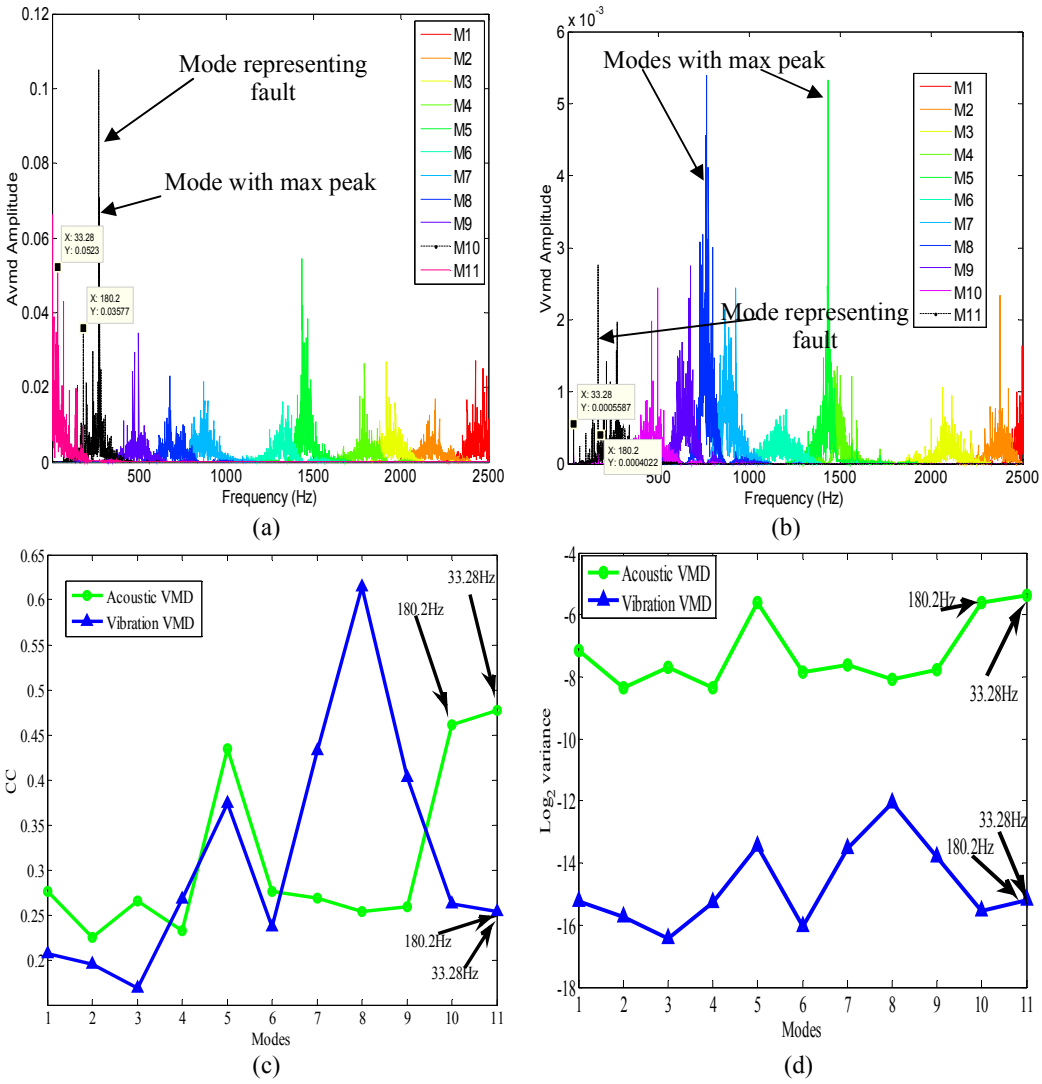

Figure 5.17 VMD modes at 2000 RPM (a) FFT acoustic signal (b) FFT vibration signal (c) $\boldsymbol{CC}$ (d) Log_2 (variance)

Case Study 9: Vibro-Acoustic Signals Analysis at 1500 RPM

The test is performed at a speed of 1500 RPM using VMD, and its effects on the vibro-acoustic modes are detailed in Fig. 5.18. The M10 in Fig. 5.18(a) detects the observed fault frequency at 135.2 Hz with minimal intensity in the spectrum. Fig. 5.18(b) shows the vibration modes and the observed fault frequency in M11. Fig. 5.18(c) shows the maximum correlation at M5 with frequency of 1429.2 Hz. Even if the fault is matched and identified at M10, but, if the mathematical formulation is not considered then the identifier may assume M5 as the actual mode representing the fault. The performance randomly shows 770 Hz at M10 for vibration signal as the actual mode and fails to provide qualitative information related to the fault. The log-variance in Fig. 5.18(d) performs better than CC, but the

performance still lacks in accurately predicting the exact mode. It can be compared that the performance of EMD is better than VMD at 1500 RPM (as CC is maximum at M5). Therefore, the decomposition process carried out by these algorithms can affect the analysis and extraction process.

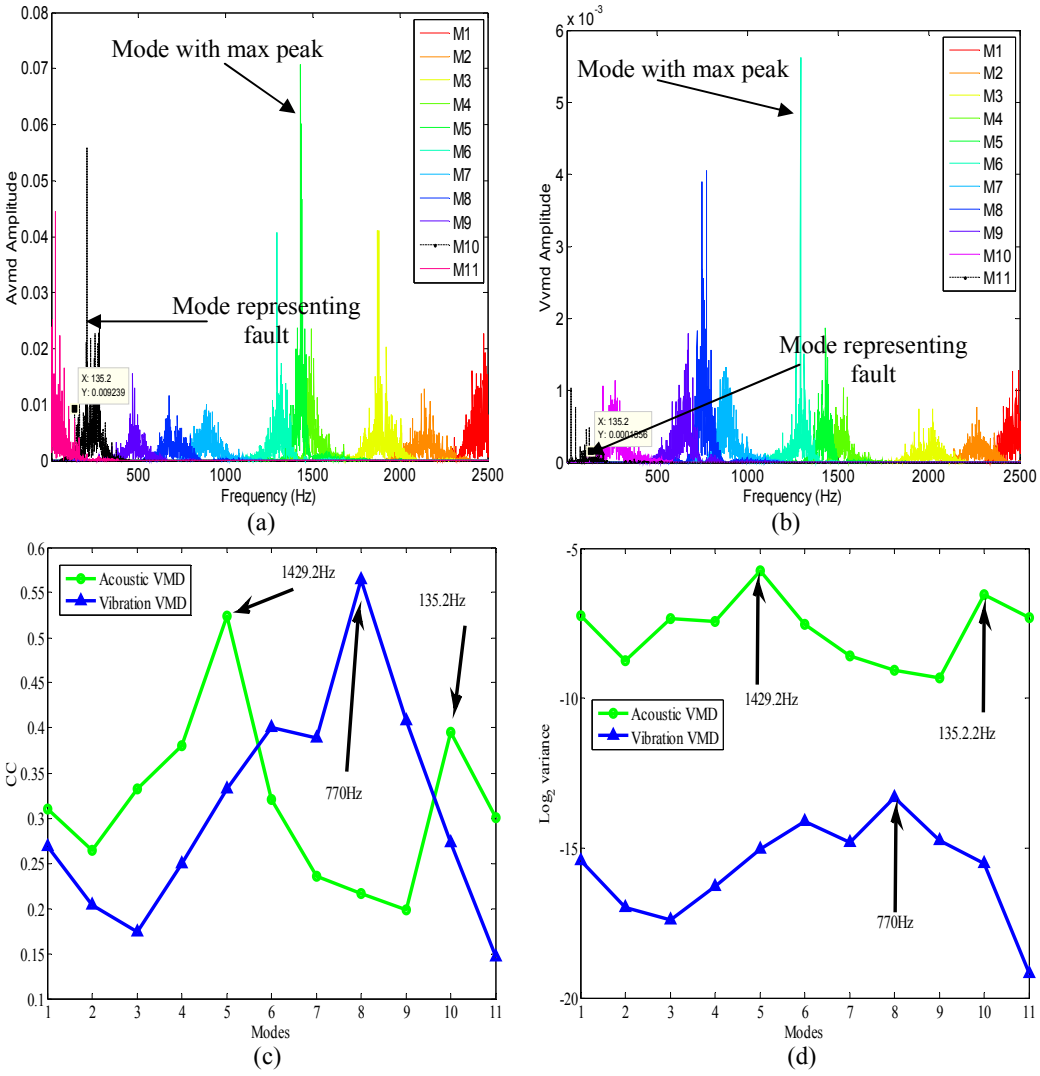

Figure 5.18 VMD modes at 1500 RPM (a) FFT acoustic signal (b) FFT vibration signal (c) $\boldsymbol{CC}$ (d) Log_2 (variance)

Case Study 10: Vibro-Acoustic Signals Analysis at 1000 RPM

Figs. 5.19(a) and (b) represent the acoustic and vibration spectrum for the decomposed modes. It can be observed from Fig. 5.19(a) that the shaft and fault frequencies of 16.38 Hz and 90.11 Hz are noticed in M11. The vibration spectrum in Fig. 5.19(b) reflects the shaft and fault frequencies, but the signals are dipped inside noise. The CC and log_variance for acoustic and vibration in Figs. 5.19(c) and (d) fail to predict the frequencies. It can be concluded that the fault frequency identifications are significant at higher speed, but its performance degrades drastically for lower speed while using CC and log-variance approaches.

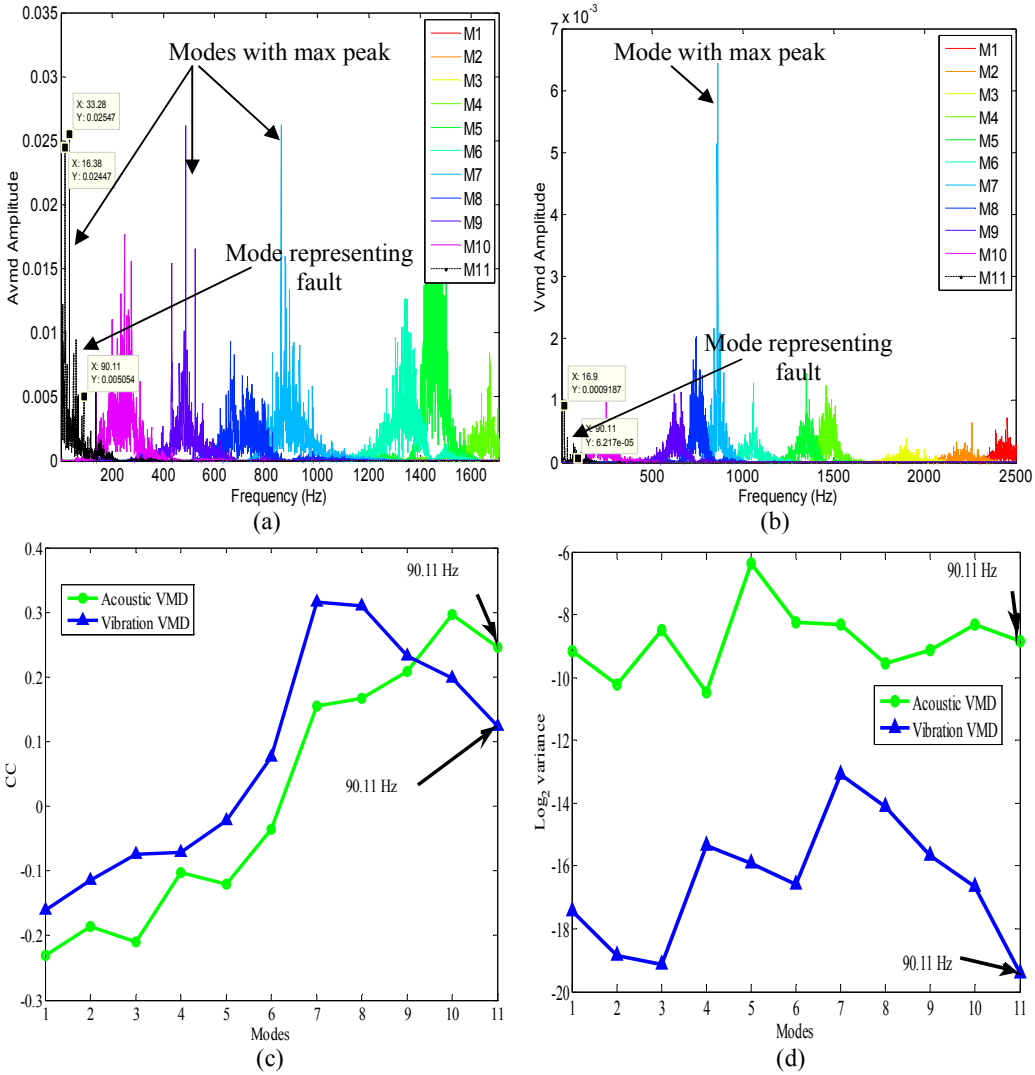

Figure 5.19 VMD modes at 1500 RPM (a) FFT acoustic signal (b) FFT vibration signal (c) CC (d) Log_2 (variance)

5.6 Conclusion

The vibro-acoustic signal analysis and mode selections using CC and log-variance, based on EMD and VMD techniques, have shown favorable results in fault detection at variable speeds. The mode mixing issues faced by EMD during signal decomposition are mitigated using VMD. It is observed that the performance of EMD is better than VMD at 1500 RPM and detects the shaft speed and fault frequencies effectively using CC and log-variance selection methods. But, the analysis shows that for lower RPM of 1000, both EMD and VMD fail to identify the mode significantly using CC and log-variance plots. However, this analysis shows that the performances of VMD are better than EMD for the acoustic signal at higher RPM i.e. above 1500, and clearly depict the actual mode representing the fault and shaft frequencies. It is observed that the vibration signals are responsive in detecting higher order shaft rotating frequencies for certain cases. This analysis suggests that VMD is more immune to noise compared to EMD as the noise floor increases with increase in speed. Similarly, the mode selection using CC and log-variance are in congruence and show the concentration of high energy for the VMD as compared to EMD.

CHAPTER 6
Conclusions and Future Works

6.1 Contributions

Traditionally, the fault diagnosis using vibration has contributed its majority share in identifying faults related to bearings. For verification and identification of faults related to the bearing, three different signal processing approaches are proposed and validated on the CWRU and experimental data sets. In the first approach, standardized EMD-PCA based average kurtosis technique followed by envelope, cepstral and cepstral envelope analysis (FECCV) are used to diagnose faults in the bearings adaptively. This proposed EMD-PCA based average kurtosis technique concurrently decomposes as well as de-correlates the mixed modes, thereby increasing the detection sensitivity of fault. It is observed that the envelope detection is more sensitive to noise as compared to the cepstral envelope method. It is also observed that it helps in detecting lower dimensional defects of IRD, ORD, and BD effectively.

In the second approach, the IRD and ORD are tested using unitary sample shifted Laplacian and rectangular framed based FCF, FKS and FE techniques. Initially, KS test is performed on healthy, IRD, ORD and BD signals to identify the actual distribution function. It is observed that the healthy and BD signals are closely related to the normal distribution, whereas, the IRD and ORD signals to Laplacian distribution. To segregate the faults, Laplacian and rectangular distribution functions are used to generate unitary sliding time series. These time series, i.e. FCF, FKS and FE are observed to be beneficial in detecting faults and their harmonics, in the signals. It is also observed that the proposed Laplacian distribution functions closely match with the faulty signals and reduce the leakages in the signal extraction process. This method is found to be free from traditional demodulation method, as it concurrently suppresses the carrier frequencies during the generation of frame based time series.

In the third approach, the performances of vibroacoustic sensors are tested to detect faults. Initially, the vibration and acoustic signals are processed using EMD-VMD techniques. It is observed, EMD shows mode mixing issues in the spectrum, whereas VMD is free from it. The performance of VMD is better than EMD for almost all the cases except

at 1500 RPM for the acoustic signal. The faulty modes are selected using CC and log-variance and it is found that the acoustic signals perform better in detecting faults and shaft rotation under variable speed. Whereas, the vibration sensor merely traces the fault in the signal, except the shaft rotating frequency for certain cases. These results clearly show the usability of pressure microphone in the area of fault detection.

Finally, it is observed from the discussions and analysis that the BCM is complicated and needs intuitive signal analysis. It is observed that the probability density function is the most vital factor, which can be used to predict the signal behavior. The nonlinear signal processing techniques can be adapted to segregate fault signal from the noise. Apart from signal processing, it is inferred that sensors play a major role in acquiring signals. This analysis shows that the microphone can be used to detect faults. During experimental observations, it is inferred that the detection and acquisition of signals depend on the test bench, and it is very difficult to project this analysis for other BCM systems.

6.2 Future Works

The observations from the experimental results show that the algorithms are sensitive to the applications, system components, and the environment; therefore, these cannot be applied directly to diverse fields. Hence, in future studies the main focus will be to characterize the signals i.e. chaotic, random or Brownian, and the why and how factors that change their behavior.

References

[1] Case Western university Bearing Data Center, Accessed on 19/06/2014
https://csegroups.case.edu/bearingdatacenter/pages/download-data-file

[2] Hightower T. V., The Harmony of the Spheres, Accessed on 19/06/2013.
http://vaczy.dk/htm/spheres.htm

[3] Marketsandmarkets.com, Machine condition monitoring market by monitoring type (vibration monitoring, ultrasound monitoring, thermography, & others), components, monitoring process (portable & online condition monitoring), applications, and geography-global trend & forecast to 2020, November 2015, Accessed on 08/07/2016.
http://www.marketsandmarkets.com/Market-Reports/machine-health-monitoring-market-29627363.html

[4] Zhao, R., Yan, R., Wang, J. and Mao, K., 2017. Learning to monitor machine health with convolutional bi-directional LSTM networks. *Sensors*, *17*(2), pp. 1-18.

[5] National Instruments, 2016. Machine condition monitoring technical library. Accessed on 06/05/2016.
http://www.ni.com/white-paper/6511/en/

[6] SKF, SKF condition monitoring-Vibration Sensors, Accessed on 08/08/2015.
http://www.exvalos.cz/soubory/File/SKF/SNIMACE_VIBRACI.pdf

[7] Da Silva, A.M., 2006. *Induction motor fault diagnostic and monitoring methods* (Doctoral dissertation, Marquette University).

[8] Kontargyri, V., Tsirekis, C., Kabanaros, S., Sakarellos, A., Moronis, A., Kolliopoulos, N. and Kaminaris, S., 2007, May. An expert system for fault diagnosis, repairing and maintenance of electrical machines. In *Proceedings of the 6th conference on Applications of electrical engineering* (pp. 166-171). World Scientific and Engineering Academy and Society (WSEAS).

[9] NSK, Type and classification of roller bearings, Accessed on 18/03/2015.
http://www.nsk.com.br/upload/file/NSK_CAT_E1102m_A7-141.pdf

[10] Mechanical failure prevention group,1972. Detection, diagnosis and prognosis, Accessed on 20/03/2015.
https://www.gpo.gov/fdsys/pkg/GOVPUB-C13-fd1c3858e9b573ae7d894b949337785a/pdf/GOVPUB-C13-fd1c3858e9b573ae7d894b949337785a.pdf

[11] Graney, B.P. and Starry, K., 2012. Rolling element bearing analysis. *Materials Evaluation*, *70*(1), pp.78-85.

[12] B&K, Detecting faulty rolling-element bearings-Application notes.
Available on: https://www.bksv.com/media/doc/BO0210.pdf, Accessed on 18/05/2016.

[13] Liu, W.Y., Han, J.G. and Jiang, J.L., 2013. A novel ball bearing fault diagnosis approach based on auto term window method. Measurement, 46(10), pp.4032-4037.

[14] Rezaei, A., Dadouche, A., Wickramasinghe, V. and Dmochowski, W., 2011. A comparison study between acoustic sensors for bearing fault detection under different speed and load using a variety of signal processing techniques. *Tribology Transactions*, *54*(2), pp.179-186.

[15] Prashad, H., 1987. The effect of cage and roller slip on the measured defect frequency response of rolling-element bearings. *ASLE transactions*, *30*(3), pp.360-367.

[16] Shuang, L. and Jing, L., 2006. Fault diagnosis of bearing based on fractal method. In *Signal Processing,*

2006 8th International Conference on (Vol. 1). IEEE.

[17] Bently, D.E., Goldman, P. and Yu, J.J., 2001. Rolling element bearing defect detection and diagnostics using REBAM® probes. *Orbit*, *22*(2), pp.12-25.

[18] Guo, W., Cao, H., He, Z. and Yang, L., 2015. Fatigue life analysis of rolling bearings based on quasistatic modeling. *Shock and Vibration*, *2015*. pp.1-10.

[19] Vencl., A, Gasic, V and V,Stojanovic, B., 2017, February. Fault tree analysis of most common rolling bearing tribological failures. In *IOP Conference Series: Materials Science and Engineering* (Vol. 174, No. 1, p. 012048). IOP Publishing.

[20] National Instruments, 2016. Sensors for condition monitoring, Accessed on 12/05/2016. http://www.ni.com/white-paper/52461/en/

[21] GE, 2007. NDT Guide to non-destructive testing, Accessed on 12/04/2016. http://www.asminternational.org/documents/10192/1895041/amp16512p033.pdf/096e1126-602e-4683-acfe-fb8699244d22

[22] Sawalhi, N., Randall, R.B. and Endo, H., 2007. The enhancement of fault detection and diagnosis in rolling element bearings using minimum entropy deconvolution combined with spectral kurtosis. *Mechanical Systems and Signal Processing*, *21*(6), pp. 2616-2633.

[23] Messer A., 2015, Mechanical Remote Monitoring with Ultrasound, Accessed on 12/04/2016. http://www.bearing-news.com/mechanical-remote-monitoring-with-ultrasound/

[24] Irfan, M., Saad, N., Ibrahim, R., Asirvadam, V.S., Alwadie A.S. and Sheikh M.A., 2017. An assessment on the non-invasive methods for condition monitoring of induction motors, Fault Diagnosis and Detection, *InTech*, PP.86-129.
Available from: https://www.intechopen.com/books/fault-diagnosis-and-detection/an-assessment-on-the-non-invasive-methods-for-condition-monitoring-of-induction-motors

[25] Houser, D.R. and Drosjack, M.J., 1973. *Vibration signal analysis techniques*. Ohio State Univ. Columbus Dept of Mechanical and Aerospace Engineering.

[26] Tandon, N., 1994. A comparison of some vibration parameters for the condition monitoring of rolling element bearings. *Measurement*, *12*(3), pp.285-289.

[27] Peton, N., 2011. Balancing with the presence of a rub. *Mechanics & Industry*, *12*(5), pp.409-418.

[28] Shieh, J., Huber, J.E., Fleck, N.A. and Ashby, M.F., 2001. The selection of sensors. *Progress in Materials Science*, *46*(3), pp.461-504.

[29] Article on vibration measurement instruments and analyzers: specs and apps, IEEE, Accessed on:16/7/16 http://insights.globalspec.com/article/1166/vibration-measurement-instruments-and-analyzers-specs-and-apps

[30] Lally, J., 2005. Technical notes on accelerometer selection considerations charge and ICP ® integrated circuit piezoelectric. PCB Piezotronics, pp.1-5.

[31] Slifka, L.D., 2004. An accelerometer based approach to measuring displacement of a vehicle body. *Master of Science in Engineering, Department of Electrical and Computer Engineering, University of Michigan–Dearborn*.

[32] Han, S. and Lee, J. B., 2001. Analysis of errors in the conversion of acceleration into displacement. In *Proceedings of SPIE, the International Society for Optical Engineering* (Vol. 4359, pp. 1408-1413). Society of Photo-Optical Instrumentation Engineers.

[33] Ribeiro, J.G., De Castro, J.T. and Freire, J.L., 2003. Using the FFT-DDI method to measure displacements with piezoelectric, resistive and ICP accelerometers. In *Conference and exposition on structural dynamics*.

[34] Emerson Process Management, 2014. Measurement types in machinery monitoring, Accessed on 12/07/2015
http://www2.emersonprocess.com/siteadmincenter/PM%20Asset%20Optimization%20Documents/ProductWhitePapers/MHM_wp_MsrmntTypes.pdf

[35] MacDonald, G.A., 1990. A review of low cost accelerometers for vehicle dynamics. *Sensors and Actuators A: Physical*, *21*(1-3), pp.303-307.

[36] Albarbar, A., Mekid, S., Starr, A. and Pietruszkiewicz, R., 2008. Suitability of MEMS accelerometers for condition monitoring: An experimental study. *Sensors*, *8*(2), pp.784-799.

[37] Monajemi, P. and Ayazi, F., 2006. Design optimization and implementation of a microgravity capacitive HARPSS accelerometer. *IEEE Sensors Journal*, *6*(1), pp.39-46.

[38] Voldman, J., 2007. Case study: A capacitive accelerometer. *Massachusetts Institute of Technology*.

[39] Saeed S., and Farhad A., 2014, July. Effects of accelerometer mounting methods on quality of measured FRF's, *The 21st International Congress on Sound and Vibration* (pp.1-8). ICSV.

[40] Mohanty, S., Gupta, K.K., Raju, K.S., Mishra, V., Kumar, V. and Prasad, P.B., 2014, February. Characterization of wireless accelerometer sensor and its industrial applications. In *Communications (NCC), 2014 Twentieth National Conference on* (pp.1-5). IEEE.

[41] Cristalli, C., Paone, N. and Rodríguez, R.M., 2006. Mechanical fault detection of electric motors by laser vibrometer and accelerometer measurements. *Mechanical Systems and Signal Processing*, *20*(6), pp.1350-1361.

[42] Pingle, P., Sailhamer, J. and Avitabile, P., 2009. Comparison of 3D laser vibrometer and accelerometer frequency measurements. *Proceedings of the IMAC-XXVII*, *9*, pp.1-12.

[43] Dzwonkowski, A., Swedrowski, L. and Swędrowski, L., 2011, September. Motor bearing diagnostics performed by means of laser vibrometer. In *Diagnostics for Electric Machines, Power Electronics & Drives (SDEMPED), 2011 IEEE International Symposium on* (pp.482-486). IEEE.

[44] Rodriguez, R.M., Cristalli, C. and Paone, N., 2002, May. Comparative study between laser vibrometer and accelerometer measurements for mechanical fault detection of electric motors. In *Fifth International Conference on Vibration Measurements by Laser Techniques* (pp.521-529). International Society for Optics and Photonics.

[45] Goyal, D. and Pabla, B.S., 2016. The vibration monitoring methods and signal processing techniques for structural health monitoring: A review. *Archives of Computational Methods in Engineering*, *23*(4), pp.585-594.

[46] Johansmann, M., Siegmund, G. and Pineda, M., 2005. Targeting the limits of laser Doppler vibrometry. *Proceedings IDEMA*, pp.1-12.

[47] Whittaker, G.A., Shives, T.R. and Philips, G.J. eds., 1983. *Technology Advances in Engineering and Their Impact on Detection, Diagnosis and Prognosis Methods: Proceedings of the 36th Meeting of the Mechanical Failures Prevention Group, La Posada Hotel, Scottsdale, Arizona, December 6-10, 1982* (Vol. 36). CUP Archive.

[48] Fujicera.co, Acoustic Emission Sensor. Accessed on 5/04/2014
http://www.fujicera.co.jp/product/e/05/index.html

[49] Tandon, N. and Choudhury, A., 1999. A review of vibration and acoustic measurement methods for the detection of defects in rolling element bearings. *Tribology international*, *32*(8), pp.469-480.

[50] Morhain, A. and Mba, D., 2003. Bearing defect diagnosis and acoustic emission. *Proceedings of the Institution of Mechanical Engineers, Part J: Journal of Engineering Tribology*, *217*(4), pp.257-272.

[51] Capgo, Condition monitoring. Accessed on 23/07/2015
http://www.capgo.com/Resources/ConditionMonitoring/index.html

[52] McLaskey, G.C. and Glaser, S.D., 2012. Acoustic emission sensor calibration for absolute source measurements. *Journal of Nondestructive Evaluation*, *31*(2), pp.157-168.

[53] Qu, Y., He, D., Yoon, J., Van Hecke, B., Bechhoefer, E. and Zhu, J., 2014. Gearbox tooth cut fault diagnostics using acoustic emission and vibration sensors-A comparative study. *Sensors*, *14*(1), pp.1372-1393.

[54] UE Systems Inc. Ultrasonic predictive maintainance, How to locate mechanical problems. Accessed on 23/07/2016
http://media.noria.com/sites/WhitePapers/WPFILES/UESYSTEMS200904-2.pdf

[55] Rockwell Automation, Ultrasonic sensing, Accessed on 23/07/2016
http://www.ab.com/en/epub/catalogs/12772/6543185/12041221/12041229/Ultrasonic-Advantages-and-Disadvantages.html

[56] Kim, Y.H., Tan, A.C., Mathew, J. and Yang, B.S., 2006. Condition monitoring of low speed bearings: A comparative study of the ultrasound technique versus vibration measurements. In *Engineering asset management* (pp. 182-191). Springer London.

[57] Sawalhi, N., Randall, R.B. and Endo, H., 2007. The enhancement of fault detection and diagnosis in rolling element bearings using minimum entropy deconvolution combined with spectral kurtosis. *Mechanical Systems and Signal Processing*, *21*(6), pp.2616-2633.

[58] Rezaei, A., Dadouche, A., Wickramasinghe, V. and Dmochowski, W., 2011. A comparison study between acoustic sensors for bearing fault detection under different speed and load using a variety of signal processing techniques. *Tribology Transactions*, *54*(2), pp.179-186.

[59] Raharjo, P., Abdusslam, S.A., Gu, F. and Ball, A., 2012, June. Vibro-acoustic characteristic of a self aligning spherical journal bearing due to eccentric bore fault. In: *The Ninth International Conference on Condition Monitoring and Machinery Failure Prevention Technologies* (pp.1-28).

[60]Bellaj, S., Pouzet, A., Mellet, C., Vionnet, R. and Chavance, D., 2011, May. Vibroacoustic Measurement for Bearing Fault Detection on High Speed Trains. In *WCRR (World Congress Railway Research)* (pp. 2-7).

[61] Rodriguez, P. H., 2014. Advances in preventive monitoring of machinery through audio and vibration signals, PHD Thesis, Universidad De Las Palmas De Gran Canaria.

[62] Bagavathiappan, S., Lahiri, B.B., Saravanan, T., Philip, J. and Jayakumar, T., 2013. Infrared thermography for condition monitoring–a review. *Infrared Physics & Technology*, *60*, pp.35-55.

[63] Schulz, R., Verstockt, S., Vermeiren, J., Loccufier, M., Stockman, K. and Van Hoecke, S., 2014, July. Thermal imaging for monitoring rolling element bearings. In *12th International Conference on Quantitative InfraRed Thermography* (pp. 7-11).

[64] Feng, L., Jianfeng, L., Yu, M., Rui, T., Ren, L., Bo, Z., Wei, L., Lin, L., Zhaoxia, W., Xingjun, C., Guorui, C., and Min, L., 2016, Feb. An infrared detection method used in electrical equipment fault diagnosis. *4th International Conference on Machinery, Materials and Computing Technology* (pp.1-4).

[65] Miljkovic, D., 2015. Brief review of motor current signature analysis. *HDKBR INFO Magazine*, *5*(1), pp.14-26.

[66] Cristaldi, L., Faifer, M., Lazzaroni, M. and Toscani, S., 2009. An inverter-fed induction motor diagnostic tool based on time-domain current analysis. *IEEE Transactions on Instrumentation and Measurement*, *58*(5), pp.1454-1461.

[67] Singh, S., Kumar, A., and Kumar, N., 2014. Detection of bearing faults in mechanical systems using motor current signature and acoustic signatures. The 21st international congress on sound and vibration, Beijing/China, pp. 1–8.

[68] Nandi, S., Toliyat, H.A. and Li, X., 2005. Condition monitoring and fault diagnosis of electrical motors-a review. *IEEE transactions on energy conversion*, *20*(4), pp.719-729.

[69] Yang, T., Pen, H., Wang, Z. and Chang, C.S., 2016. Feature knowledge based fault detection of induction motors through the analysis of stator current data. *IEEE Transactions on Instrumentation and Measurement*, *65*(3), pp.549-558.

[70] Tsoumas, I., Mitronikas, E., Georgoulas, G. and Safacas, A., 2005, September. A comparative study of induction motor current signature analysis techniques for mechanical faults detection. In *Diagnostics for Electric Machines, Power Electronics and Drives, 2005. SDEMPED 2005. 5th IEEE International Symposium on* (pp. 1-6). IEEE.

[71] Gong, X. and Qiao, W., 2013. Bearing fault diagnosis for direct-drive wind turbines via current-demodulated signals. *IEEE Transactions on Industrial Electronics*, *60*(8), pp.3419-3428.

[72] Bellini, A., Immovilli, F., Rubini, R. and Tassoni, C., 2008, October. Diagnosis of bearing faults of induction machines by vibration or current signals: A critical comparison. In *Industry Applications Society Annual Meeting, 2008. IAS'08. IEEE* (pp. 1-8). IEEE.

[73] Hodge, V.J., O'Keefe, S., Weeks, M. and Moulds, A., 2015. Wireless sensor networks for condition monitoring in the railway industry: A survey. *IEEE Transactions on Intelligent Transportation Systems*, *16*(3), pp.1088-1106.

[74] Emerson process management. 2014. White paper on measurement types in machinery monitoring.

[75] Saeed, S. and Farhad, A., 2014, July. Effects of accelerometer mounting methods on quality of measured FRF'S. *ICSV international congress on acoustic and vibration* (pp.1-8).

[76] Jiang, K., Xu, G., Liang, L., Tao, T. and Gu, F., 2014. The recovery of weak impulsive signals based on stochastic resonance and moving least squares fitting. *Sensors*, *14*(8), pp.13692-13707.

[77] Shannon, B. 2008, March. Vibration measurement systems and guidelines for centrifugal fans- a field perspective. *AMCA International Engineering Conference* (pp.1-24).

[78] Smith, W.A. and Randall, R.B., 2015. Rolling element bearing diagnostics using the Case Western Reserve University data: A benchmark study. *Mechanical Systems and Signal Processing*, *64*, pp.100-131.

[79] Duan, F., Elasha, F., Greaves, M. and Mba, D., 2016, June. Helicopter main gearbox bearing defect identification with acoustic emission techniques. In *Prognostics and Health Management (ICPHM), 2016 IEEE International Conference on* (pp. 1-4). IEEE.

[80] He, Y.Y., Chu, F.L. and Wang, Q.Y., 2001. Acoustic emission technique based rubbing identification for Rotor-bearing systems. *Science in China Series A-Mathematics Physics Astronomy*, *44*, pp.459-465.

[81] Wirtz, S.F., Beganovic, N., Tenberge, P. and Söffker, D., 2016. Frequency-based damage detection of spur

gear using wavelet analysis. In *Proceedings of 8th European Workshop on Structural Health Monitoring, Bilbao, Spain*(pp. 1-10).

[82] Berger, H., 1977. *Nondestructive Testing Standards: a Review: A Symposium Gaithersburg, MD., 19-21 May 1976* (Vol. 624). ASTM International.

[83] Bandes, A., 2012. Ultrasonic Condition Monitoring. *Materials Evaluation*, *70*(1), pp. 1-9.

[84] NI, 2017, G.R.A.S. selection guide for microphones and preamplifiers, Accessed on 23/09/2016 http://www.ni.com/white-paper/14044/en/

[85] Henriquez, P., Alonso, J.B., Ferrer, M.A. and Travieso, C.M., 2014. Review of automatic fault diagnosis systems using audio and vibration signals. *IEEE Transactions on Systems, Man, and Cybernetics: Systems*, *44*(5), pp.642-652.

[86] Verma, N.K., Singh, S., Gupta, J.K., Sevakula, R.K., Dixit, S. and Salour, A., 2012, December. Smartphone application for fault recognition. In *Sensing Technology (ICST), 2012 Sixth International Conference on* (pp. 1-6). IEEE.

[87] Zhou, W., Habetler, T.G. and Harley, R.G., 2007, September. Bearing condition monitoring methods for electric machines: A general review. In *Diagnostics for Electric Machines, Power Electronics and Drives, 2007. SDEMPED 2007. IEEE International Symposium on* (pp. 3-6). IEEE.

[88] Lifshits, A., Simmons, H.R. and Smalley, A.J., 1986. More comprehensive vibration limits for rotating machinery. *Journal of engineering for gas turbines and power*, *108*(4), pp.583-590.

[89] Corne, B., Vervisch, B., Debruyne, C., Knockaert, J. and Desmet, J., 2015, May. Comparing MCSA with vibration analysis in order to detect bearing faults-A case study. In *Electric Machines & Drives Conference (IEMDC), 2015 IEEE International* (pp. 1366-1372). IEEE.

[90] Carullo, A., Casassa, F., Castellana, A., Astolfi, A., Pavese, L. and Puglisi, G.E., 2015, June. Performance comparison of different contact microphones used for voice monitoring. In *22nd Interntion congress on sound and vibration* (pp.1-8).

[91] NI, White paper on Complete guide to building a measurement system http://download.ni.com/evaluation/daq/Measurement_System_Build_Guide.pdf

[92] Stack, J.R., Harley, R.G., and Habetler, T.G., 2004. An amplitude modulation detector for fault diagnosis in rolling element bearings. *IEEE Transactions on Industrial Electronics*, *51*(5), pp.1097-1102.

[93] Sheen, Y.T., 2007. An analysis method for the vibration signal with amplitude modulation in a bearing system. *Journal of Sound and Vibration*, *303*(3), pp.538-552.

[94] Lacey, S.J., 2008. An overview of bearing vibration analysis. *Maintenance & Asset Management*, *23*(6), pp.32-42.

[95] Jones, R.M., 1996. Enveloping for bearing analysis. *Sound and vibration*, *30*(2), pp.10-15.

[96] Finley, W.R., 2000. Troubleshooting induction motors. In *Industry Applications Conference, 2000. Conference Record of the 2000 IEEE* (Vol. 5, pp. 3491-3498). IEEE.

[97] Siringoringo, D.M., Nagayama, T., Fujino, Y., Su, D., Tandian, C. and Miura, H., vibration study and application of outlier analysis to the s101 bridge full-scale destructive testing, pp.305-330.

[98] Subramaniam, S., Palpanas, T., Papadopoulos, D., Kalogeraki, V. and Gunopulos, D., 2006, September. Online outlier detection in sensor data using non-parametric models. In *Proceedings of the 32nd international conference on Very large data bases* (pp. 187-198). VLDB Endowment.

[99] Kaiser, R. and Maravall, A., 1999. Seasonal outliers in time series. *Statistics and Econometrics Series 15,* pp.1-27.

[100] Jayaswal, P., Wadhwani, A.K. and Mulchandani, K.B., 2008. Machine fault signature analysis. *International Journal of Rotating Machinery*, *2008*, pp.1-10.

[101] Howard, I., 1994. *A review of rolling element bearing vibration detection, diagnosis and prognosis* (No. DSTO-RR-0013).Defence Science and Technology Organization Canberra (Australia).

[102] Yang, H., Mathew, J. and Ma, L., 2003, Nov. Vibration feature extraction techniques for fault diagnosis of rotating machinery: a literature survey, In *Asia-Pacific Vibration Conference* (pp.1-8).

[103] Almeida, F.R.D.V. and Almeida, M.T.D., 2005, Nov. Statistical analysis of vibration signals for condition monitoring of defects in rolling element bearings. In *Proceedings of the COBEM 2005: 18th International Congress of Mechanical Engineering* (pp.1-8).

[104] Nikias, C.L. and Mendel, J.M., 1993. Signal processing with higher-order spectra. *IEEE signal processing magazine*, *10*(3), pp.10-37.

[105] Igba, J., Alemzadeh, K., Durugbo, C. and Eiriksson, E.T., 2016. Analysing RMS and peak values of vibration signals for condition monitoring of wind turbine gearboxes. *Renewable Energy*, *91*, pp.90-106.

[106] Fu, S., Liu, K., Xu, Y. and Liu, Y., 2016. Rolling bearing diagnosing method based on time domain analysis and adaptive fuzzy-means clustering. *Shock and Vibration*, *2016*. pp.1-8.

[107] Liang, Z., Wei, J., Zhao, J., Liu, H., Li, B., Shen, J. and Zheng, C., 2008. The statistical meaning of kurtosis and its new application to identification of persons based on seismic signals. *Sensors*, *8*(8), pp.5106-5119.

[108] Gomez-Villegas, M.A., Main, P., Navarro, H. and Susi, R., 2013. Assessing the effect of kurtosis deviations from Gaussianity on conditional distributions. *Applied Mathematics and Computation*, *219*(21), pp.10499-10505.

[109] Osuagwu, C.C., 1989. Fault detection using the zero crossing rate. *Nigerian Journal of Technology*, *13*(1), pp.16-25.

[110] Tom, K.F., 2015. *A primer on vibrational ball bearing feature generation for prognostics and diagnostics algorithms* (No. ARL-TR-7230). Army Research Lab Adelphi MD Sensors and Electron Devices Directorate.

[111] Han, L., Li, C. and Liu, H., 2015. Feature extraction method of rolling bearing fault signal based on EEMD and cloud model characteristic entropy. *Entropy*, *17*(10), pp.6683-6697.

[112] Rosser, G., Fletcher, A.G., Maini, P.K. and Baker, R.E., 2013. The effect of sampling rate on observed statistics in a correlated random walk. *Journal of The Royal Society Interface*, *10*(85), pp. 1-11.

[113] Sreejith, B., Verma, A.K. and Srividya, A., 2008, December. Fault diagnosis of rolling element bearing using time-domain features and neural networks. In *Industrial and Information Systems, 2008. ICIIS 2008. IEEE Region 10 and the Third international Conference on* (pp. 1-6). IEEE.

[114] Immovilli, F., Cocconcelli, M., Bellini, A. and Rubini, R., 2009. Detection of generalized-roughness bearing fault by spectral-kurtosis energy of vibration or current signals. *IEEE Transactions on Industrial*

Electronics, *56*(11), pp.4710-4717.

[115] Kang, M., Kim, J., Wills, L.M. and Kim, J.M., 2015. Time-varying and multiresolution envelope analysis and discriminative feature analysis for bearing fault diagnosis. *IEEE Transactions on Industrial Electronics*, *62*(12), pp.7749-7761.

[116] Jia, F., Lei, Y., Shan, H. and Lin, J., 2015. Early fault diagnosis of bearings using an improved spectral kurtosis by maximum correlated kurtosis deconvolution. *Sensors*, *15*(11), pp.29363-29377.

[117] Tian, J., Morillo, C., Azarian, M. H., and Pecht, M., 2016. Kurtosis-based feature extraction coupled with k-nearest neighbor distance analysis. *IEEE Transactions on Industrial Electronics, 63*(3), pp. 1793–1803.

[118] Antoni, J., 2006. The spectral kurtosis: a useful tool for characterising non-stationary signals. *Mechanical Systems and Signal Processing*, *20*(2), pp.282-307.

[119] Wang, Y. and Liang, M., 2011. An adaptive SK technique and its application for fault detection of rolling element bearings. *Mechanical Systems and Signal Processing*, *25*(5), pp.1750-1764.

[120] Cocconcelli, M., Zimroz, R., Rubini, R. and Bartelmus, W., 2012. STFT based approach for ball bearing fault detection in a varying speed motor. In *Condition Monitoring of Machinery in Non-Stationary Operations* (pp. 41-50). Springer Berlin Heidelberg.

[121] Bechhoefer, E., Kingsley, M. and Menon, P., 2011, June. Bearing envelope analysis window selection using spectral kurtosis techniques. In *Prognostics and Health Management (PHM), 2011 IEEE Conference on* (pp. 1-6). IEEE.

[122] Tian, Q., Hou, C. and Li, S., 2013, July. Adaptive resonant demodulation for early fault diagnosis of ball bearing. In *Signal and Information Processing (ChinaSIP), 2013 IEEE China Summit & International Conference on* (pp. 34-38). IEEE.

[123] Lau, E.C. and Ngan, H.W., 2010. Detection of motor bearing outer raceway defect by wavelet packet transformed motor current signature analysis. *IEEE Transactions on Instrumentation and measurement*, *59*(10), pp.2683-2690.

[124] Liu, J., Wang, W. and Golnaraghi, F., 2008. An extended wavelet spectrum for bearing fault diagnostics. *IEEE Transactions on Instrumentation and Measurement*, *57*(12), pp.2801-2812.

[125] Yan, R. and Gao, R.X., 2009. Energy-based feature extraction for defect diagnosis in rotary machines. *IEEE Transactions on Instrumentation and Measurement*, *58*(9), pp.3130-3139.

[126] Saidi, L., Ali, J.B., Benbouzid, M. and Bechhoefer, E., 2016. The use of SESK as a trend parameter for localized bearing fault diagnosis in induction machines. *ISA transactions*, *63*, pp.436-447.

[127] Mohanty, S., Gupta, K.K. and Raju, K.S., 2017. Adaptive fault identification of bearing using empirical mode decomposition–principal component analysis-based average kurtosis technique. *IET Science, Measurement & Technology*, *11*(1), pp.30-40.

[128] Chen, B., Yan, Z. and Chen, W., 2014. Defect detection for wheel-bearings with time-spectral kurtosis and entropy. *Entropy*, *16*(1), pp.607-626.

[129] Soualhi, A., Medjaher, K. and Zerhouni, N., 2015. Bearing health monitoring based on Hilbert–Huang transform, support vector machine, and regression. *IEEE Transactions on Instrumentation and Measurement*, *64*(1), pp.52-62.

[130] Picot, A., Obeid, Z., Regnier, J., Poignant, S., Darnis, O. and Maussion, P., 2014. Statistic-based spectral indicator for bearing fault detection in permanent-magnet synchronous machines using the stator current. *Mechanical systems and signal processing*, *46*(2), pp.424-441.

[131] Leite, V.C., da Silva, J.G.B., Veloso, G.F.C., da Silva, L.E.B., Lambert-Torres, G., Bonaldi, E.L. and de Oliveira, L.E.D.L., 2015. Detection of localized bearing faults in induction machines by spectral kurtosis and envelope analysis of stator current. *IEEE Transactions on Industrial Electronics*, *62*(3), pp.1855-1865.

[132] Feng, Z., Liang, M. and Chu, F., 2013. Recent advances in time–frequency analysis methods for machinery fault diagnosis: a review with application examples. *Mechanical Systems and Signal Processing*, *38*(1), pp.165-205.

[133] Boudiaf, A., Moussaoui, A., Dahane, A. and Atoui, I., 2016. A comparative study of various methods of bearing faults diagnosis using the Case Western Reserve University Data. *Journal of Failure Analysis and Prevention*, *16*(2), pp.271-284.

[134] Mohanty, S., Gupta, K. K. and Raju, K.S., 2014, December. Comparative study between VMD and EMD in bearing fault diagnosis. In *2014 9th International Conference on Industrial and Information Systems (ICIIS)* (pp. 1-6). IEEE.

[135] Lahmiri, S., 2014. Comparative study of ECG signal denoising by wavelet thresholding in empirical and variational mode decomposition domains. *Healthcare technology letters*, *1*(3), pp.104-109.

[136] Li, Y., Xu, M., Wei, Y. and Huang, W., 2016. Health condition monitoring and early fault diagnosis of bearings using SDF and Intrinsic characteristic-scale decomposition. *IEEE Transactions on Instrumentation and Measurement*, *65*(9), pp.2174-2189.

[137] Huang, N.E., Wu, M.L., Qu, W., Long, S.R. and Shen, S.S., 2003. Applications of Hilbert–Huang transform to non-stationary financial time series analysis. *Applied stochastic models in business and industry*, *19*(3), pp.245-268.

[138] Betta, G., Liguori, C., Paolillo, A. and Pietrosanto, A., 2001, May. A DSP-based FFT-analyzer for the fault diagnosis of rotating machine based on vibration analysis. In *Instrumentation and Measurement Technology Conference, 2001. IMTC 2001. Proceedings of the 18th IEEE* (Vol. 1, pp. 572-577). IEEE.

[139] Chen, G., 2012. *Design, Implementation and Comparison of Demodulation Methods in AM and FM* (Doctoral dissertation, Blekinge Institute of Technology).

[140] Djebala, A., Ouelaa, N. and Hamzaoui, N., 2008. Detection of rolling bearing defects using discrete wavelet analysis. *Meccanica*, *43*(3), pp.339-348.

[141] Kankar, P.K., Sharma, S.C. and Harsha, S.P., 2011. Rolling element bearing fault diagnosis using wavelet transform. *Neurocomputing*, *74*(10), pp.1638-1645.

[142] Lin, J. and Qu, L., 2000. Feature extraction based on Morlet wavelet and its application for mechanical fault diagnosis. *Journal of sound and vibration*, *234*(1), pp.135-148.

[143] Zhou, Y., Chen, J., Dong, G.M., Xiao, W.B. and Wang, Z.Y., 2011. Wigner–Ville distribution based on cyclic spectral density and the application in rolling element bearings diagnosis. *Proceedings of the Institution of Mechanical Engineers, Part C: Journal of Mechanical Engineering Science*, *225*(12), pp.2831-2847.

[144] Smith, J.S., 2005. The local mean decomposition and its application to EEG perception data. *Journal of the Royal Society Interface*, *2*(5), pp.443-454.

[145] Lei, Y., Lin, J., He, Z. and Zuo, M.J., 2013. A review on empirical mode decomposition in fault diagnosis of rotating machinery. *Mechanical Systems and Signal Processing*, *35*(1), pp.108-126.

[146] Li, H., Zhang, Y. and Zheng, H., 2009. Hilbert-Huang transform and marginal spectrum for detection and diagnosis of localized defects in roller bearings. *Journal of Mechanical Science and Technology*, *23*(2), pp.291-301.

[147] Benbouzid, M., 2015. Advanced signal processing techniques for condition monitoring of electric machines and drives. Proposal for IECON '15 Tutorial. IEEE.

[148] Du, Q. and Yang, S., 2007. Application of the EMD method in the vibration analysis of ball bearings. *Mechanical Systems and Signal Processing*, *21*(6), pp.2634-2644.

[149] Mohanty, S., Gupta, K.K., Raju, K.S., Singh, A. and Snigdha, S., 2013, September. Vibro acoustic signal analysis in fault finding of bearing using empirical mode decomposition. In *Advanced Electronic Systems (ICAES), 2013 International Conference on* (pp. 29-33). IEEE.

[150] Thameur, K., Marc, T. and Raynald, G., 2013. Comparison between the efficiency of LMD and EMD algorithms for early detection of gear defects. *Mechanics & Industry*, *14*(2), pp.121-127.

[151] Lei, Y., Lin, J., He, Z. and Zuo, M.J., 2013. A review on empirical mode decomposition in fault diagnosis of rotating machinery. *Mechanical Systems and Signal Processing*, *35*(1), pp.108-126.

[152] Dragomiretskiy, K. and Zosso, D., 2014. Variational mode decomposition. *IEEE transactions on signal processing*, *62*(3), pp.531-544.

[153] Peng, Z.K., Peter, W.T. and Chu, F.L., 2005. A comparison study of improved Hilbert–Huang transform and wavelet transform: application to fault diagnosis for rolling bearing. *Mechanical systems and signal processing*, *19*(5), pp.974-988.

[154] Randall, R.B. and Antoni, J., 2011. Rolling element bearing diagnostics-a tutorial. *Mechanical Systems and Signal Processing*, *25*(2), pp.485-520.

[155] Li, W., Zhu, Z., Jiang, F., Zhou, G. and Chen, G., 2015. Fault diagnosis of rotating machinery with a novel statistical feature extraction and evaluation method. *Mechanical Systems and Signal Processing*, *50*, pp.414-426.

[156] Mohanty, S., Gupta, K.K. and Raju, K.S., 2015, February. Multi-channel vibro-acoustic fault analysis of ball bearing using wavelet based multi-scale principal component analysis. In *Communications (NCC), 2015 Twenty First National Conference on* (pp. 1-6). IEEE.

[157] Feng, Z., Ma, H. and Zuo, M.J., 2016. Amplitude and frequency demodulation analysis for fault diagnosis of planet bearings. *Journal of Sound and Vibration*, *382*, pp.395-412.

[158] Du, Q. and Yang, S., 2006. Improvement of the EMD method and applications in defect diagnosis of ball bearings. *Measurement Science and Technology*, *17*(8), pp. 2355–2361.

[159] Raj, A.S. and Murali, N., 2013. Early classification of bearing faults using morphological operators and fuzzy inference. *IEEE Transactions on Industrial Electronics*, *60*(2), pp.567-574.

[160] Batista, L., Badri, B., Sabourin, R. and Thomas, M., 2013. A classifier fusion system for bearing fault diagnosis. *Expert Systems with Applications*, *40*(17), pp.6788-6797.

[161] McInerny, S.A. and Dai, Y., 2003. Basic vibration signal processing for bearing fault detection. *IEEE Transactions on education*, *46*(1), pp.149-156.

[162] Shakya, P., Darpe, A.K. and Kulkarni, M.S., 2013. Vibration-based fault diagnosis in rolling element bearings: ranking of various time, frequency and time-frequency domain data-based damage identification parameters. *International journal of condition monitoring*, *3*(2), pp.53-62.

[163] Sun, W., Yang, G.A., Chen, Q., Palazoglu, A. and Feng, K., 2013. Fault diagnosis of rolling bearing based on wavelet transform and envelope spectrum correlation. *Journal of Vibration and Control*, *19*(6), pp.924-941.

[164] Li, F., Meng, G., Ye, L. and Chen, P., 2008. Wavelet transform-based higher-order statistics for fault diagnosis in rolling element bearings. *Journal of Vibration and Control*, *14*(11), pp.1691-1709.

[165] Peng, B., Wei, X., Deng, B., Chen, H., Liu, Z. and Li, X., 2014. A sinusoidal frequency modulation Fourier transform for radar-based vehicle vibration estimation. *IEEE Transactions on Instrumentation and Measurement*, *63*(9), pp.2188-2199.

[166] Nandi, A.K., Liu, C. and Wong, M.D., 2013. Intelligent vibration signal processing for condition monitoring. *Surveillance*, *7*, pp.29-30.

[167] Mohanty, A. R., 2015. Machinery condition monitoring: principles and practices, CRC press T&F.

[168] Heller, A., 2015. *Condition Monitoring* (Doctoral dissertation, TU Chemnitz).

[169] Dong, S., Sun, D., Tang, B., Gao, Z., Yu, W. and Xia, M., 2014. A fault diagnosis method for rotating machinery based on PCA and Morlet kernel SVM. *Mathematical Problems in Engineering*, *2014*, pp.1-8.

[170] Mohamad, I.B. and Usman, D., 2013. Standardization and its effects on K-means clustering algorithm. *Research Journal of Applied Sciences, Engineering and Technology*, *6*(17), pp.3299-3303.

[171] Zhao, M., Lin, J., Xu, X. and Li, X., 2014. Multi-fault detection of rolling element bearings under harsh working condition using IMF-based adaptive envelope order analysis. *Sensors*, *14*(11), pp.20320-20346.

[172] Barszcz, T., 2009. Decomposition of vibration signals into deterministic and nondeterministic components and its capabilities of fault detection and identification. *International Journal of Applied Mathematics and Computer Science*, *19*(2), pp.327-335.

[173] Smith, W.A. and Randall, R.B., 2015. Rolling element bearing diagnostics using the Case Western Reserve University data: A benchmark study. *Mechanical Systems and Signal Processing*, *64*, pp.100-131.

[174] Hu, H., 2009. Cyclostationary Approach to signal detection and classification in cognitive radio systems. *INTECH*, pp. 51-76.

[175] National Instruments Inc., 2016, Zero padding does not buy spectral resolution. Accessed on 27/03/2016 http://www.ni.com/white-paper/4880/en/

[176] Verma, N.K., Agrawal, A.K., Sevakula, R.K., Prakash, D. and Salour, A., 2013, December. Improved signal preprocessing techniques for machine fault diagnosis. In *Industrial and Information Systems (ICIIS), 2013 8th IEEE International Conference on* (pp. 403-408). IEEE.

[177] Huang, N.E., Wu, M.L.C., Long, S.R., Shen, S.S., Qu, W., Gloersen, P. and Fan, K.L., 2003, September. A confidence limit for the empirical mode decomposition and Hilbert spectral analysis. In *Proceedings of the royal society of london a: Mathematical, physical and engineering sciences* (Vol. 459, No. 2037, pp. 2317-2345). The Royal Society.

[178] Ren, H., Wang, Y.L., Huang, M.Y., Chang, Y.L. and Kao, H.M., 2014. Ensemble empirical mode decomposition parameters optimization for spectral distance measurement in hyperspectral remote sensing data. *Remote Sensing*, *6*(3), pp.2069-2083.

[179] Wu, Z. and Huang, N.E., 2009. Ensemble empirical mode decomposition: a noise-assisted data analysis method. *Advances in adaptive data analysis*, *1*(1), pp.1-41.

[180] Smith, L.I., 2002. A tutorial on principal components analysis. *Cornell University, USA*, *51*(52), pp.1-27.

[181] Hall, S., 2014. Implementation and verification of robust PLS regression algorithm. *Chalmers University of Technology:* Master's Thesis in Engineering Mathematics and Computational Science.

[182] Haykin, S., 2008. *Communication Systems*. John Wiley & Sons.

[183] Verma, N.K., Sevakula, R.K., Dixit, S. and Salour, A., 2016. Intelligent condition based monitoring using acoustic signals for air compressors. *IEEE Transactions on Reliability*, *65*(1), pp.291-309.

[184] De Lorenzo, F. and Calabro, M., 2007. Kurtosis: a statistical approach to identify defect in rolling bearings. In *Proceedings of 2nd International Conference on Marine Research and Transportation, Naples* (pp. 17-24).

[185] Walck, C., 2007. Handbook on statistical distributions for experimentalists.

[186] Rosser, G., Fletcher, A.G., Maini, P.K. and Baker, R.E., 2013. The effect of sampling rate on observed statistics in a correlated random walk. *Journal of The Royal Society Interface*, *10*(85), pp.1-11.

[187] Schwede, R. L., Cirpka, O.A., Nowak, W. and Neuweiler, I., 2008. Impact of sampling volume on the probability density function of steady state concentration. *Water Resources Research*, *44*(12), pp.1-16.

[188] Broom, M., Nouvellet, P., Bacon, J.P. and Waxman, D., 2007. Parameter-free testing of the shape of a probability distribution. *Biosystems*, *90*(2), pp.509-515.

[189] Park, H.M., 2008. Univariate analysis and normality test using SAS, Stata, and SPSS. *The University Information Technology Services (UITS) Center for Statistical and Mathematical Computing, Indiana University*, pp.1-38.

[190] Cococcioni, M., Lazzerini, B. and Volpi, S.L., 2013. Robust diagnosis of rolling element bearings based on classification techniques. *IEEE Transactions on Industrial Informatics*, *9*(*4*), pp.2256-2263.

[191] Kihm, F., Rizzi, S.A., Ferguson, N.S. and Halfpenny, A., 2013. Understanding How Kurtosis Is Transferred from Input Acceleration to Stress Response and Its Influence on Fatigue Llife. *RASD 2013 , Pisa, IT,* 01 - 03 Jul.,pp. 1-16.

[192] Westfall, P.H., 2014. Kurtosis as peakedness, 1905–2014. RIP. *The American Statistician*, *68*(3), pp.191-195.

[193] Balakrishnan, A.V., 1964. Effect of line*ar and nonlinear signal processing on signal statistics*. Radio Science *Journal of Research NBS/USNC-URSI*, *68D*(9*)*, pp.953-965.

[194] Klingspor, M., 2015. Hilbert transform: Mathematical theory and applications to signal processing. *Master Thesis*, Department of Mathematics, Mathematics and Applied Mathematics. Linkoping University.

[195] Johansson, M., 1999. The Hilbert transform. *Mathematics Master's Thesis. Vaxjo University.*

[196] Randall, R.B., 2017. A history of cepstrum analysis and its application to mechanical problems. *Mechanical Systems and Signal Processing*, *97*, pp.3-19.

[197] Cong, F., Chen, J. and Pan, Y., 2011. Kolmogorov-Smirnov test for rolling bearing performance degradation assessment and prognosis. *Journal of vibration and control*, *17*(9), pp.1337-1347.

[198] Sun, P., Liao, Y. and Lin, J., 2017. The shock pulse index and its application in the fault diagnosis of rolling element bearings. *Sensors*, *17*(*3*), pp.1-23.

[199] Batista, F.B., Lamim Filho, P.C.M., Pederiva, R. and Silva, V.A.D., 2016. An Empirical Demodulation for Electrical Fault Detection in Induction Motors. *IEEE Transactions on Instrumentation and Measurement*, *65*(3), pp.559-569.

[200] Reineke, D.M., Baggett, J. and Elfessi, A., 2003. A note on the effect of skewness, kurtosis, and shifting on one-sample t and sign tests. *Journal of Statistics Education*, *11*(3), pp.1-13.

[201] Gaikwad, A. D., Sugumaran, V., and Amarnath, M., 2016. Fault diagnosis of roller bearings with sound signals using wavelets and decision tree algorithm. *Indian Journal of Science and Technology*. *9*(33), pp. 1–7.

[202] Zhong, J.H., Wong, P.K. and Yang, Z.X., 2016. Simultaneous-fault diagnosis of gearboxes using probabilistic committee machine. *Sensors*, *16*(2), pp.2-19.

[203] Stanik, Z., 2014. Vibro-acoustic Diagnostics of Rolling Bearings in Vessels. *Transactions on Maritime Science*, *3*(02), pp.111-118.

[204] Dai, J., Chen, C.P., Xu, X.Y., Huang, Y., Hu, P., Hu, C.P. and Wu, T., 2008, September. Machinery vibration signals analysis and monitoring for fault diagnosis and process control. In *International Conference on Intelligent Computing* (pp. 696-703). Springer Berlin Heidelberg.

[205] Alonso, J.B., Ferrer, M.A. and Travieso, C.M., 2012. Fault diagnosis using audio and vibration signals in a circulating pump. In *Journal of Physics: Conference Series* (Vol. 364, No. 1, p. 012135). IOP Publishing.

[206] Iorgulescu, M., Alexandru, M., Beloiu. R., 2012. Noise and vibration monitoring for diagnosis of DC motor's faults. Optimization of Electrical and Electronic Equipment (OPTIM), 2012 13th International Conference on. IEEE.

[207] Wei, Q., Liu, Q., Fan, S.Z., Lu, C.W., Lin, T.Y., Abbod, M.F. and Shieh, J.S., 2013. Analysis of EEG via multivariate empirical mode decomposition for depth of anesthesia based on sample entropy. *Entropy*, *15*(9), pp.3458-3470.

[208] Ren, Y., Suganthan, P.N. and Srikanth, N., 2015. A comparative study of empirical mode decomposition-based short-term wind speed forecasting methods. *IEEE Transactions on Sustainable Energy*, *6*(1), pp.236-244.

[209] Li, H., Zheng, H. and Tang, L., 2006, September. Wigner-Ville distribution based on EMD for faults diagnosis of bearing. In *International Conference on Fuzzy Systems and Knowledge Discovery* (pp. 803-812). Springer Berlin Heidelberg.

[210] Wang, Y., Markert, R., Xiang, J. and Zheng, W., 2015. Research on variational mode decomposition and its application in detecting rub-impact fault of the rotor system. *Mechanical Systems and Signal Processing*, *60*, pp.243-251.

[211] Xiong, Q., Zhang, W., Lu, T., Mei, G. and Liang, S., 2015. A fault diagnosis method for rolling bearings based on feature fusion of multifractal detrended fluctuation analysis and alpha stable distribution. *Shock and Vibration*, 2016, pp.1-12.

[212] Liu, Y., Yang, G., Li, M. and Yin, H., 2016. Variational mode decomposition denoising combined the detrended fluctuation analysis. *Signal Processing*, *125*, pp.349-364.

[213] Siljak, H. and Seker, S., 2014. Hurst analysis of induction motor vibrations from aging process. *Balkan Journal of Electrical and Computer Engineering*, *2*(1).pp.16-19.

[214] Nunes, J.C. and Deléchelle, E., 2009. Empirical mode decomposition: Applications on signal and image processing. *Advances in Adaptive Data Analysis*, *1*(01), pp.125-175.

[215] Liao, W., Han, P. and Liu, X., 2009, November. Fault diagnosis for engine based on EMD and wavelet packet BP neural network. In *Intelligent Information Technology Application, 2009. IITA 2009. Third International Symposium on* (Vol. 1, pp. 672-676). IEEE.

[216] Liu, H., Song, B., Qin, H. and Qiu, Z., 2013. An adaptive-ADMM algorithm with support and signal value detection for compressed sensing. *IEEE Signal Processing Letters*, *20*(4), pp.315-318.

[217] Flandrin, P., Goncalves, P. and Rilling, G., 2005. EMD equivalent filter banks, from interpretation to applications. *Hilbert-Huang transform and its applications*, *16*, pp.57-74.

[218] Zhang, S., Wang, Y., He, S. and Jiang, Z., 2016. Bearing fault diagnosis based on variational mode decomposition and total variation denoising. *Measurement Science and Technology*, *27*(7), pp.1-10.

[219] Wunder, G. and Boche, H., 2003. Peak value estimation of bandlimited signals from their samples, noise enhancement, and a local characterization in the neighborhood of an extremum. *IEEE Transactions on Signal Processing*, *51*(3), pp.771-780.

[220] Brandt, A. and Ahlin, K., 2010. Sampling and Time-Domain Analysis. *Sound and Vibration*, *44*(5), pp.13-16.

[221] Antoni, J. and Randall, R.B., 2004. Unsupervised noise cancellation for vibration signals: part II-a novel frequency-domain algorithm. *Mechanical Systems and Signal Processing*, *18*(1), pp.103-117.

[222] Shaw, P.K., Saha, D., Ghosh, S., Janaki, M.S. and Iyengar, A.S., 2015. Investigation of coherent modes in the chaotic time series using empirical mode decomposition and discrete wavelet transform analysis. *Chaos, Solitons & Fractals*, *78*, pp.285-296.

[223] Nava, N., Di Matteo, T. and Aste, T., 2016. Anomalous volatility scaling in high frequency financial data. Physica A: Statistical Mechanics and its Applications, 447, pp.434-445.

[224] Stack, J.R., Harley, R.G. and Habetler, T.G., 2004. An amplitude modulation detector for fault diagnosis in rolling element bearings. *IEEE Transactions on Industrial Electronics*, *51*(5), pp.1097-1102.

[225] Konstantin-Hansen, H. and Herlufsen, H., 2010. Envelope and cepstrum analyses for machinery fault identification. *Sound and Vibration*, *44*(5), pp.10-12.

List of Publications

Journals

1. S. Mohanty, K. K. Gupta, Kota Solomon Raju, "Unitary Sample Shifted time Series FCF, FKS, and FE in Fault Identification of Bearing, " IET - Science, Measurement & Technology, Vol-11, issue -4, pp. 516 - 524, July 2017.
2. S. Mohanty, K. K. Gupta, Kota Solomon Raju, "Adaptive Fault Identification of Bearing using EMD-PCA based average Kurtosis technique," IET - Science, Measurement & Technology, Vol-11, issue -1, pp. 30-40, Jan 2017.
3. S. Mohanty, K. K. Gupta, Kota Solomon Raju, "Hurst based Vibro-acoustic Feature Extraction of Bearing using EMD and VMD," Elsevier Measurement Science. (revision submitted)

Book Chapter

1. S. Mohanty, K. K. Gupta, and Kota Solomon Raju, "Vibro-Acoustic Fault Analysis of Bearing using FFT, EMD, EEMD, and CEEDMAN and Their Implications", Advances in Machine Learning and Signal Processing, Springer Lecture Notes in Electrical Engineering, Chapter 25, pp. 281 - 292, Vol. 387, 2016.

Conferences

1. S. Mohanty, K. K. Gupta, Kota Solomon Raju, "Multi-Channel Vibro Acoustic Fault Analysis of Ball Bearing Using Wavelet Based Multi-Scale Principal Component Analysis," Proceedings of 21st National Conference on Communications (NCC 2015), IIT, Mumbai, 27-1st March, 2015.
2. S. Mohanty, K. K. Gupta, and Kota Solomon Raju, "Comparative Study between VMD and EMD in Bearing Fault Diagnosis," 9th IEEE International Conference on Industrial and Information Systems (ICIIS -2014), IIIT, Gwalior, 2014.
3. S. Mohanty, K. K. Gupta, and Kota Solomon Raju, "Vibration Analysis in Fault finding of Ball Bearing using VMD," 9th IEEE International Conference on Industrial and Information Systems (ICIIS -2014), IIIT, Gwalior, 2014.
4. S. Mohanty, K. K. Gupta, S. Snigdha, "Bearing Health Monitoring and Fault Diagnosis by Analyzing Vibration Signal," International Conference on Communication Systems (ICCS 2013), BKBIT, Pilani, 2013.
5. S. Mohanty, K. K. Gupta, K. Solomon Raju, Arvind Singh, S. Snigdha, "Vibro Acoustic Signal Analysis in Fault Finding of Bearing Using Empirical Mode Decomposition," International IEEE Conference on Advanced Electronic Systems (ICAES-2013), CEERI, Pilani, 2013.

PUBLICATIONS OUT OF THESIS

Journals

1. S. Mohanty, K. K. Gupta, Kota Solomon Raju, "Vibration Feature Extraction and Analysis of Industrial Ball Mill using MEMS Accelerometer Sensor and Synchronized Data Analysis Technique", Procedia Computer Science Journal, vol. 58, pp. 217-224, 2015.

Conferences

1. Satish Mohanty, Karunesh Kumar Gupta, Kota Solomon Raju, "Multi-Channel Vibration Feature Extraction of Ball Mill Using Synchronized Wavelet Based Multi-Scale Principal Component Analysis," Proceedings of the 9th International Conference on Circuits, Systems, Signal and Telecommunications (CSST '15), Dubai, United Arab Emirates, February 22-24, 2015.
   http://www.wseas.us/e-library/conferences/2015/Dubai/CSST/CSST-17.pdf.
2. S. Mohanty, K. K. Gupta, and Kota Solomon Raju, "Effective Sample Length Selection to Avoid Dead Zone Effect in Ball Mill Vibration Signal Analysis and Applications," 2nd IEEE International Conference on Signal Processing and Integrated Networks (SPIN-2015), AMITY University, Noida, February 19-20, 2015.
3. S. Mohanty, K. K. Gupta, Kota Solomon Raju, Vikrant Mishra, Vipin Kumar, P. Bhanu Prasad, "Characterization of Wireless Accelerometer Sensor and its Industrial Applications," Proceedings of 20th National Conference on Communications (NCC 2014), IIT, Kanpur, 2014.

Brief Biography of Candidate

Satish Mohanty received his B.Tech degree in Electronics & Communication Engineering from IEI (India), and M.Tech degree in Communication Engineering from Vellore Institute of Technology, Vellore, India in 2003 and 2008 respectively. He worked as a Project fellow in Central Electronics Engineering Research Institute, Pilani, India from 2009-2012 in the area of vibration signal processing related to ball mill to characterize material size from their vibration signatures. He joined the department of Electrical and Electronics Engineering at B.I.T.S. Pilani, India as a research scholar in 2012. His area of research includes signal analysis related to vibration and acoustic signals, and statistical signal processing.

Brief Biography of Supervisor

Dr. Karunesh Kumar Gupta received his B.Tech. degree in Electronics & Communication Engineering from IET, Lucknow University; M.E. in Control & Instrumentation Engineering from Motilal Nehru National institute of technology (MNNIT), Allahabad; and Ph.D. from Birla Institute of Technology & Sciences (BITS-Pilani), Pilani, India in 1991, 1994, 2007 respectively. Before joining BITS, he had worked with many industries and involved in designing, fabrication, installation and commissioning of Process plant, Machine & Factory Automation Industries (EMA India Limited, Kanpur; DEUTEK Controls (India) Ltd, New Delh; LML Scooter Pvt Ltd, Kanpur; Sanchar Antennas & Communication Systems, New Delhi; MESSUNG Systems Pvt Ltd, Pune). Currently he is working as a faculty member in the department of Instrumentation & EEE Engineering. He has published many research papers in National and International Conferences and in International Journals of repute. His areas of interests are Image processing, Vibration and Acoustic signal processing, drinking water quality sensors and Biometrics.

Brief Biography of Co-Supervisor

Dr. Kota Solomon Raju received the Bachelor of Engineering degree in 1997 from Andhra University, Master of Engineering in 2003 from Birla Institute of Technology and Science (BITS), Pilani and Ph.D. in 2008 from department of Electronics and Computer Engineering, IIT Roorkee, India. He has been working as Principal Scientist in Digital Systems Group, CSIR-Central Electronics Research Institute (CSIR-CEERI), Pilani, Rajasthan, India. His research work focused on reconfigurable computing systems (RCS), advanced embedded systems design and wireless sensor network (WSN) based embedded systems design and included hardware/software codesign, parallelizing applications, customized computing, and high-level synthesis, ad hoc networking, Zigbee based networking, and other sensor based embedded systems, protocols design and CAD tools for electronic systems design. He is the author and co-author of many Journals and Conference papers of repute.